CATALYTIC HYDROGENOLYSIS OF BIORENEWABLE SUBSTRATES TO PREPARE POLYOLS

By

Yaoyan Xi

A DISSERTATION

Submitted to
Michigan State University
In partial fulfillment of the requirement
For the degree of

DOCTOR OF PHILOSOPHY

Chemical Engineering

2010

ABSTRACT

CATALYTIC HYDROGENOLYSIS OF BIORENEWABLE SUBSTRATES TO PREPARE POLYOLS

By

Yaoyan Xi

Heterogeneous hydrogenolysis of glycerol to propylene glycol was carried out in both batch and trickle bed reactors. A kinetic study was done in both reaction systems by changing temperature, pressure, glycerol concentration, base concentration, and catalyst loading. Different solvents were tested to determine to what extent the solvent affected kinetics. The catalysts prepared by our collaborator were characterized.

A combined mass transfer-kinetic model, which integrated mass and energy balances, was developed and optimized to find kinetic parameters for the reaction. Prediction of outlet glycerol concentration and temperature profile with model was in good agreement with experimental data. In order to improve model's prediction accuracy, empirical correction factor was numerically fitted; adjusted model gives more accurate prediction and facilitates the understanding of overall reaction rate and its components in the model. Moreover, model's assumptions were examined and checked by developing simplified models.

Finally, lactic acid hydrogenation to prepare propylene glycol was studied in batch and trickle bed reactors with the same reaction conditions to correlate their intrinsic reaction rates. The research shows both reactors, under the intrinsic reaction regime, are correlated. Simulation was performed with the model incorporating the intrinsic kinetics specifically developed for lactic acid hydrogenation, and results are in good agreement with experimental data.

ACKNOWLEDGEMENTS

I would like to thank my academic advisor, Dr. Dennis J. Miller, for his guidance and support in my research projects. I would also like to thank Dr. Bruce Dale, Dr. Lawrence Drzal, Dr. Ramini Narayan, and Dr. James Jackson for serving on my graduate committee. Finally, I would like to acknowledge the generous financial and technical support provided by Department of Energy, Pacific Northwestern National Laboratory, and Michigan Economic Development Cooperation.

TABLE OF CONTENTS

LIST OF TABLES

LIST OF FIGURES

LIST OF SYMBOLS

C_{GO} glycerol concentration (kmol/m^3 fluid)

$C_{H2,L}$ hydrogen concentration in bulk liquid phase (kmol/m^3 fluid)

$C_{H2,S}$ hydrogen liquid phase concentration at catalyst surface (kmol/m^3 fluid)

$C_{GA \cdot S}$ glyceraldehyde concentration (kmol/m^3 fluid)

C_S free site concentration on catalyst surface (kmol/m^3 fluid)

C_{OH^-} base concentration (kmol/m^3 fluid)

C_{total} total site concentration on catalyst surface (kmol/m^3 fluid)

C_{LA} lactic acid concentration, kmol/m^3 fluid

C^*_{H2} equivalent hydrogen bulk concentration, kmol/m^3 fluid

$C_{H2,\,L}$ hydrogen concentration on gas-liquid interface, kmol/m^3 fluid

$C_{H2,S}$ hydrogen concentration on liquid-solid interface, kmol/m^3 fluid

$C_{I \cdot S}$ adsorbed intermediate concentration (kmol/m^3 fluid)

C_p specific heat of solution (kJ/kg/K)

d_p catalyst particle diameter (m)

$D_{e,H2}$ hydrogen effective diffusivity (m^3 fluid/m cat/sec)

D_{H2} hydrogen diffusivity, m^2/sec

E_a activation energy in k_f (kJ/kmol)

H_A Henry's Law constant, MPa·m^3/kmol

$k_{GL,H2}a$ hydrogen gas-liquid interfacial mass transfer coefficient (m^3 fluid/m^3 reactor/sec)

$k_{SL,H2}a$ hydrogen solid-liquid interfacial mass transfer coefficient (m^3 fluid/m^3 eactor/sec)

k_0 pre-exponential coefficient of k_f (m^3 fluid/m^3 catalyst/sec)

k_f rate constant (m^3 fluid/m^3 catalyst/sec)

K_H hydrogen rate constant (unitless)

K reaction rate constant, m^3/kg catalyst/MPa/sec

K_{H2} reaction rate constant, MPa^{-1}

K_{LA} reaction rate constant, m^3/kmol

k_1,k_{-1} dehydrogenation rate constants (m^6/m^3 catalyst/kmol/sec)

k_2,k_{-2} dehydration rate constants (m^6/m^3 catalyst/kmol/sec)

k_3 hydrogenation rate constant (m^6/m^3 catalyst/kmol/sec)

L catalyst particle characteristic length, m

P_{H2} hydrogen partial pressure, MPa

$-R_{LA,G}$	lactic acid global reaction rate, kmol/kg catalyst/sec
$-R_{LA,obs}$	lactic acid intrinsic reaction rate, kmol/kg catalyst/sec
r_1	dehydrogenation rate (kmol/m^3 catalyst/sec)
r_2	dehydration rate (kmol/m^3 catalyst/sec)
r_3	hydrogenation rate (kmol/m^3 catalyst/sec)
R	reactor radius (m)
R_{obv}	observed reaction rate (kmol/m^3 reactor/sec)
t	time (sec)
T	temperature (K)
T_c	coolant temperature (K)
ΔH_R	heat of reaction (kJ/kmol)
U_o	overall heat transfer coefficient, J/m^2/K/sec
X_{GO}	glycerol conversion at trickle bed outlet
ε_W	fraction of bed wetted
ε_P	catalyst particle porosity
ε_B	bed porosity (m^3 void/m^3 reactor)
η_{H2}	hydrogen effectiveness factor
ρ	fluid density (kg/m^3)

τ trickle bed residence time (m^3 reactor·sec/m^3 fluid)

φ Thiele modulus

Part I General Introduction

Chapter 1 Literature Review

1.1. Current Developments in Glycerol Applications

At present, the chemical industry worldwide is heavily dependent on petroleum and its derivatives. Given that petroleum resources are limited and will be depleted sooner rather than later, it is important for chemical industries to find alternatives to sustain their growth.[1-5] Biomass is a promising choice given that it (1) is available in large amounts, (2) is easily accessed, and (3) has potential for a broad spectrum of products via environmentally friendly processes.[6-10] Glycerol can be readily derived from biomass sources such as sugarcane and straw and is currently produced mainly by the petrochemical and biodiesel industries without efficient use despite its tremendous potential. Therefore, this research project is to join the global effort to explore chemicals from biomass and to develop value added processes in the face of the current bleak conventional energy future. Propylene glycol is selected as the value added synthesis product from glycerol in this project, based on its current various applications in the pharmaceuticals, cosmetics, and auto cooling media.[11,12] At the same time, propylene glycol's unique molecular structure, two hydroxyls, allows derivatization for potential monomers for the polymer industry.[13,14]

1.2. Prior Arts in Glycerol Hydrogenolysis

A great number of papers and patents have been published regarding the preparation of propylene glycol by glycerol hydrogenolysis.[15-17] Previous research focused mainly on either

(1) catalyst formulation followed by reaction condition optimization, (2) mechanistic investigations, or (3) propylene glycol preparation by hydrogenolysis of glycerol on metal or alloy catalysts. Casale et al.[18] tried ruthenium catalyst modified with sulfides in a basic environment. Main products were 1,2-propanediol and lactic acid. Ratio of sulfide ions to ruthenium in the catalyst was chosen to range from 0.2 to 5 moles of sulfur ions per mole of ruthenium. The base was a compound selected from the group consisting of hydroxides of alkali metal, alkaline earth metal, sodium carbonates, and quaternary ammonium salts and was used in a quantity to bring pH within a range of 8 to 13. Reaction temperature was over 200°C, and pressure was between 5~20 MPa. According to data provided in the patent, glycerol is completely converted, and selectivity toward propylene glycol, lactic acid, ethylene glycol, ethanol, and i-propanol is 75.2%, 13.4%, 5.1%, 0.6%, and 2.0%, respectively. The remainder is gaseous side products. This result can apply to impure glycerol, which brings huge leverage for this patent.

Schuster et al.[19] investigated a process where glycerol was hydrogenated to propylene glycol with a catalyst containing active metals such as cobalt, copper, manganese, and molybdenum. Weight percentage for each metal was suggested as 40-70% of cobalt, 10-20% of copper, 0 to 10% of manganese, and 0-10% of molybdenum. This catalyst might additionally contain inorganic polyacids and/or heteropolyacids in an amount of up to 10% by weight, based on the total weight. Reactions were conducted at temperatures ranging from 200~250°C and pressures ranging from 200~325 bars. Analysis with HPLC shows that reaction mixture contains 95.8 wt% of 1,2-propanediol, 3.2 wt% n-propanol, and no glycerol.

Werpy et al.[20] studied a catalyst as a multi-metallic system in their patent. Different combinations were examined, and Ni-Re turned out to be the best. Reactions were carried out at temperature range of 170~220°C and pressure range of 600~1800 psi in a basic solution for 0.3 ~ 30 hours.

In addition to the discussion of catalyst preparation and composition in hydrogenolysis processes, it is equally important to investigate the current knowledge about the catalysis mechanism and surface chemistry. Hass et al.[21] proposed an acidic solid catalyst to synthesize 1,2-propanediol and 1,3-propanediol simultaneously with the mechanism consisting of three steps: (1) glycerol is first dehydrated by feeding a gaseous glycerol-water mixture with 10~40 wt% glycerol at 250~340°C over solid catalyst to get acrolein as the intermediate, (2) acrolein is hydrated, and (3) the reaction mixture derived is catalytically hydrogenated to the polyols. The products, including 3-hydroxypropionaldehyde, hydroxyacetone, 1,2-propanediol, and 1,3-propanediol, are separated by distillation. Analysis shows the total yield toward 1,3-propanediol relative to glycerol is 60% and 1,2-propanediol 10%. In addition, Miyazawa[22] experimented with heat-resistant ion-exchange resin combined with Ru/C for glycerol hydrogenolysis to 1,2-propanediol. Maris et al.[15] also studied the hydrogenolysis mechanism: glycerol is dehydrogenated to glyceraldehyde, which is converted to ethylene glycol via hydrogenolysis; glyceraldehyde can also dehydrate to 2-hydroxyl acrolein, which is hydrogenated to propylene glycol; 2-Hydroxyl acrolein can be converted to pyruvaldehyde via keto-enol tautomerization; from there, pyruvaldehyde will be hydrated to lactic acid and hydrogenolysis of 2-hydroxyl acrolein will lead to propylene glycol.

Beyond the discussion of catalyst preparation and reaction mechanism, a great number of kinetic studies have been done. Suppes et al.[23] studied the effects of temperature, hydrogen pressure, initial water content, choice of catalyst and its reduction temperature, and catalyst loading. This study also validated a new reaction pathway for converting glycerol to propylene glycol via the acetol intermediate. Shanks et al.[24] studied ruthenium on carbon catalyst in batch reactor at two pH levels to obtain kinetic data. Langmuir-Hinshelwood type models were developed from experimental data to describe glycerol hydrogenolysis to propylene glycol, ethylene glycol, and further degradation of glycols. Their study also determined the competitive adsorption coefficients for reaction species.

1.3. Prior Arts in Trickle Bed Reactor Modeling

Our research project is designed to prepare for the scale-up of glycerol hydrogenolysis after initial research conducted in the batch reactors to provide insight into the catalysis mechanism and kinetics. Therefore, moving on to a multiphase reactor environment is an obvious choice in order to achieve the ultimate goal of commercial production. Multiphase reactors are widely used in the production of petroleum-based fuels, commodity and specialty chemicals, pharmaceuticals, and polymers.[25-30] Trickle bed reactors are especially favored, thanks to their easy installation, various configurations, flexible operating conditions, and good mass transfer between phases. They are widely employed in hydro-treating processes such as hydrogenolysis, hydrodesulfurization, hydrocracking, and hydrorefining.[31-33]

Studies that correlate trickle bed reactor performance with operating conditions have been conducted. Larachi et al.[34] investigated the gas-liquid interfacial mass transfer in a trickle

bed reactor at the elevated pressure, and proposed a rigorous thermodynamic model accounting for liquid and gas nonidealities along with pressure, gas and liquid superficial velocities, liquid viscosity, and packing size. Iliuta et al.[35] studied the fluid dynamics and the gas-liquid mass transfer characteristics in a trickle bed reactor. A more quantitative model was established by Al-Dahhan et al.[36] taking into account flow regime transition, liquid holdup, pressure drop, gas-liquid interfacial area, mass transfer coefficient, and catalyst wetting efficiencies in both the liquid-limited and the gas-limited scenarios. Huang et al.[37] studied the heat transfer characteristics of a trickle bed reactor on the laboratory scale and determined four factors influencing the local fluid-solid convective heat transfer coefficient. A correlation for catalyst wetting efficiency in a pressurized trickle bed reactor was developed by Al-Dahhan et al.[38] to correlate the laboratory and pilot scale reactors' data. Tronconi et al.[39] developed a mathematical model to characterize carbohydrate hydrogenolysis.

Despite the studies mentioned above, little work has been done to integrate mass and energy transport and fluid dynamics in the trickle bed reactor with operating parameters in a single model. On the other hand, trickle bed reactor modeling is a powerful tool that enables a better understanding of glycerol hydrogenolysis in terms of trickle bed geometry, gas-liquid-solid mass and heat transport, and intrinsic reaction kinetics. In Chapter 5 and 6, research will focus on the establishment and development of this integral model based on the experimental data.

Chapter 2 Experimental Systems and Methods

This chapter will mainly introduce the chemicals, the apparatus, and the analytical instruments and methods employed in the research.

2.1. Chemicals

Ultrahigh purity gases used in our research - hydrogen (99.999%), nitrogen (99.99%), helium (99.999%), and oxygen (99.99%) - are produced by Linde Gas LLC. The gas mixture serving as a gas chromatography (GC) analysis standard is produced by AGA Specialty Gas, where methane, carbon monoxide, carbon dioxide, and hydrogen volume percentages are 2.15%, 2.05%, 2.10%, and 93.7%, respectively. Anhydrous glycerol, or 1,2,3-propanetriol (99.9%), sodium hydroxide pellets (98.7%), 2-propanol (99.9%), lactic acid (88.9%), and water (99.99%) are produced by J.T. Baker. Potassium hydroxide pellets (85%), 1-propanol (98%), and sodium stearate (99%) are manufactured by Sigma-Aldrich, Inc. Sodium chloride (96%) and 1-butanol (99.56%) are produced by Mallinckrodt, Inc. Propylene glycol (99.5%) is produced by Jade Scientific, Inc. Ethylene glycol (99.0%) is produced by Spectrum, Inc. Finally, anhydrous ethanol and sulfuric acid (98%) are produced by Pharmco-Aaper, Inc. and Columbus Chemical Industries, Inc., respectively.

2.2. Catalysts and Characterization

All catalysts used in our research were prepared by vendors or our collaborators at Pacific Northwest National Laboratory (PNNL) and consist of active metals such as ruthenium, nickel, and rhenium loaded onto active carbon. Proprietary catalysts prepared by PNNL were provided

with a wide variety of active metal combinations. The catalyst used for the lactic acid hydrogenolysis study is a 5 wt% ruthenium on coal-based activated carbon (-15+30 mesh, Calgon Carbon Corp). Inert glass beads (150 to 220 μm) were purchased from Sigma-Aldrich Co. Catalysts used in glycerol hydrogenolysis were characterized and are listed in Table 2-1.

Table 2-1. Catalyst characterization summaries

Description(Unit)	Re/Ni/C	59260-33E	58969-10-1-R	58959-10-1
B.E.T. Area (m^2/g catalyst)	1500±35	840±20	790±15	745±15
Quantity H_2 adsorbed (μmol/g catalyst)	18.42	2.04	26.31	62.39
Metal Dispersion (%)	5.60	0.07	0.63	9.18
Metallic Surface Area (m^2/ g catalyst)	1.23	0.02	0.31	4.47

All the physisorption analyses used nitrogen, and chemisorption experiments were done with hydrogen. Catalyst characterization was done with a Micromeritics 2010 Accelerated Surface And Porosimetry (ASAP) Analyzer, and catalyst porosimetry test was done with an Micromeritics AutoPore IV 9500.

2.3. Apparatus and Operations

2.3.1. Batch Reactors and Operations

Two types of batch reactors were used in our research: 1) a Parr 4560 mini reactor (300 ml capacity) with a Parr 3960 M process controller, and 2) a Parr 5000 multiple reactor system (6

× 75 ml capacity) with a Parr 4871 process controller. Figure 2-1 shows the configuration of a 300 ml batch reactor.

Catalyst was ground to fine powder and loaded into a 300 ml or 75 ml autoclave and reduced at 280°C in the hydrogen atmosphere at 500 psi overnight. The magnetic stirrer operated at 1000 rpm to reduce the heat transfer resistance. The reactor was cooled to room temperature, and the feedstock was transferred into the autoclave. After being purged several times, the batch reactor was heated to the temperature set point (180~230°C) and pressurized to the reaction pressure (1000~1500 psi), and the reaction was started. Agitation speed was maintained at 1000 rpm for all the batch runs to ensure catalyst suspension in the reacting fluid and to minimize gas-liquid mass transport resistance.

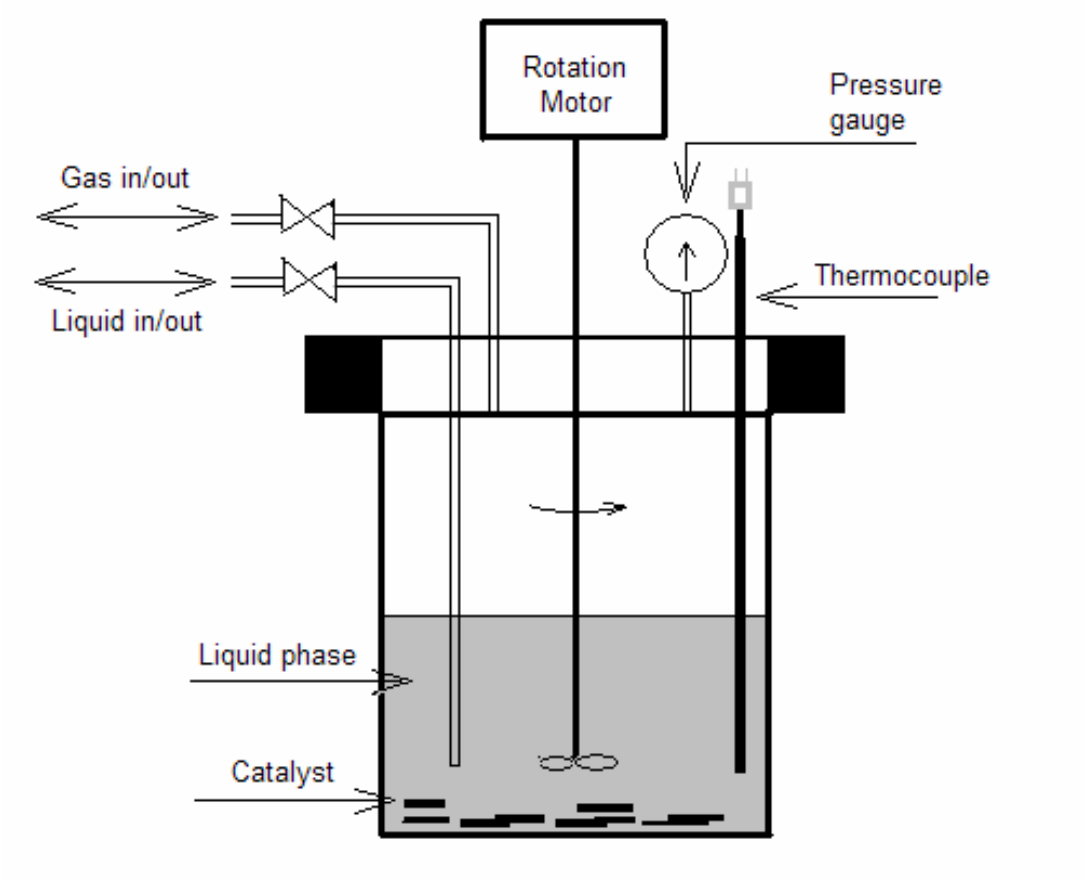

Figure 2-1. Schematic configuration of a batch reactor (Parr 300ml).

2.3.2. Trickle Bed Reactors and Operations

Unlike the experiments performed in the batch reactors where the reactor design and geometry played a less important role in determining mass transfer limits, the trickle bed reactor and catalyst bed configuration influences, if not heavily, reaction kinetics. Therefore, a catalyst bed was built to utilize the specific configuration of the trickle bed reactor constructed in the Miller-Jackson group. The trickle bed reactor consists of a 316 stainless steel tube of 2.5 cm outer diameter and 1.3 cm inner diameter with a length of 22 cm (45 cm^3) catalyst bed. The entire tube length is 71 cm. Top layer of stainless steel balls takes up 0.15 m, and bottom layer of glass beads uses 0.24 m. Stainless steel balls (2 mm diameter) were used to facilitate heat transfer and even liquid feedstock distribution, and glass beads (2 mm diameter) were situated to support the catalyst bed at the elevated pressure. The reactor features an oil jacket to control temperature and an internal thermowell to accommodate thermocouple. A Chromel- Alumel thermocouple (Omega KQXL-116U-24, ungrounded junction, and 1.5 mm × 60 cm in length) was used to measure temperature profile. Reactor temperature was maintained by a Julabo SE-6 recirculating oil bath that circulates silicon oil through the reactor jacket. The schematic configuration of the trickle bed reactor is shown in Figure 2-2. In the reactor, pressure was maintained constant (8.3 MPa in most runs) via a back pressure regulator, and hydrogen flow rate was monitored by a Porter mass flow controller. Hydrogen was saturated with water in the saturation tank (2 × 300 ml, Whitney 304L) at the reaction temperature before it entered the top of trickle bed. Liquid feed solution was fed to the reactor through a Bio-Rad HPLC pump. Accessories used along with the trickle bed reactor include a stainless steel feedstock charger, funnels, filters, magnetic stirrers, graduated glass cylinders, stainless steel screens, and an A&D electronic balance.

For the glycerol hydrogenolysis experiments, the amount of catalyst in the trickle bed reactor was calculated to achieve the same retention time for liquid feedstock as in the trickle bed reactor of our collaborator PNNL. The catalysts prepared by PNNL needed to be preliminarily reduced and passivated. The catalyst was heated at 1.5°C/min to 290°C with a combination of 15/85 (V/V) hydrogen/nitrogen flowing through the trickle bed within a range of 100 to 200 standard cubic centimeters per minute (sccm) at 200 psi. After 290°C was reached and catalyst bed was held there for 3 hours, the flow was switched to 100% hydrogen. Passivation followed by flowing 5 vol% oxygen in helium to cool the trickle bed reactor to room temperature. The procedure was repeated for the whole batch of catalyst to make it ready for the secondary reduction before each experiment.

For the lactic acid hydrogenolysis experiments, the catalyst was packed into the trickle bed reactor between a section of glass beads (below) to support the catalyst particles and a set of stainless steel beads (above) to help preheat the liquid feed prior to contacting the catalyst. Following the initial packing of a catalyst into the trickle bed, the catalyst was reduced by heating the trickle bed from room temperature at 1.5°C /min to 290°C and kept for 3 hours in 100 psi hydrogen atmosphere at 100 sccm flow rate. After reduction, the trickle bed was cooled to reaction temperature with hydrogen still flowing. Once the system pressure and hydrogen flow rate were steady, the liquid feed pump was started, and cocurrent flow of hydrogen and lactic acid solution were delivered to the trickle bed top.

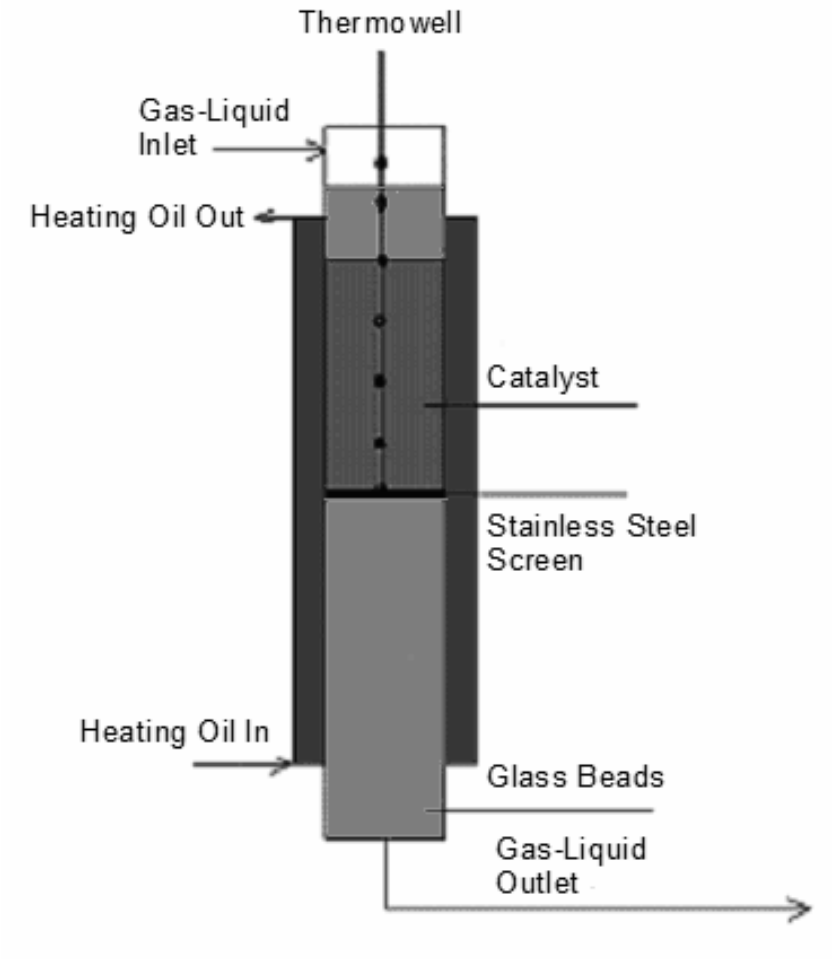

Figure 2-2. Schematic configuration of a trickle bed reactor.

2.4. Sampling and Analysis

Samples were usually taken every hour in the batch reactors during the course of the reactions and analyzed afterwards. Sampling in the trickle bed runs is slightly different: samples were taken every hour by directing the exiting liquid phase from trickle bed reactor to a sampling tank (50 ml, Whitney 304L stainless steel) for five minutes; otherwise, this continuous liquid phase was directed to a collection tank (500 ml, Whitney 304L stainless steel). The complete process and instrument diagram (P&ID) is shown in Figure 2-3. A Varian gas chromatograph (GC, Model 2300) was used to analyze gas samples taken to close the carbon balance. Liquid

phase samples were analyzed with HPLC after being diluted 15-50 times depending on feedstock initial concentration.

Two HPLC's were used for liquid phase samples, and they use different detectors: an LC 90 UV detector and a Waters 410 LC RI detector were used in the first HPLC with a Bio-Rad XP-87H column, and the samples were injected with a Waters 717 auto sampler with a Perkin-Elmer 410 LC pump. The second HPLC used an LDC Analytical RI detector and a Spectra System UV 3000 detector with a Bio-Rad XP-87H column. Species concentrations were determined from the comparison with a multipoint calibration curve using an external standard. A material balance was then conducted by entering species concentrations into an Excel spreadsheet.

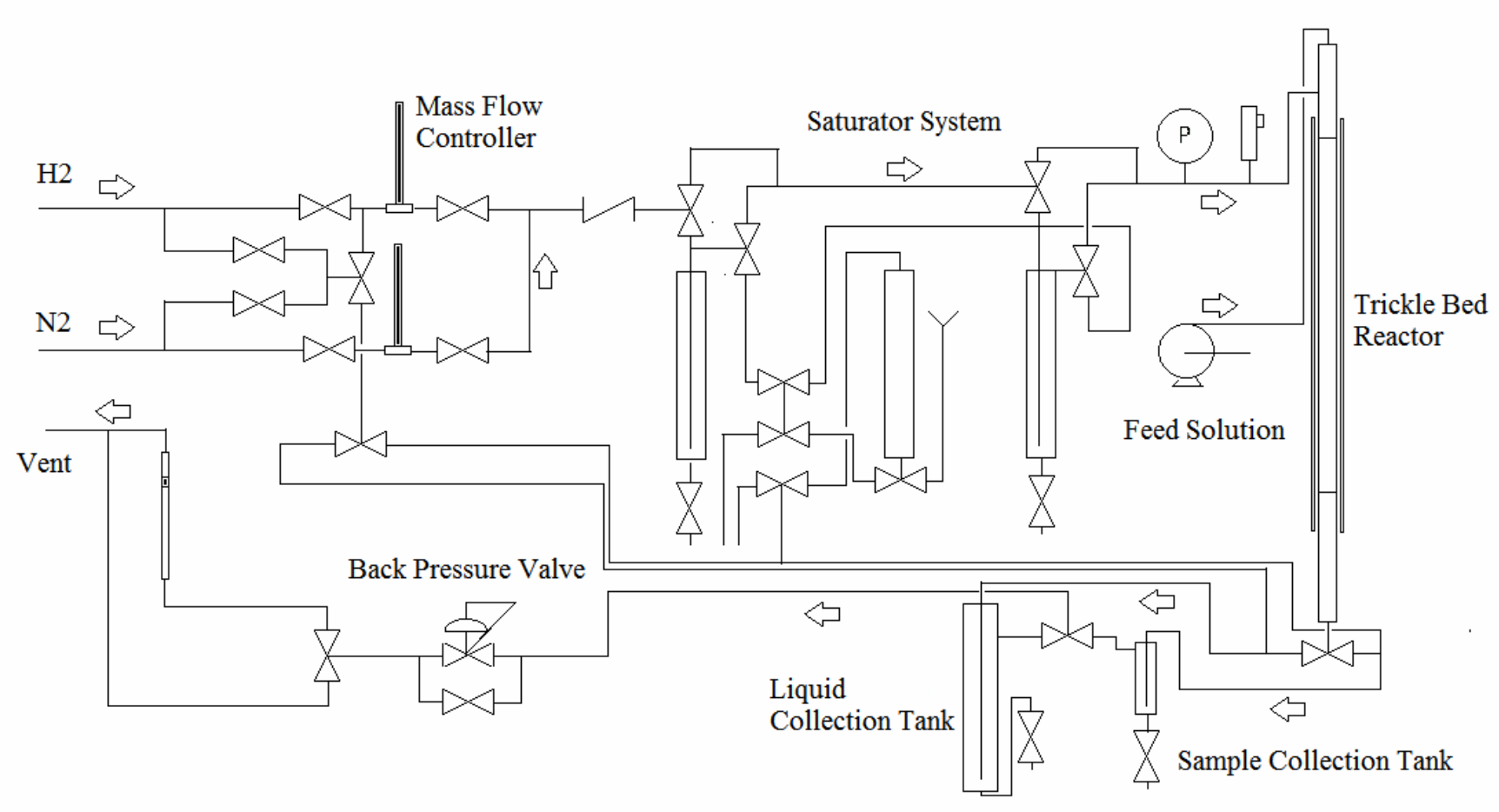

Figure 2-3. Trickle bed reactor entire process schematic.

Part II Experiments and Discussions

Chapter 3 Experiments in the Batch Reactors

This chapter mainly focuses on the experiments with various catalysts and their kinetic performance for a better understanding of the hydrogenolysis mechanism and therefore, optimizing the catalyst performance in the batch reactors.

3.1. Experiments in Batch Reactors

For the experiments carried out in the batch reactors, four catalysts were studied: Re/Ni/C, PNNL-59260-33E, PNNL-58969-10-1-R, and PNNL-58959-10-1. All the catalysts are PNNL's proprietary materials. Reaction conditions, such as temperature and pressure, were changed to investigate their effects on the reaction kinetics and catalyst performance. Different base promoters and solvents were also tested and compared. To bring this study closer to industrial reality, impurities were added to feedstock, and their effects on the system were studied. More details for each subtopic will be discussed. Reaction conditions for the batch reactors are listed in Table 3-1.

Control experiments were conducted with no base present (BAT 3, 1000 psi H_2) and with no hydrogen present (BAT 11, 0.11 M KOH). No glycerol conversion was observed in these experiments. The carbon balance for each reaction is excellent. Given the excellent mass conservation and the fact that reactant solution density does not change much, carbon balance was calculated with compounds' concentrations from HPLC analysis and then compared with the initial glycerol concentration. For instance, in BAT 3

Table 3-1. Batch reaction conditions

Serial No.	Tempera-ture (℃)	Pressure (psi)	Initial Glycerol Concentration (mol/l)	Base	Initial Base concentration (mol/l)	Solvent	Feedstock volume (ml)	Catalyst Weight (g)	Catalyst ID
BAT 3	200	1000	1.0	-	-	water	150	1.5	Re/Ni/C
BAT 4	200	1000	1.0	KOH	1.0	water	150	1.5	Re/Ni/C
BAT 6	200	1000	1.0	KOH	1.0	water	100	0.75	Re/Ni/C
BAT 8	200	1000	1.0	KOH	1.0	water	150	0.75	Re/Ni/C
BAT 9	200	1000	1.0	KOH	0.11	water	100	0.5	Re/Ni/C
BAT 10	200	1000	1.0	KOH	0.11	water	100	0.5	Re/Ni/C
BAT 11	200	225	1.0	KOH	0.11	water	100	0.5	Re/Ni/C
BAT 12	200	1500	1.0	KOH	0.11	water	100	0.5	Re/Ni/C
BAT 13	220	1500	1.0	KOH	0.11	water	100	0.5	Re/Ni/C
BAT 15	200	1000	1.0	KOH	0.11	ethanol	50	0.25	Re/Ni/C
BAT 16	200	1000	1.0	KOH	0.11	n-propanol	50	0.25	Re/Ni/C
BAT 18	200	1000	1.0	KOH	0.11	isopropanol	50	0.25	Re/Ni/C
BAT 19	200	1000	1.0	KOH	0.11	water	50	0.25	Re/Ni/C
BAT 29	200	1000	1.0	KOH	0.11	water	100	0.5	58959-10-1
BAT 30	200	1000	1.0	KOH	0.11	water	100	0.5	58959-10-1
BAT 35	190	1200	4.86	NaOH	0.57	water	100	0.5	58969-10-1-R
BAT 36*	190	1200	4.86	NaOH	0.57	water	100	0.5	58969-10-1-R
BAT 37**	190	1200	4.86	NaOH	0.57	water	100	0.5	58969-10-1-R
BAT 40	190	1200	4.86	NaOH	0.57	water	100	0.5	58959-72-1-R&P
BAT 46	190	1200	4.86	NaOH	0.57	water	100	1.0	59260-33E
BAT 47	175	1200	4.86	NaOH	0.57	water	100	1.0	59260-33E

* 0.5 g Na stearate was added to feedstock to study the impurity's effect on the reaction.
** 0.5 g NaCl was added to feedstock to study the impurity's effect on the reaction.

the initial glycerol concentration was 0.99 M. After one hour, HPLC analysis showed glycerol concentration was 0.98 M and propylene glycol concentration was 0.014 M. Therefore, at 1 hour, reaction carbon balance equals

$$(0.98 + 0.014) / 0.99 \times 100\%$$

that is, 100.40%. In this light, analysis precision and reproducibility must be ensured.

3.2. Result Reproducibility (BAT 9 and BAT 10)

To test system reproducibility and reliability, two experiments, BAT 9 and BAT 10, were done with identical reaction conditions (200°C,1000 psi, 1.0 M glycerol initial concentration, 0.11 M KOH, 0.5g Re/Ni/C, 100 ml feedstock), where no samples were collected before the reactions were finished. Table 3-2 shows the final product concentrations after the 7-hour long reaction. Each sample was analyzed twice to test HPLC reproducibility and reliability.

Table 3-2. Analysis reproducibility

Description	BAT 9			BAT 10		
Compounds	Sample 1	Sample 2	Final Concentration (mol/l)	Sample 1	Sample 2	Final Concentration (mol/l)
Lactic Acid	0.227	0.219	0.223±0.004	0.160	0.159	0.159±0.003
Glycerol	0.0138	0.0130	0.0134 ±0.0004	0.05049	0.05032	0.05041 ±0.00005
Ethylene glycol	0.0540	0.0530	0.0535 ±0.0005	0.0467	0.0478	0.0472 ±0.0005
Propylene glycol	0.426	0.420	0.423±0.003	0.418	0.414	0.416±0.002

Table 3-2 shows the reasonably reliable performances both from the reaction system and from the analysis system. Glycerol concentration disparity shown in both reactions is relatively

large due to high conversion of glycerol and low glycerol concentration at the end of reactions. Also, on the magnitude of 0.01 to 0.05 mol/l, analysis error from HPLC plays a more significant role, which explains the difference of glycerol final concentrations from BAT 9 and BAT 10. Lactic acid concentration from both reactions is also different due to the early stage of the research and experiments.

3.3. Effect of Base Promoter (BAT 3 and BAT 4)

The majority of experiments were done with Re/Ni/C catalyst at the early stages of our research. The first experiments were designed to test if the base promoter's presence was necessary for this hydrogenolysis process because the typical reaction mechanism involves dehydrogenation and rearrangement steps. BAT 3 and BAT 4 results are shown in Figures 3-1 to 3-3.

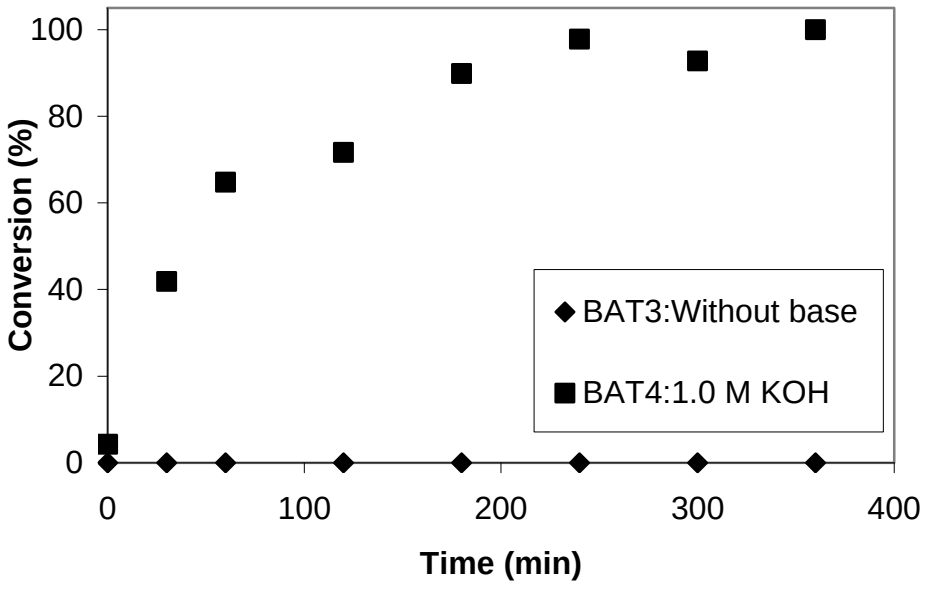

Figure 3-1. Effect of base promoter on glycerol conversion (200°C, 1000 psi, initial glycerol concentration:1.0M, 1.5g Re/Ni/C catalyst, 150 ml feedstock).

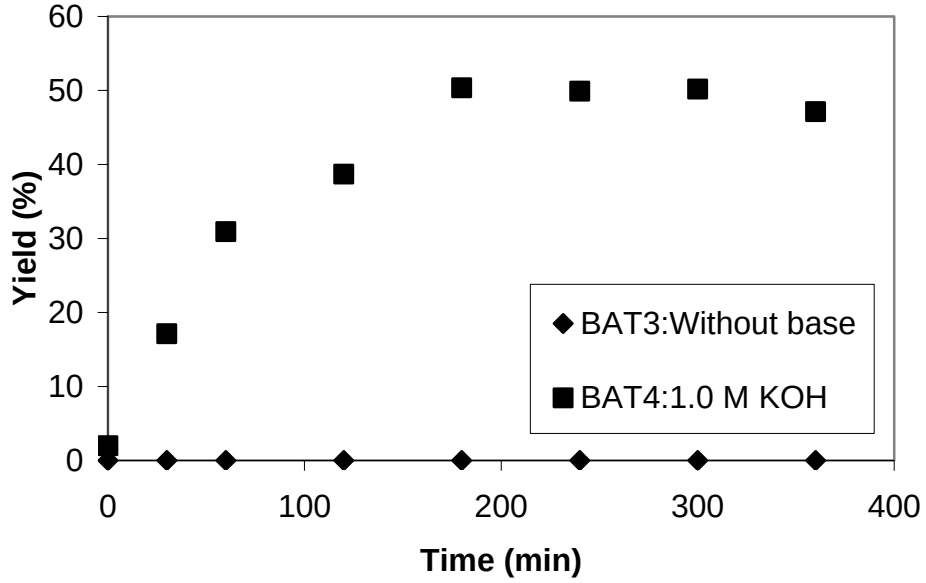

Figure 3-2. Effect of base promoter on propylene glycol yield (200°C, 1000 psi, initial glycerol concentration: 1.0 M, 1.5 g Re/Ni/C catalyst, 150 ml feedstock).

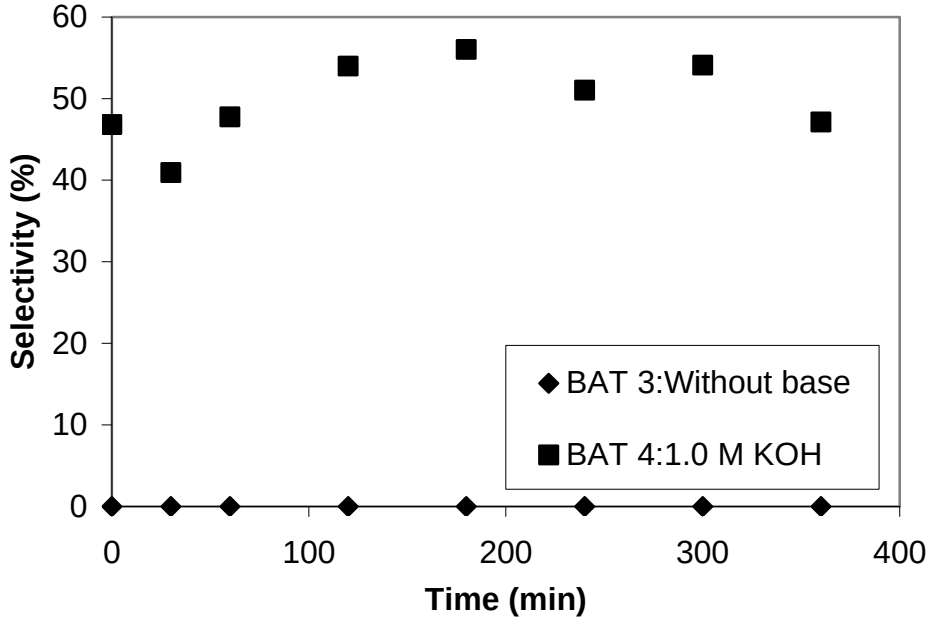

Figure 3-3. Selectivity toward propylene glycol versus time with and without base (200°C, 1000 psi, initial glycerol concentration: 1.0 M, 1.5 g Re/Ni/C catalyst, 150 ml feedstock).

From these figures, no glycerol was converted in BAT 3 (no base) versus ready conversion in BAT 4 with KOH in the feedstock. At the early stages of this study, KOH was applied mainly at 0.11M concentration in order to be comparable with our project collaborator, PNNL; later, NaOH was used for the same reason.

3.4. Effect of Catalyst Loading (BAT 4, BAT6, and BAT 8)

The amount of catalyst used in experiments decides the amount of active surface where reactions take place. Therefore, catalyst loading was changed in BAT 4, BAT 6, and BAT 8 to investigate how loading affects reaction rate.

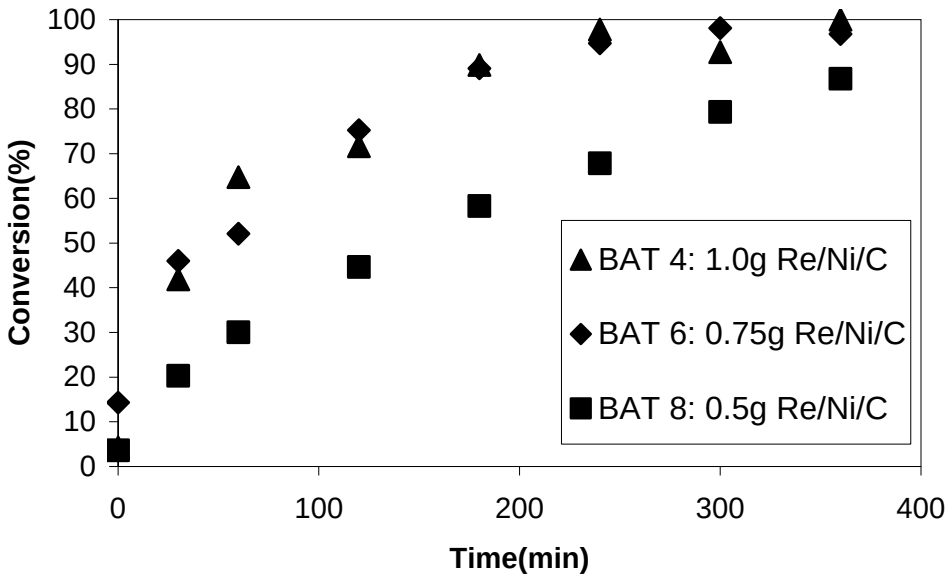

Figure 3-4. Effect of catalyst loading on glycerol conversion (200°C, 1000 psi, 1.0 M glycerol initial concentration, 1.0 M KOH, and designated catalyst loading per 100 ml feedstock for each reaction).

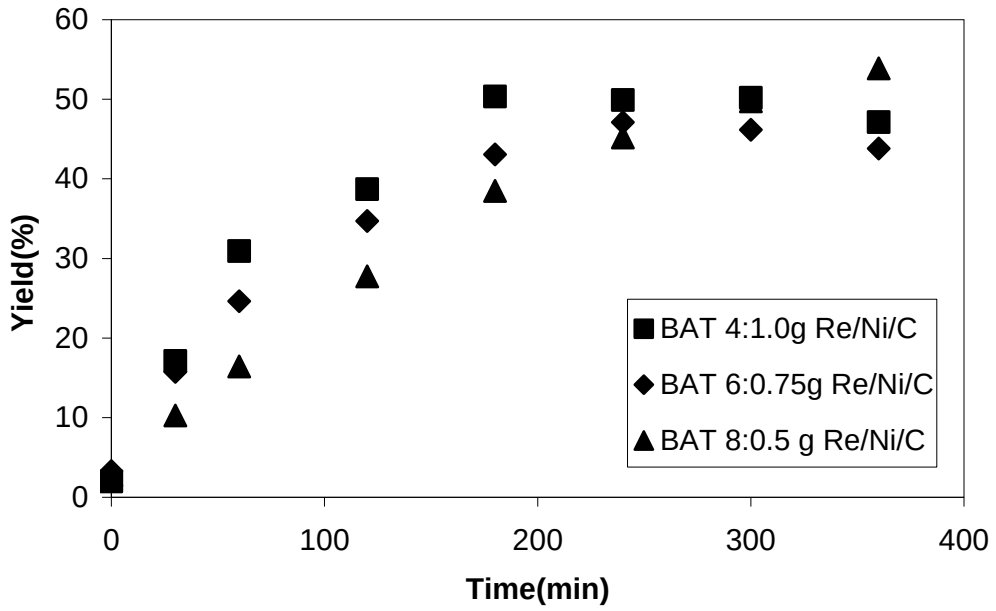

Figure 3-5. Effect of catalyst loading on propylene glycol yield (200°C, 1000 psi, 1.0 M glycerol initial concentration, 1.0 M KOH, and designated catalyst loading per 100 ml feedstock for each reaction).

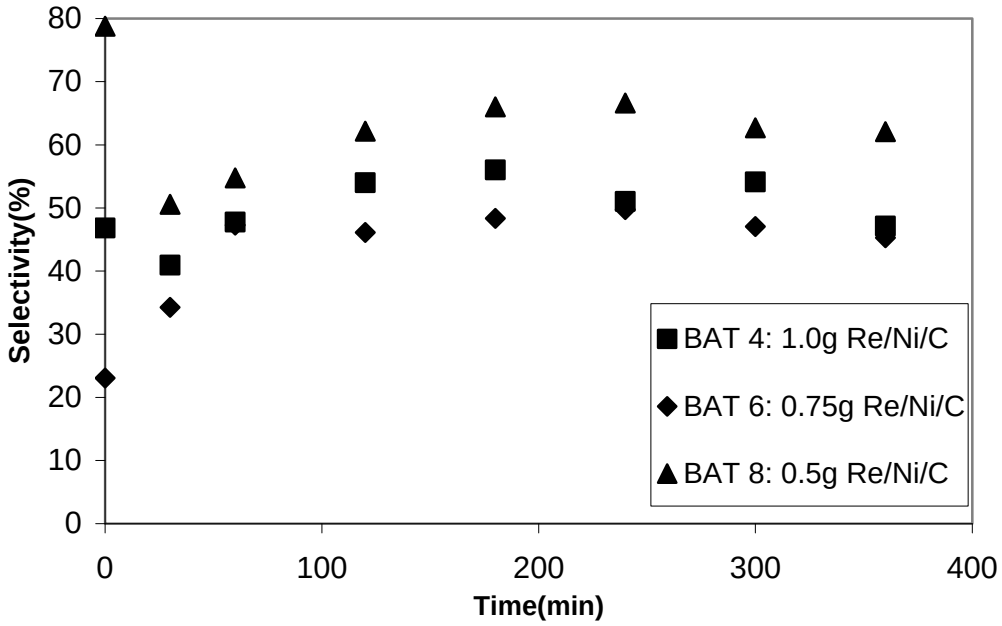

Figure 3-6. Effect of catalyst loading on selectivity toward propylene glycol (200°C, 1000 psi, 1.0 M glycerol initial concentration, 1.0 M KOH, and designated catalyst loading per 100 ml feedstock for each reaction).

At higher catalyst loading such as in BAT 4 and BAT 6, glycerol conversion was higher, and so was propylene glycol yield. Since propylene glycol yield difference was more pronounced relative to glycerol conversion, selectivity toward propylene glycol was lower at the higher catalyst loading. Given that our research focused mainly on boosting reaction selectivity, a lower catalyst loading was adopted. In the subsequent batch reaction studies, catalyst loading was always 0.5 grams per 100 ml feedstock. To better understand the kinetic effect of catalyst loading, reaction rate was calculated for three reactions as following:

Microsoft Excel was used to fit a trend line for all glycerol concentration data derived from HPLC analysis. Linear or exponential correlations usually work well in our study. Differentiation of this trend line at time equals zero allowed initial reaction rates to be calculated. Finally, the units of reaction rate were converted from mol/l/hr to mol/hr/g catalyst. Since data from three experiments are scattered, uncertainty will arise when initial reaction rate is calculated with data points at the early stage of reaction. Several fitting options were tried, and results are listed in Table 3-3. Initial reaction rate is relatively close for all three loadings.

Table 3-3. Initial reaction rates with various catalyst loadings

Run	Catalyst loading per 100 ml solution (g)	Low initial rate (mol/g cata./hr)	High initial rate (mol/g cata./hr)
BAT 4	1.0	0.0228	0.0660
BAT 6	0.75	0.0256	0.0760
BAT 8	0.5	0.0276	0.0514

3.5. Mass Transfer Analysis

As a matter of fact, BAT 6 boasts one of the highest glycerol conversions of all the batch reactions, and therefore mass transfer analysis was done for glycerol and hydrogen in this experiment to determine if internal diffusion limits reaction rate. The Weisz-Prater modulus was calculated for both species with the following formula:

$$C_{WP} = \frac{-r'_A(obs)\rho_c R^2}{D_e C_{As}} \qquad (3\text{-}1)$$

where $r'_A(obs)$ stands for observed actual reaction rate, ρ_c for catalyst dry density, R for catalyst particle radius, D_e for diffusivity, and C_{AS} for the reactant concentration on the catalyst particle external surface. A spreadsheet was created according to this formula and the computation shows the Weisz-Prater modulus for glycerol and hydrogen is significantly less than one, which means that the reaction is not mass transfer limited. Calculation results are listed in Table 3-4.

Table 3-4. Weisz-Prater calculation results

Compound	C_{WP}
Glycerol	4.7E-2
Hydrogen	1.8E-4

3.6. Effect of Reaction Temperature (BAT 12 and BAT 13)

BAT 12 (200°C, 1500 psi, 0.11M KOH, 0.5 g Re/Ni/C, 100 ml feedstock, and 1.0 M initial glycerol solution) and BAT 13 (220°C, 1500 psi, 0.11M KOH, 0.5 g Re/Ni/C, 100 ml feedstock, and 1.0 M initial glycerol solution) were done to test the effect of reaction temperature

and to estimate the activation energy, E_a. No samples were taken until the reactions ended after 6 hours. Table 3-5 shows the initial and final glycerol concentration for both reactions.

Table 3-5. BAT 12 and BAT 13 glycerol concentrations

Description	BAT 12	BAT 13
Temperature (°C)	200	220
Glycerol Initial Concentration(mol/l)	0.958	0.938
Glycerol final Concentration (mol/l)	0.837	0.755
Average Glycerol Reaction Rate(mol/l/hr)	0.0201	0.0304
Activation Energy (kJ/kmol)	39,827	

3.7. Effect of Different Solvents

After the above exploration of the reaction system, several experiments were conducted to investigate the effect of solvents other than water on catalyst performance. Results of these solvent experiments are given in Figures 3-7 to 3-9.

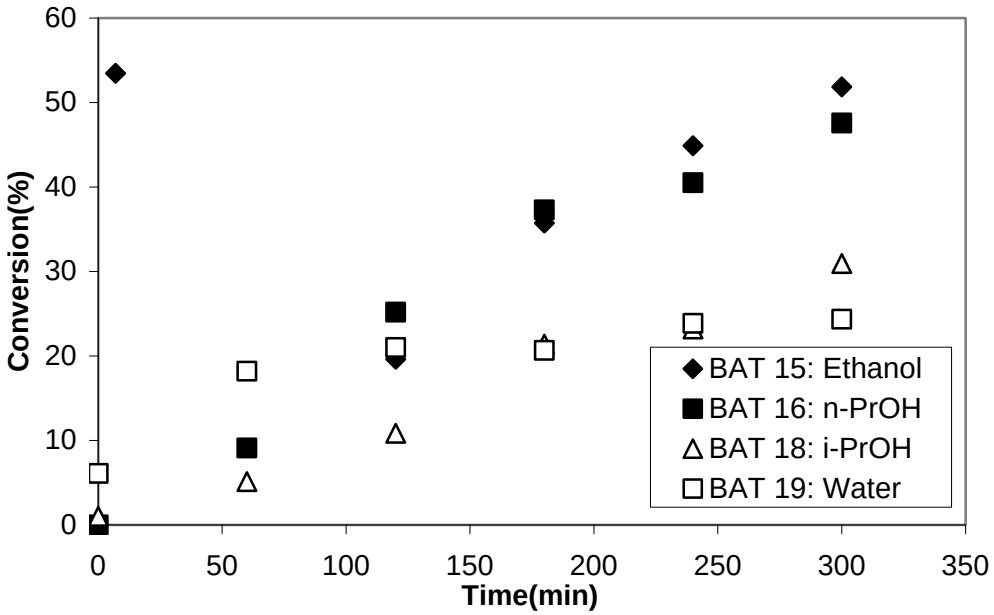

Figure 3-7. Effect of solvents on glycerol conversion (200°C, 1000 psi, 1.0 M glycerol initial concentration, 0.11M KOH, 0.25 g Re/Ni/C, 50 ml feedstock).

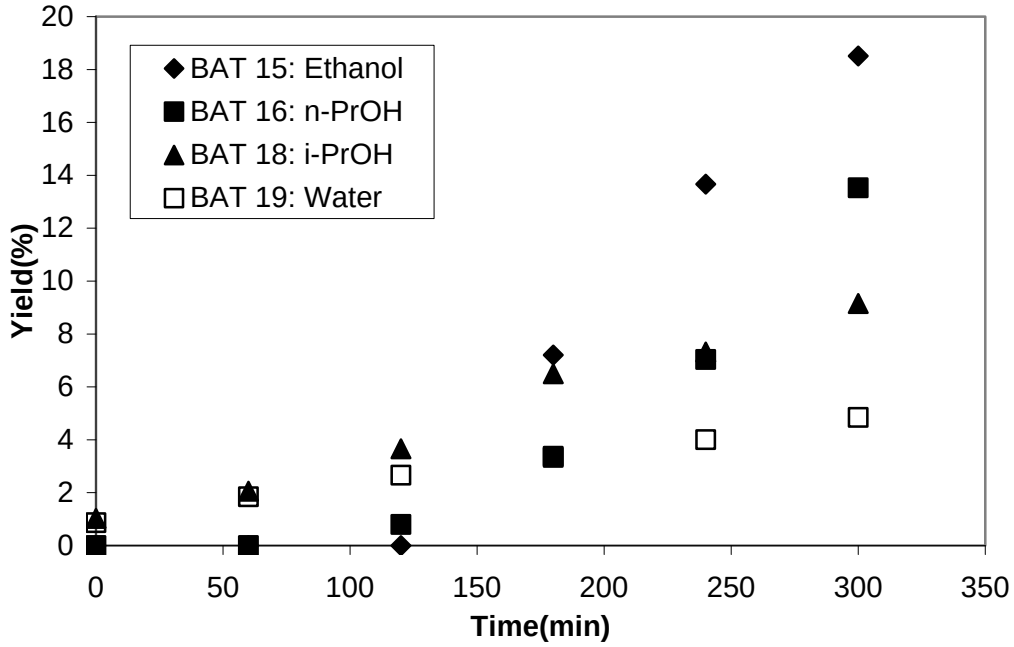

Figure 3-8. Effect of solvents on propylene glycol yield (200°C, 1000 psi, 1.0 M glycerol initial concentration, 0.11M KOH, 0.25 g Re/Ni/C, 50 ml feedstock).

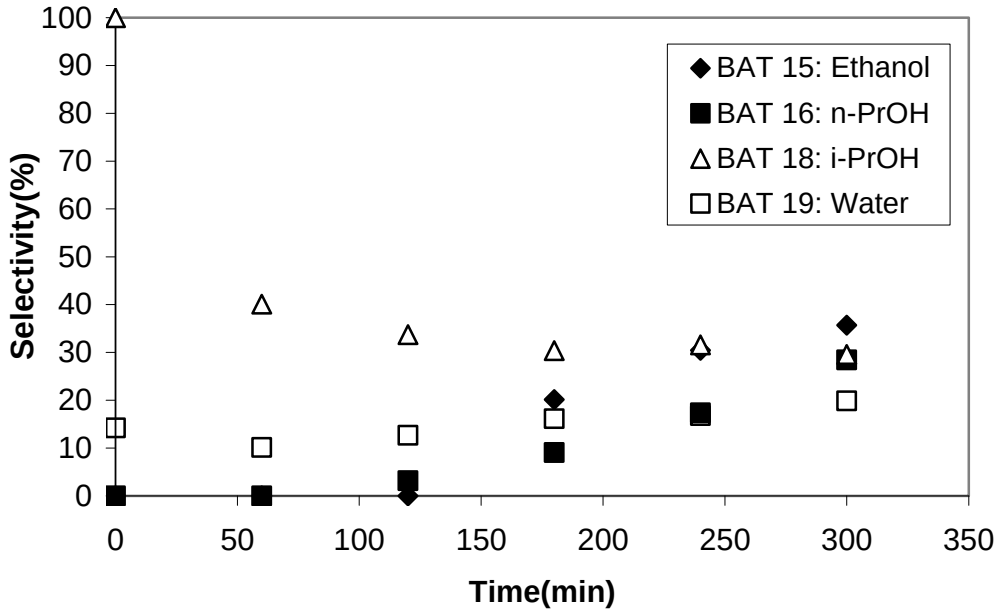

Figure 3-9. Effect of solvents on propylene glycol selectivity (200°C, 1000 psi, 1.0 M glycerol initial concentration, 0.11M KOH, 0.25 g Re/Ni/C, 50 ml feedstock).

As the figures show, organic solvents boost glycerol conversion, propylene glycol yield, and selectivity towards propylene glycol relative to water. Reaction rates were calculated for each reaction, and results are listed in Table 3-6 along with hydrogen solubility at 25°C and 1000 psi.[40]

Table 3-6. Initial reaction rates with different solvents

Solvent	Ethanol	1-Propanol	2-Propanol	Water
Initial rate (mol/g. cata/hr)	0.0237	0.0183	0.0036	0.0069
Solubility (ml STP/g solvent)	5.88	N/A	4.81	1.22

Neither solvent vapor pressure nor hydrogen solubility exhibits a defining correlation between solvent and reaction kinetics. Group member Dr. Simona Marincean did a similar series of experiments, and also could not correlate solvent properties with kinetics.

3.8. Effect of Impurities in Feedstock

In addition to different solvents used in our research, impurities arising as byproducts of industrial biodiesel production were studied as well. Sodium salts are the typical impurities in the industrial feedstock, and our research tested two: sodium chloride and sodium stearate. The results are shown in Figures 3-10 to 3-12.

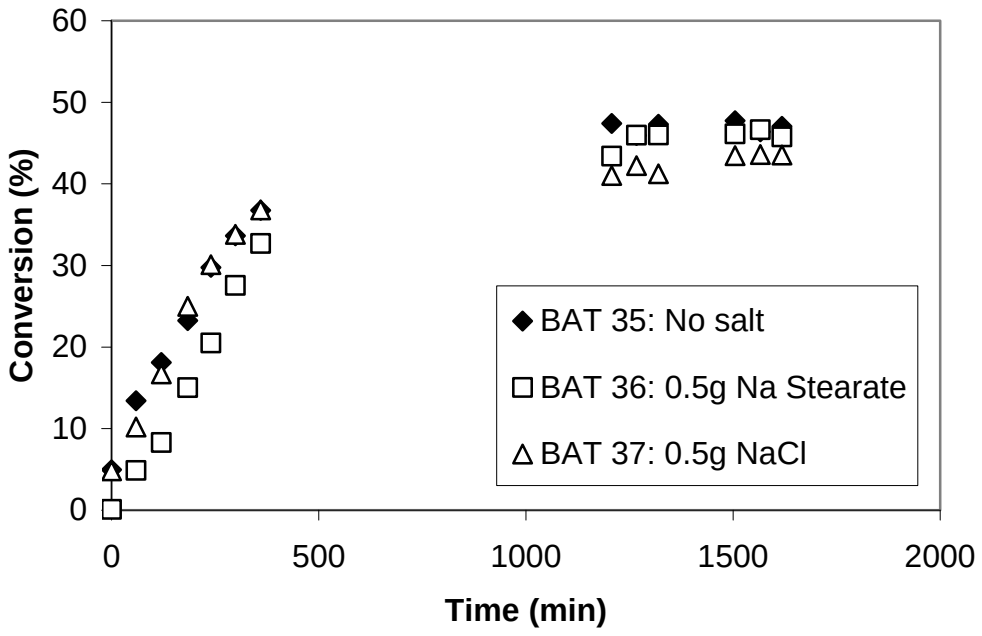

Figure 3-10. Effect of feedstock impurities on glycerol conversion (190°C, 1200 psi, 40 wt% glycerol solution, 2 wt% NaOH, 0.5 g PNNL-58969-10-1-R, 100 ml feedstock).

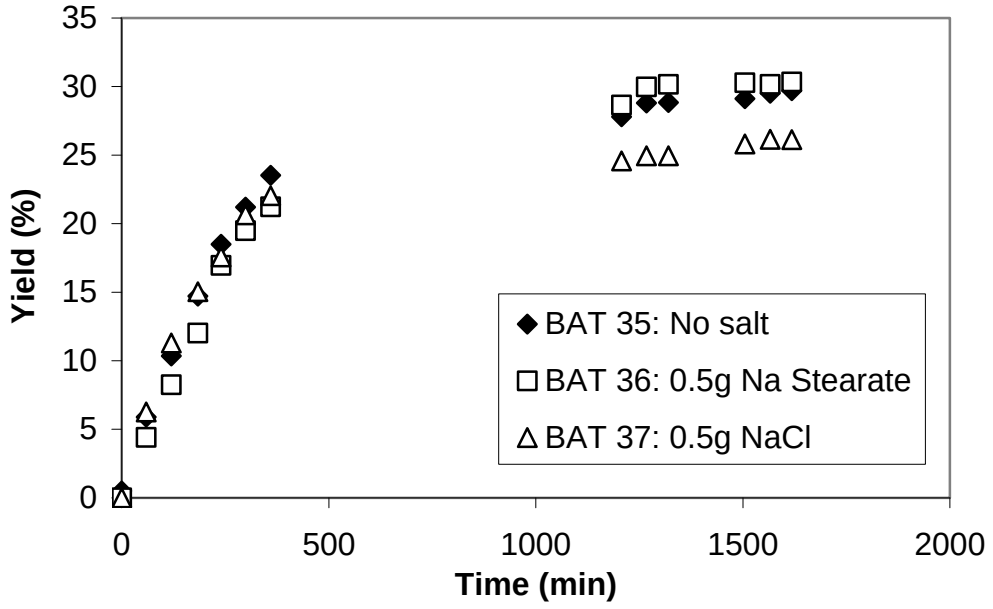

Figure 3-11. Effect of feedstock impurities on propylene glycol yield (190°C, 1200 psi, 40 wt% glycerol solution, 2 wt% NaOH, 0.5 g PNNL-58969-10-1-R, 100 ml feedstock).

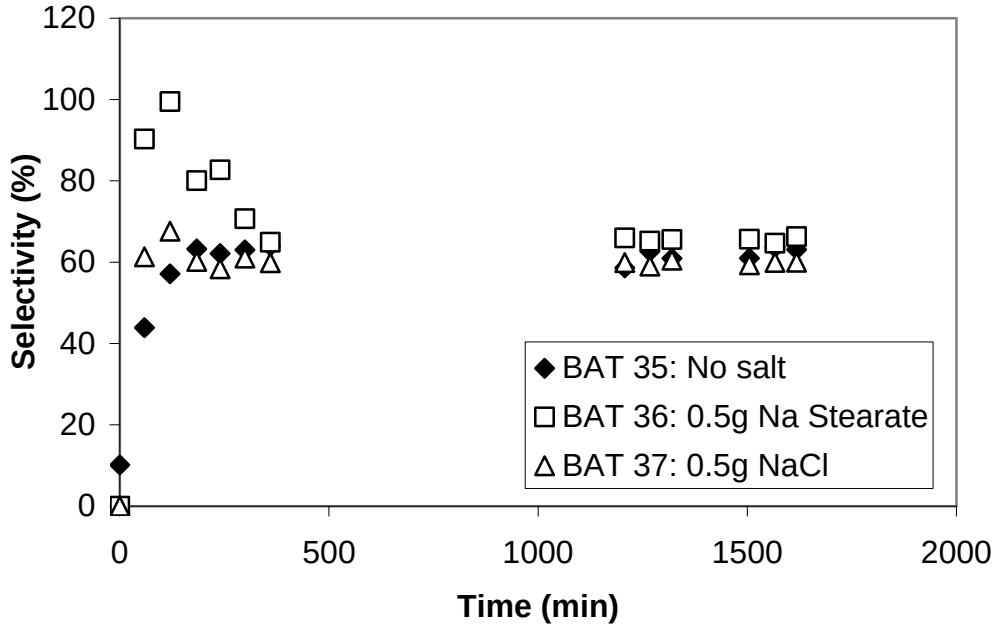

Figure 3-12. Effect of feedstock impurities on selectivity toward propylene glycol (190°C, 1200 psi, 40 wt% glycerol solution, 2 wt% NaOH, 0.5 g PNNL-58969-10-1-R, 100 ml feedstock).

The three experiments show similar conversion, yield, and selectivity, despite the addition of the impurities NaCl and Na stearate. These salts are usually present in the feedstock during industrial production and possibly poison the catalyst. BAT 35 through BAT 37 show the presence of impurities does not impose a serious danger to the catalyst and reaction.

3.9. Catalyst Specific Kinetic Study

The third catalyst tested in the batch reactor was PNNL-59260-33E. This catalyst was also the first catalyst studied in the trickle bed reactor. In order to get the information about reaction activation energy and preexponential factor in the Arrhenius equation, reactions were done at three different temperatures: 160°C, 175°C, and 190°C at the pressure of 1200 psi in a 40 wt% glycerol and 2.1 wt% NaOH solution. No reaction was detected with HPLC for BAT 48, which was carried out at 160°C. Figures 3-13 and 3-14 show glycerol conversion and propylene glycol yield versus time. Glycerol conversion is very low due to the low activity of 59260-33E catalyst. At this narrow and small range of glycerol concentration, conversion is also quite scattered between 1% and 6%, which produces fluctuation for the selectivity toward propylene glycol. The overall carbon balance, however, is good.

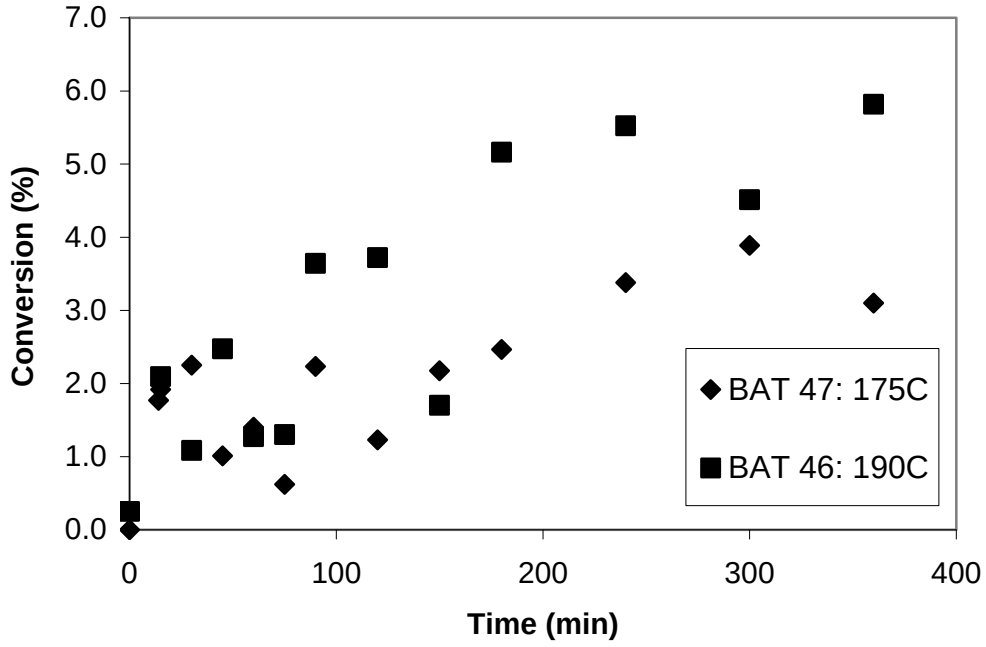

Figure 3-13. Glycerol conversions with catalyst 59260-33E at different temperatures.

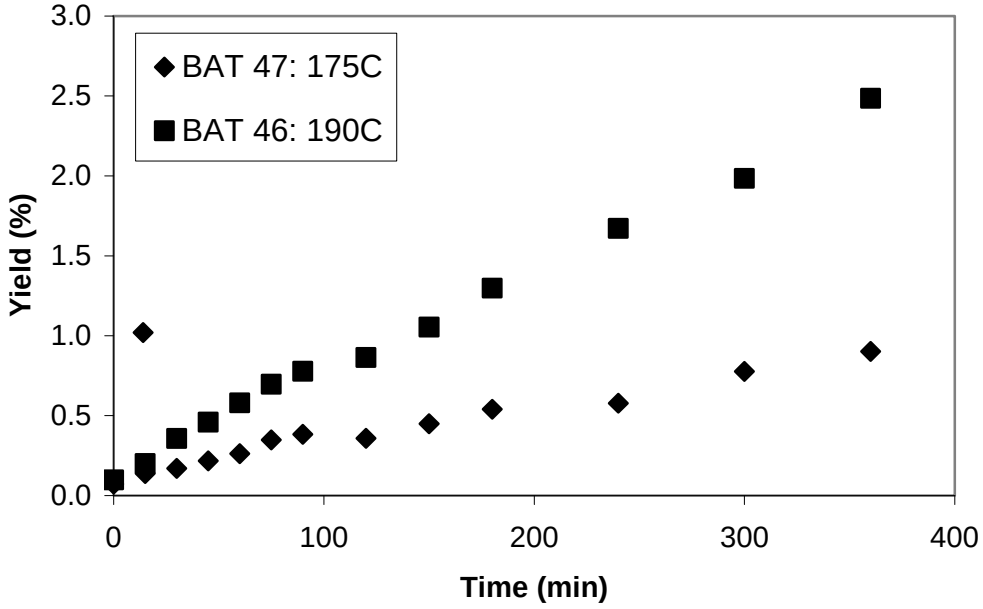

Figure 3-14. Propylene glycol yield versus time at different temperatures.

From Figure 3-14, reaction activation energy can be calculated based on propylene glycol concentration relative to time. This value is 99,064 kJ/kmol. Reaction rates were calculated for these two catalysts and listed in Table 3-7.

Table 3-7. Reaction rates of different catalysts

Catalyst	58969-10-1-R	59260-33E
Reaction rate(mol/ m^2 metallic surface area/hr)	0.2103	0.2915

Both PNNL catalysts give an excellent carbon balance, and PNNL-58969-10-1-R used in BAT 35 shows better conversion and yield. This difference is due to the metal constituents' molar ratio in the catalysts. This information is crucial, as feedback, to optimize catalyst preparation and process design in the future.

Chapter 4 Experiments in Continuous Trickle Bed Reactor

The trickle bed reactor is one of the most commonly used reactors for hydrogenolysis on the manufacturing scale. In order to scale up catalysts and processes, a pilot scale trickle bed reactor was built in our research facilities, and catalysts were packed and tested to study the effects of conditions and hydrodynamics on glycerol hydrogenolysis rate. Three catalysts were tested in the trickle bed reactor: reaction conditions are summarized in Table 4-2 on following page.

4.1. Reaction Mass Conservation

Liquid feedstock flow rate was controlled by a HPLC pump and could be varied, based on the experiment conditions desired. Gas flow rate was monitored by an electronic mass flow controller and was also variable. During start up and between sample collections, reactor effluent was collected to purge the product collection system. At steady state, samples were collected every 30 to 60 minutes and analyzed via HPLC using an external standard method. Before each sample, effluent was collected in a sample vial for four minutes to purge the sample tank. Then the sample was collected in the sample tank for five minutes before being transferred to the vial. All the samples were diluted with the mobile phase before HPLC analysis. After the sample collection was complete, the continuous liquid phase product was again directed to a collection tank. At the end of the experiment, the weights of the collection tank, purge effluent, and samples were measured, recorded, and compared with the actual quantity of feed solution consumed. Table 4-1 shows that the overall mass conservation during reaction was good. Water (150 g) was loaded into the hydrogen saturation tank each time before reaction and was

recovered and its mass measured at the end of the experiment (Table 4-1, water recovered). Table 4-1 shows that water loss was within a very reasonable scope of acceptance, and its influence on the sample concentration was negligible.

Table 4-1. Mass balance of TBR 7, TBR 8, and TBR 9

Exp. S/N	Collection tank recovery (g)	Mass of Samples (g)	Mass of sample purge (g)	Total recovery (g)	Feed Consumption (g)	Water Recovered (g)
TBR 7	307.8	57.3	18.6	383.7	382.7	142.0
TBR 8	441.7	52.9	20.7	515.3	546.8	134.3
TBR 9	465.5	52.3	24.5	542.3	529.2	142.3

Table 4-2. Trickle bed reaction conditions

Experiment Serial No.	Temperature (℃)	Pressure (psi)	Initial Glycerol Concentration (mol/l)	Base	Initial Base concentration (mol/l)	Solvent	Feedstock flow rate (ml/hr)	Catalyst volume (cm^3)	Catalyst ID
TBR 7	230	1100	1.0	NaOH	0.25	water	50	30	58959-72-1
TBR 8	190	1100	1.0	NaOH	0.25	water	50	30	58959-72-1
TBR 9	210	1100	1.0	NaOH	0.25	water	50	30	58959-72-1
TBR 10	230	1100	1.0	NaOH	0.25	water	25	30	58959-72-1
TBR 11	230	1100	1.0	NaOH	0.25	water	75	30	58959-72-1
TBR 12	230	1100	1.0	NaOH	0.25	water	100	30	58959-72-1
TBR 15	190	1200	1.0	NaOH	0.25	water	25	45	59260-33E
TBR 17	190	1200	1.0	NaOH	0.25	water	50	45	59260-33E
TBR 18	190	1200	1.0	NaOH	0.25	water	100	45	59260-33E
TBR 19	190	1200	1.0	NaOH	0.25	water	200	45	59260-33E
TBR 20 *	190	1200	0	NaOH	0.25	water	50	45	59260-33E
TBR 21	195	1200	4.86	NaOH	0.285	water	37.5	45	59260-51-65
TBR 22	195	1200	4.86	NaOH	0.285	water	52.5	45	59260-51-65
TBR 23	195	1200	4.86	NaOH	0.285	water	75	45	59260-51-65
TBR 24	195	1200	4.86	NaOH	0.285	water	100	45	59260-51-65
TBR 25	195	1200	4.86	NaOH	0.285	water	200	45	59260-51-65
TBR 26	180	1200	4.86	NaOH	0.285	water	37.5	45	59260-51-65
TBR 27	180	1200	4.86	NaOH	0.285	water	52.5	45	59260-51-65
TBR 28	180	1200	4.86	NaOH	0.285	water	75	45	59260-51-65
TBR 29	180	1200	4.86	NaOH	0.285	water	100	45	59260-51-65
TBR 30	180	1200	4.86	NaOH	0.285	water	200	45	59260-51-65

* Propylene glycol was added to replace glycerol in the feedstock to investigate if propylene glycol degrades during the reaction.
** Propylene glycol concentration was 1.0 mol/l.

4.2. Catalyst Specific Kinetic Study

4.2.1. PNNL 58959-72-1 Catalyst

For catalyst PNNL-58959-72-1, reaction temperature and liquid feedstock pumping rate were varied to test their effects on the reaction system. TBR 7 and TBR 9 were done at 230°C and 210°C, respectively, with the same pressure (1100 psi), pumping rate (50 ml/hr), feedstock (1.0 M glycerol and 0.25M NaOH), and molar ratio (hydrogen: glycerol = 5:1). Figures 4-1 through 4-3 show the glycerol conversion, propylene glycol yield, and selectivity toward propylene glycol versus time during the course of the reactions.

Higher temperature boosts glycerol conversion and propylene glycol yield. Selectivity toward propylene glycol is modestly higher at 230°C in TBR 7. Also, Figure 4-4 gives the carbon balance during reaction; experiments always reclaim more than 90% of the carbon from the reaction system at steady state. Based on the steady state conversion, average reaction rate in the trickle bed for both temperatures could be calculated, and the results are listed in Table 4-3.

Table 4-3. Glycerol consumption rate in TBR 7 and TBR 9

Run	Temperature (°C)	Reaction rate (mol/hr/g catalyst)
TBR 7	230	5.727E-4
TBR 9	210	3.783E-4

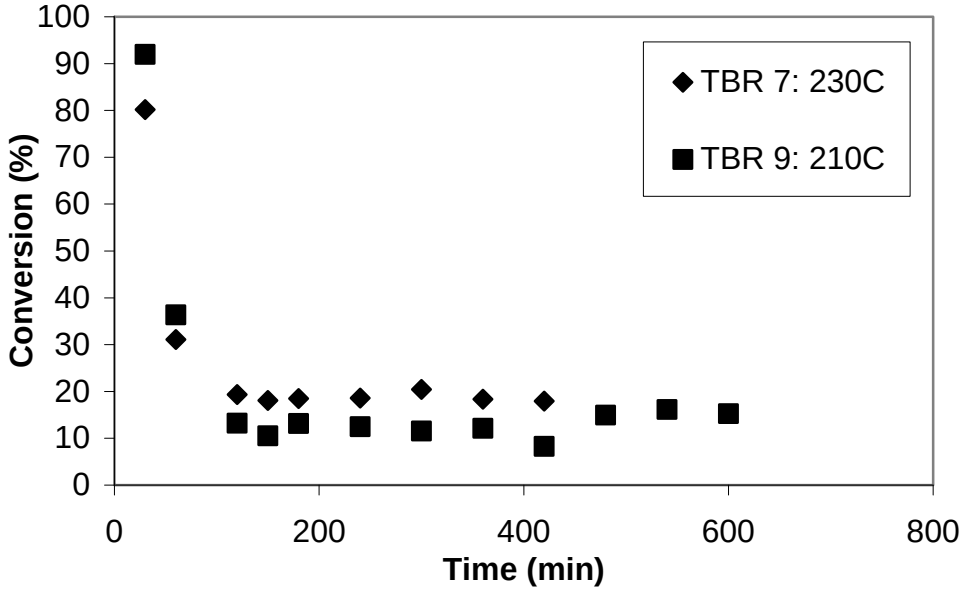

Figure 4-1. Effect of temperature on glycerol conversion in trickle bed reactor.

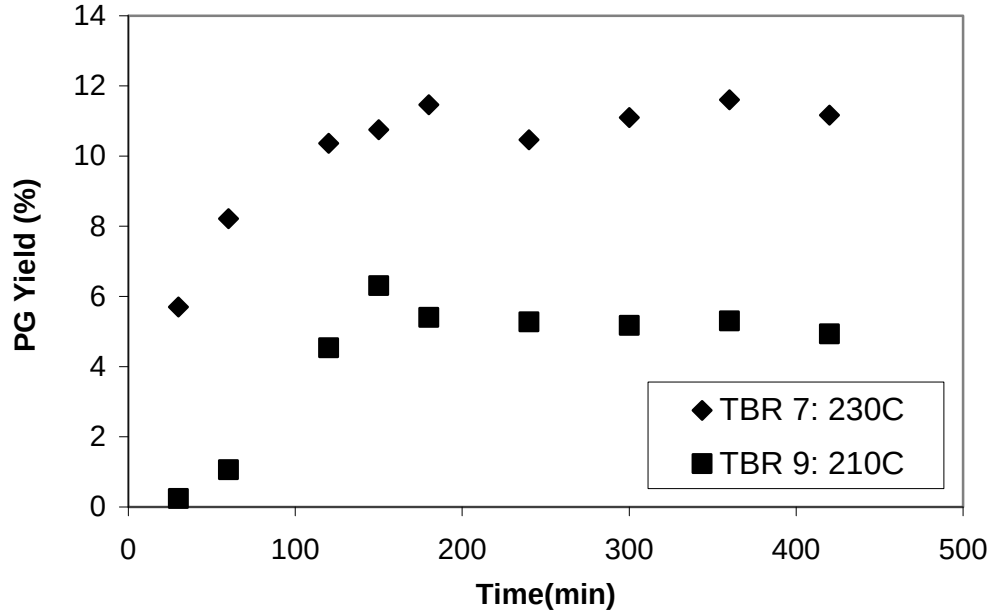

Figure 4-2. Effect of temperature on propylene glycol yield in trickle bed reactor.

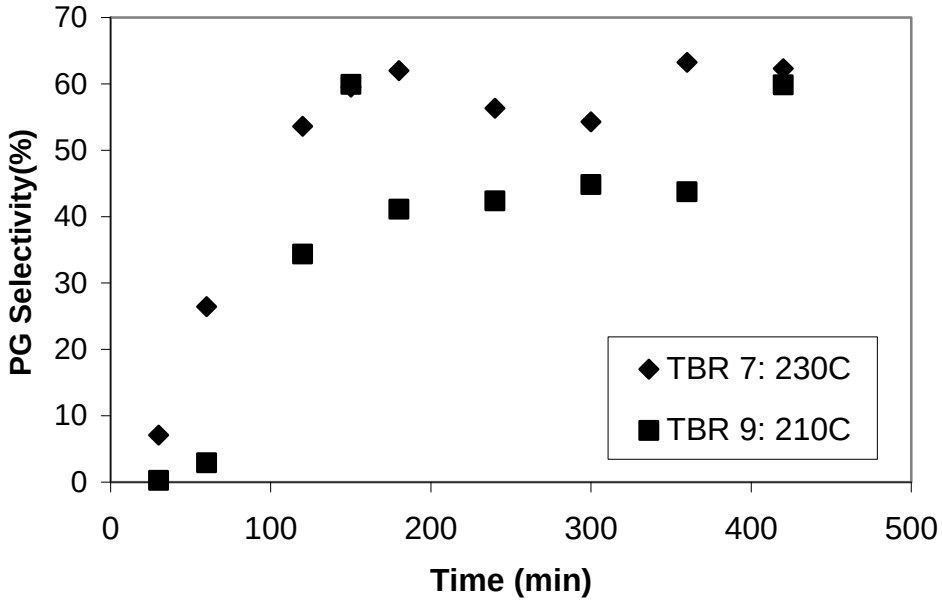

Figure 4-3. Effect of temperature on selectivity toward propylene glycol in trickle bed reactor.

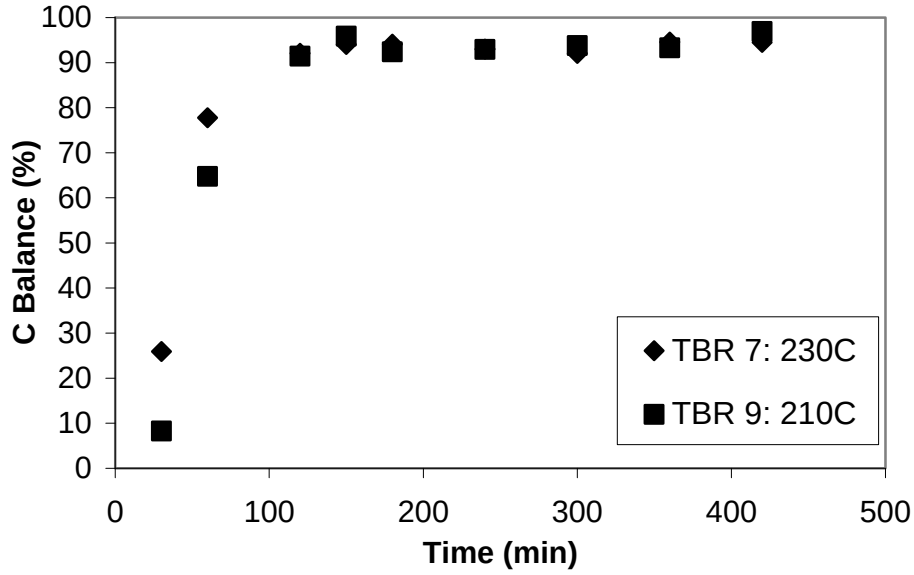

Figure 4-4. Carbon balance versus time in trickle bed reactor.

To test the effect of partial wetting of catalyst particles, the liquid feed rate was changed from 25 ml/hr to 100 ml/hr in TBR 7 to TBR 12, with all other conditions being the same. In

addition to reducing the residence time of liquid in the trickle bed reactor, a higher liquid feed rate will make catalyst particles more fully wetted and limit hydrogen access to the catalyst surface. On the other hand, a slower feedstock flow rate will make catalyst particles partially wetted, where three phase mass transfer will be carried out. Since the reaction rate is not hydrogen limited inside the catalyst particles (given Weisz-Prater modulus in Table 4-4), a slower flow rate will boost glycerol conversion and propylene glycol yield. This is observed in Figures 4-5 to 4-7, where the results of these reactions are presented.

In case of a higher flow rate in the trickle bed reactor where catalyst is fully wetted, the comparison can be made with the batch reactor where catalyst is also fully immersed and therefore wetted. At this point, only PNNL 59260-33E was used in both reactors but conditions were different (initial glycerol concentration). In Part III of this dissertation, we will discuss the parallel experiments with the identical reaction conditions for this investigation.

At the steady state for all four experiments, more than 90% carbon balance closure was achieved. Not much reaction happened at the higher flow rate (100 ml/hr in TBR 12). Average reaction rates in the trickle bed, in terms of glycerol consumption, were calculated and are listed in Table 4-4 along with Weisz-Prater modulus.

Table 4-4. Reaction rate for different feed flow rates

Run	TBR 10	TBR 7	TBR 11	TBR 12
Flow rate(ml/hr)	25	50	75	100
Glycerol W-P modulus	2.90E-3	5.79E-3	8.69E-3	1.16E-2
Hydrogen W-P modulus	1.12E-2	2.23E-2	3.35E-2	4.46E-2
Average reaction rate in bed (mol/hr/g catalyst)	4.432E-4	5.727E-4	5.735E-4	4.632E-4

The values used to calculate the Weisz-Prater modulus at reaction conditions are as follows:

- Hydrogen Diffusivity $D_{e,\,H2}=5.50 \times 10^{-8}$ m^2/sec
- Glycerol Diffusivity $D_{e,\,GO}=1.27 \times 10^{-8}$ m^2/sec
- Hydrogen concentration $C_{H2}=6.00 \times 10^{-2}$ $kmol/m^3$
- Effective particle radius $R=2.00 \times 10^{-4}$ m
- Catalyst density $\rho_c=1.40 \times 10^{3}$ kg/m^3

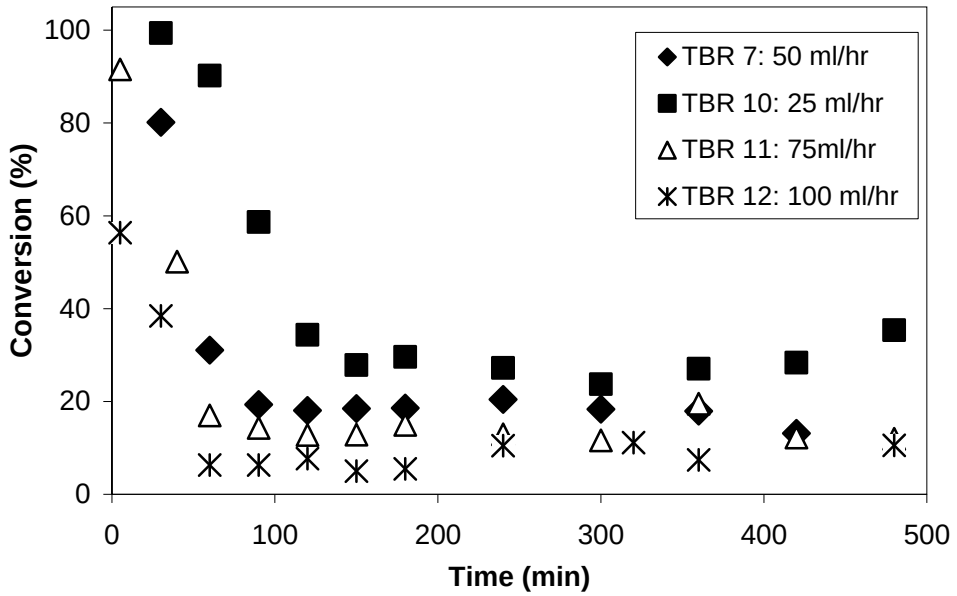

Figure 4-5. Effect of feed flow rate on glycerol conversion with catalyst 58959-72-1 (230°C, 1100 psi, 1.0 M glycerol, 0.25M NaOH, 30 ml catalyst).

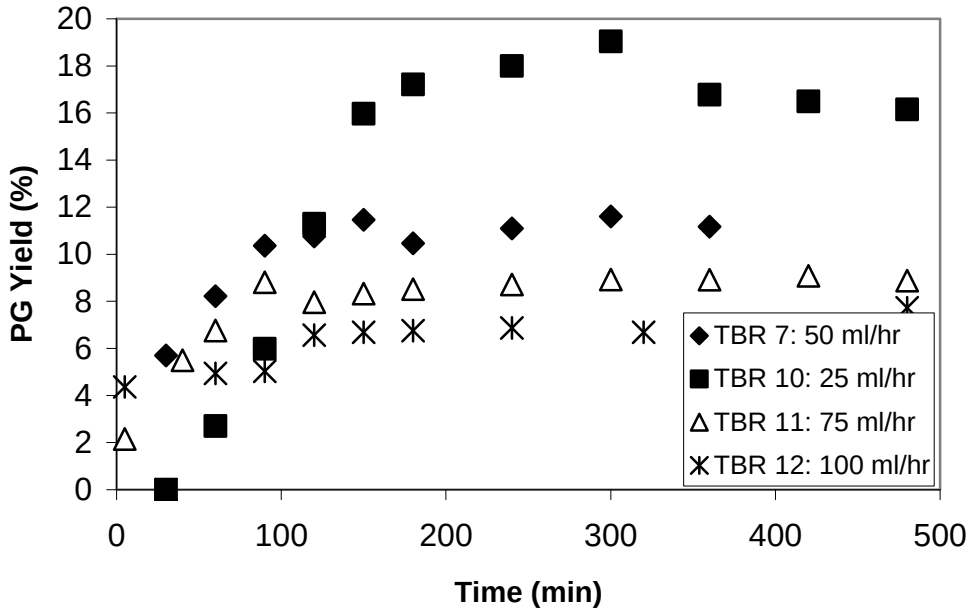

Figure 4-6. Effect of feed flow rate on propylene glycol yield with catalyst 58959-72-1 (230°C, 1100 psi, 1.0 M glycerol, 0.25M NaOH, 30 ml catalyst).

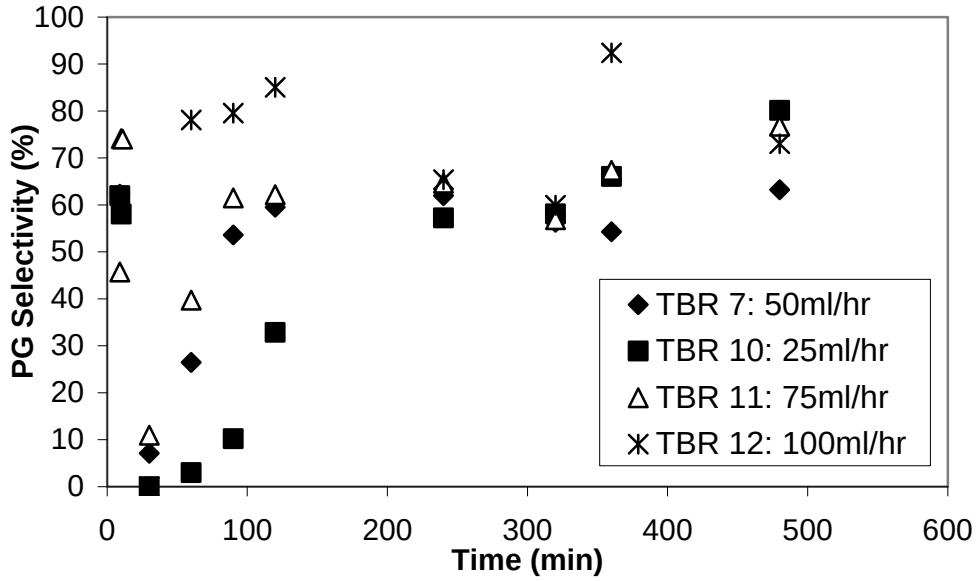

Figure 4-7. Effect of feed flow rate on selectivity toward propylene glycol with catalyst 58959-72-1 (230°C, 1100 psi, 1.0 M glycerol, 0.25M NaOH, 30 ml catalyst).

4.2.2. PNNL 59260-33E Catalyst

For the first series of experiments run in the trickle bed (catalyst PNNL-58959-72-1), performance was reasonably good, and results were indicative of catalyst reactivity. However, improvement w needed for glycerol conversion and propylene glycol yield. Therefore, the second series of experiments was carried out with catalyst 59260-33E in the trickle bed with the similar configuration. Catalyst reduction and operation procedure were the same.

Liquid feedstock flow rate was tested at 25 ml/hr, 50 ml/hr, 100 ml/hr, and 200 ml/hr in TBR 15 through 19 with all the other conditions the same: 1200 psi, 190°C, 1.0 M glycerol, 0.25 M NaOH, and hydrogen: glycerol mole ratio = 5:1. This catalyst (59260-33E) shows a higher glycerol conversion than catalyst PNNL-58959-72-1 at the same flow rate. Yield and selectivity toward propylene glycol are also boosted significantly. Conversion, yield, and selectivity are constant once reaction system reaches the steady state, as shown in Figures 4-8 to 4-10. Carbon

balance is very good for all the experiments. Average glycerol consumption rate in the trickle bed was calculated and is listed in Table 4-5.

Table 4-5. Reaction rate for different feed flow rates

Run	TBR 15	TBR 17	TBR 18	TBR 19
Flow rate (ml/hr)	25	50	100	200
Average reaction rate (mol/gcat/hr)	6.609E-4	9.254E-4	1.173E-3	1.270E-3

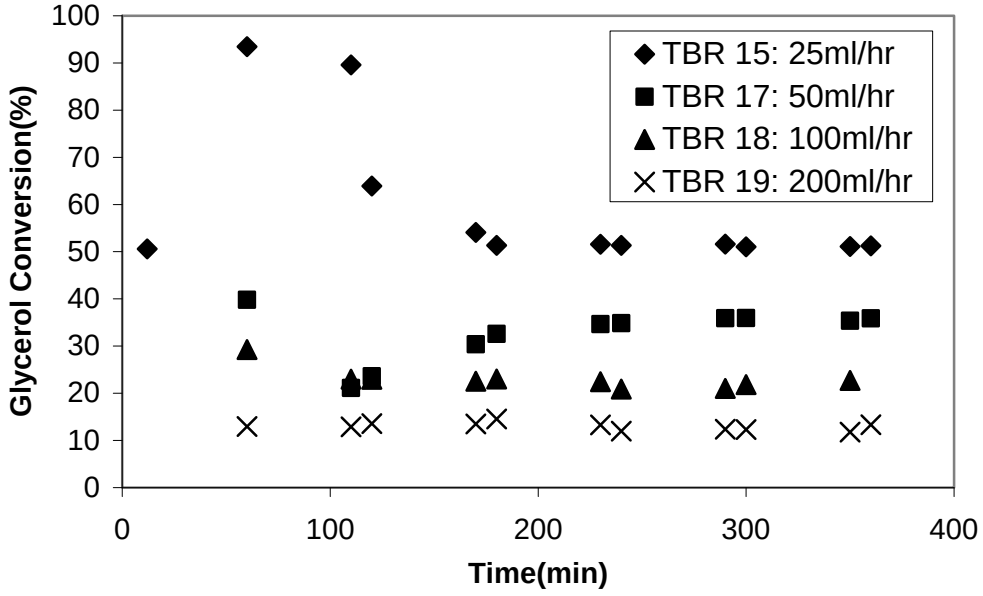

Figure 4-8. Effect of feed flow rate on glycerol conversion with catalyst 59260-33E (190°C, 1200 psi, 1.0 M glycerol, 0.25 M NaOH, 45 ml catalyst).

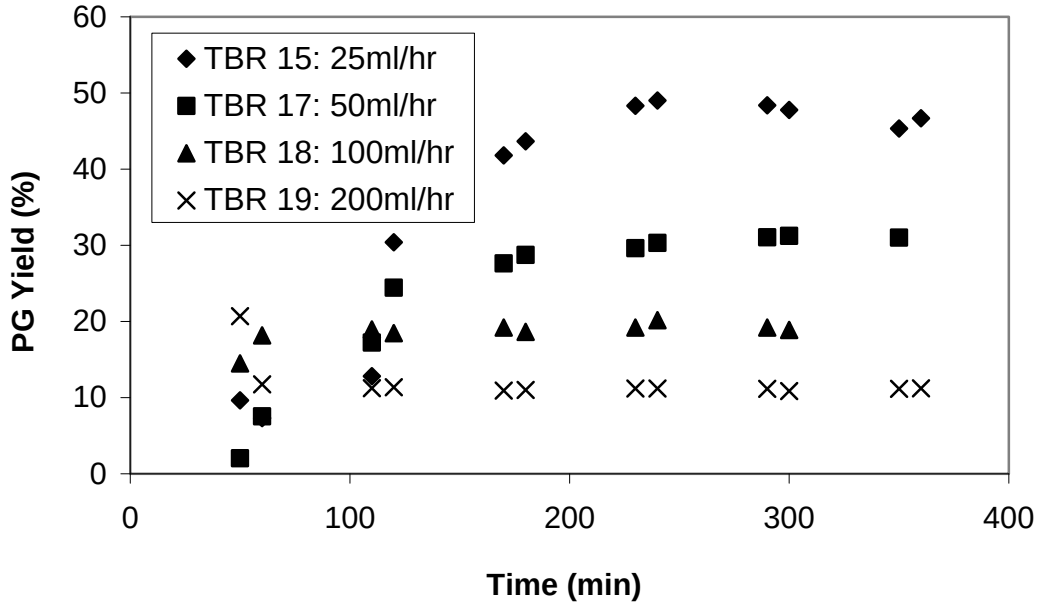

Figure 4-9. Effect of feed flow rate on propylene glycol yield with catalyst 59260-33E (190°C,1200 psi, 1.0 M glycerol, 0.25 M NaOH, 45 ml catalyst).

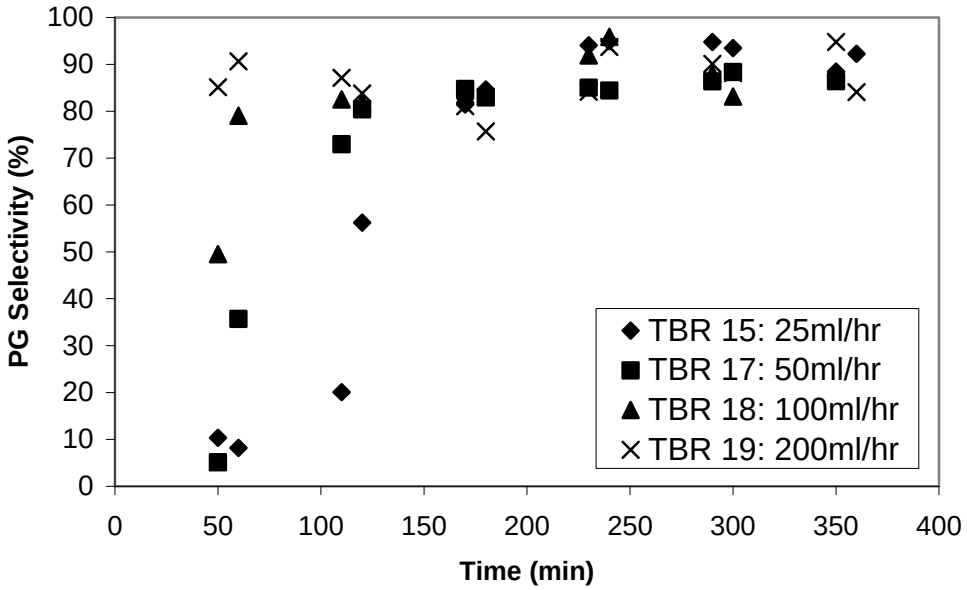

Figure 4-10. Effect of feed flow rate on selectivity toward propylene glycol with catalyst 59260-33E (190°C, 1200 psi, 1.0 M glycerol, 0.25 M NaOH, 45 ml catalyst).

4.2.3. PNNL 59260-51-65 Catalyst

Two sets of experiments were done with this catalyst, and the major objective was to further investigate how feedstock flow rate affected glycerol outlet conversion. TBR 21 to 25 were done at 195°C and TBR 26 to 30 at 180°C. Flow rate was varied, and a higher glycerol feed concentration (40 wt% glycerol (4.6 M) and 1 wt% NaOH (0.25 M) was used. Table 4-6 shows glycerol outlet conversion and propylene glycol yield.

Table 4-6. Experiment results summary (TBR 21-30)

Run	Feedstock flow rate (ml/hr)	Glycerol outlet conversion (%)	Propylene glycerol yield (%)	Propylene glycerol selectivity (%)	Carbon balance (%)
TBR 21	37.5	82.3	71.2	86.6	92.6
TBR 22	52.5	73.5	64.3	87.6	94.1
TBR 23	75	67.6	58.9	87.1	94.2
TBR 24	100	57.8	47.7	82.6	92.4
TBR 25	200	49.0	39.9	81.3	92.9
TBR 26	37.5	52.1	46.1	88.5	95.7
TBR 27	52.5	41.3	37.4	90.6	97.5
TBR 28	75	33.1	32.4	97.9	100.5
TBR 29	100	30.9	23.5	75.8	93.3
TBR 30	200	18.6	17.2	92.5	99.2

All the experiments were run at 1200 psi in hydrogen with a hydrogen: glycerol molar feed ratio of 5:1. The same trend was observed as TBR 15 to TBR19 when flow rate was changed. Selectivity to propylene glycol is also remarkably higher with this catalyst than with earlier catalysts tested.

After three series of experiments with different catalysts, the trickle bed reactor proved an efficient device for glycerol hydrogenolysis, with different active metal combinations in the catalysts deciding their performances. In the trickle bed, partial wetting of catalyst particles plays

an important role in interfacial mass transfer, which determines the quantity of active sites on the catalyst surface accessible to hydrogen to make hydrogenolysis happen. Also, the trickle bed geometry contributes to reaction kinetics; in the following chapter regarding modeling, some scenarios involving various geometries are simulated and evaluated.

Part III Reaction Rate Modeling and Correlation

Chapter 5 Integral Model for Glycerol Hydrogenolysis in Trickle Bed

A detailed model of glycerol hydrogenolysis has been developed that includes a mechanistically based kinetic rate expression, energy transport, mass transport through the liquid phase, and partial wetting of the trickle bed. Optimal kinetic parameters based on all the data collected, either at Pacific Northwest National laboratory or at MSU, from the trickle bed system were determined via regression analysis. Model predictions agree with experimental data and accurately predict trends in reactor performance with liquid flow rate, temperature, hydrogen pressure, and base promoter concentration. The kinetic rate expression represents truly intrinsic kinetics and is compared with batch reactor data to unify reactions in both environments. The model is thus a useful tool for predicting laboratory reactor performance and for preliminary design of commercial-scale trickle bed systems.

Due to a wrong stoichiometry used in the proposed catalytic mechanism, the intrinsic rate expression to be discussed in this chapter was incorrectly derived but correction will be made in Chapter 6. Since we have done the data analyses in their completeness with the current intrinsic rate expression, we decided to present the results and discussion for demonstration purposes. In Chapter 6, correct derivation and corresponding discussion will be carried out.

5.1. Kinetic Model

The establishment of the reactor model begins with development of a kinetic rate expression based on the accepted reaction mechanism for glycerol hydrogenolysis. In simplified form, the mechanism involves (i) dehydrogenolysis of glycerol to an adsorbed

glyceraldehyde analog (*GA·S*), (ii) rearrangement and dehydration of (*GA·S*) to a second adsorbed intermediate (*I·S*) analogous to pyruvaldehyde or 2-hydroxyl acrolein, and (iii) hydrogenolysis of the intermediate to propylene glycol (*PG*).

$$GO + S \underset{k_{-1}}{\overset{k_1}{\rightleftarrows}} GA \cdot S + H_2 \tag{5-1}$$

$$GA \cdot S + OH^- \underset{k_{-2}}{\overset{k_2}{\rightleftarrows}} I \cdot S + OH^- \tag{5-2}$$

$$I \cdot S + H_2 \xrightarrow{k_3} PG + S \tag{5-3}$$

The rate expression for each step shown above can be written as follows:

$$r_1 = k_1 C_{GO} \cdot C_S - k_{-1} C_{GA \cdot S} C_{H_2} \tag{5-4}$$

$$r_2 = k_2 C_{GA \cdot S} C_{OH^-} - k_{-2} C_{I \cdot S} C_{OH^-} \tag{5-5}$$

$$r_3 = k_3 C_{I \cdot S} C_{H_2} \tag{5-6}$$

Equating all three rates, invoking the site balance,

$$C_{total} = C_S + C_{GA \cdot S} + C_{I \cdot S} \tag{5-7}$$

eliminating the concentrations of adsorbed intermediates, and dismissing two terms in the denominator lead to the final expression:

$$r = \frac{k_f C_{H_2} C_{GO} C_{OH^-}}{C_{GO} C_{OH^-} + K_H C^2_{H_2}} \tag{5-8}$$

Those two terms dismissed ($C_{H2}C_{OH^-}$, $C_{H2}C_{GO}$) are cross terms whose influence on rate can adequately be described by $C_{GO}C_{OH^-}$ and C^2_{H2} terms. Thus, glycerol hydrogenolysis

reaction kinetics are described in terms of a preexponential factor k_0, a reaction activation energy E_a, and an adsorption constant K_H that is independent of temperature. This rate expression captures essential features of glycerol hydrogenolysis: partial order with respect to glycerol and hydroxide, and negative order with respect to hydrogen at high pressures. The complete derivation of the kinetic rate expression is given in Appendix A of this dissertation.

The rate expression derived for GO hydrogenolysis does not contain any information about selectivity to products, even though historically methane, ethylene glycol, and lactic acid are noted as byproducts of GO hydrogenolysis to PG. In this study, the catalyst showed selectivities to PG between 88 and 95% of theoretical over the range of operating conditions, with byproducts ethylene glycol (2-3%), lactic acid (1-3%), and alcohols (methanol, ethanol, propanol) (1.5-3.5%) consuming the remainder of GO. To include formation of these byproducts explicitly in this model would require an additional rate expression for each species; such additional complexity is not warranted because byproduct yields are relatively constant and it would be extremely difficult to obtain distinct rate expressions for byproduct formation from solely the outlet concentrations of those species.

5.2. Reactor Model

The trickle bed model for glycerol hydrogenolysis is developed for steady state operation by assuming one-dimensional plug flow and using the glycerol molar balance and the reactor energy balance. The molar balance for glycerol is given by

$$-\frac{dC_{GO}}{d\tau} = R_G \qquad (5\text{-}9)$$

where τ is defined as reactor volume divided by liquid flow rate.

For GO hydrogenolysis in the trickle bed, it is not necessary to write a molar balance for the gas-phase. The significant molar excess of hydrogen used in reactions (5:1 H_2:GO) and the formation of negligible quantities of gas-phase products (less than 1% of GO is converted to methane) means that the gas phase is essentially composed of hydrogen and water at its vapor pressure over the reacting solution. Thus, gas composition does not change down the length of the trickle bed. Further, the high gas-phase pressure (3-12 MPa) results in very small gas superficial velocities through the reactor (< 10 cm/min) and thus low pressure drop (< 10 kPa), so gas-phase has essentially no influence on liquid flow in the trickle bed.

The energy balance includes terms for heat generation by reaction and energy removal by the coolant surrounding the reactor.

$$\frac{d(\rho C_p T)}{d\tau} = (-\Delta H_R)(-R_G) + \frac{2U_0}{R}(T_c - T) \qquad (5\text{-}10)$$

The overall heat transfer coefficient (U_o) between the catalyst bed and coolant was taken as 100 J/m^2/sec/K; [41] varying this value by ±20% led to larger variations between predicted and experimental temperature profiles in the trickle bed, so this value was used for all simulations. The jacket temperature (T_c) used in the reactor model was taken as the recirculating oil bath set point temperature.

It is worth noting that temperature changes in the trickle bed should be dampened by the phase equilibrium between the liquid and gas phases. Energy liberated by reaction raises the liquid phase temperature, but that rise in temperature is offset by the corresponding increase in

water vapor pressure which forces the energy liberated in reaction to produce more water vapor to re-establish equilibrium. Thus, for a constant water mole fraction in the liquid phase and negligible pressure drop in the reactor, the reactor temperature should be approximately constant.

5.3. Mass Transfer

In order to calculate the hydrogen concentration at the catalyst particle surface ($C_{H2,\,S}$), the concentration gradient for each compound in the steady state, three-phase reactor system is defined as shown in Figure 5-1. The global reaction rate R_G is a summation of reaction rates occurring in both wetted and unwetted factions of the trickle bed (Eq. 5-11 below). This approach is taken because liquid velocities in the reactor are low under our operating conditions, and the bed is only partially wetted. In the wetted fraction, mass transport resistances across the liquid film surrounding the catalyst particles must be accounted for (Figure 5-1); hence, the rate expression must include hydrogen concentration expressed as $C_{H2,S}$. In the unwetted fraction, there is no liquid layer surrounding the catalyst particle, and thus hydrogen gas has direct access to the catalyst surface. Its concentration can be taken as the gas phase equivalent, C^{*}_{H2}. It is assumed that the liquid in both wetted and unwetted fractions is replenished continuously.

$$-R_G = \varepsilon_W (1-\varepsilon_B)\frac{\eta_{H_2} k_f C_{H_2,S} C_{GO} C_{OH^-}}{C_{GO} C_{OH^-} + K_H C^2_{H_2,S}} + (1-\varepsilon_W)(1-\varepsilon_B)\frac{\eta_{H_2} k_f C^*_{H_2} C_{GO} C_{OH^-}}{C_{GO} C_{OH^-} + K_H C^{*2}_{H_2}} \quad (5\text{-}11)$$

The hydrogenolysis reaction is hydrogen limited in the catalyst particles, because of the low solubility of hydrogen in water (~0.05 M) in comparison to the glycerol concentration used

(1.0 to 4.8 M). Therefore, a first order approximation is used for the effectiveness factor for hydrogen intraparticle diffusion:

$$\eta_{H_2} = \tanh\phi \Big/ \phi \tag{5-12}$$

where

$$\phi = \frac{d_p}{6}\sqrt{\frac{k_f}{\varepsilon_p{}^2 D_{H_2}}} \tag{5-13}$$

At the steady state in the wetted fraction of the bed, hydrogen flux across gas-liquid and liquid-solid interfaces should equal hydrogen consumption rate in the catalyst. Therefore, the following relationship can be established:

$$\begin{aligned} & k_{GL,H_2} a(C^*_{H_2} - C_{H_2,L}) = k_{SL,H_2} a(C_{H_2,L} - C_{H_2,S}) \\ & = \eta_{H_2}(1-\varepsilon_B)\frac{k_f C_{H_2,S} C_{GO} C_{OH^-}}{C_{GO} C_{OH^-} + K_H C^2_{H_2,S}} \end{aligned} \tag{5-14}$$

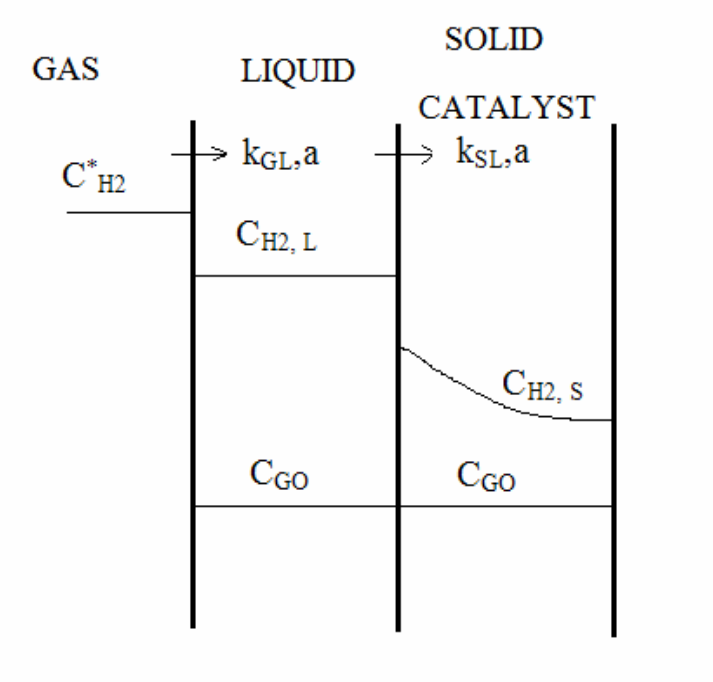

Figure 5-1. Steady state concentration profiles in the wetted fraction of the trickle bed reactor.

$C_{H2, S}$ can be solved by the following cubic equation, which is derived from Eq.5-14:

$$\frac{k_{GL,H_2}ak_{SL,H_2}ak_H}{k_{GL,H_2}a+k_{SL,H_2}a}\cdot C^3{}_{H_2,S}+\left(\frac{k_Hk^2{}_{GL,H_2}a^2C^*{}_{H_2}}{k_{SL,H_2}a+k_{GL,H_2}a}-k_{GL,H_2}ak_HC^*{}_{H_2}\right)\cdot C^2{}_{H_2,S}$$
$$+\left(\eta_{H_2}\left(1-\varepsilon_B\right)k_f+\frac{k_fk_{GL,H_2}ak_{SL,H_2}a}{k_{GL,H_2}a+k_{SL,H_2}a}\right)\cdot C_{GO}C_{OH^-}C_{H_2,S} \qquad (5\text{-}15)$$
$$+\frac{k_fk^2{}_{GL,H_2}a^2C^*{}_{H_2}{}^2C_{GO}C_{OH^-}}{k_{SL,H_2}a+k_{GL,H_2}a}-k_fk_{GL,H_2}aC^*{}_{H_2}C_{GO}C_{OH^-}=0$$

The mass transfer coefficients $k_{GL,H2}$ and $k_{LS,H2}$ were determined for the trickle bed correlations by Goto and Smith:[42]

$$k_{GL}a=\frac{7.8D\,\mathrm{Re}_L^{0.39}\,Sc_L^{1/2}}{d_p{}^{0.39}} \qquad (5\text{-}16)$$

$$k_{LS}a = \frac{45D\,\mathrm{Re}_L^{0.56}\,Sc_L^{1/3}}{{d_p}^{0.56}} \tag{5-17}$$

where *Sc* stands for Schmidt number, R_e for Reynolds number, *D* for hydrogen diffusivity, and d_p for catalyst particle diameter.

$$\mathrm{Re}_L = \frac{U_L \rho_L d_p}{\mu_L} \tag{5-18}$$

$$Sc_L = \frac{\mu_L}{\rho_L D} \tag{5-19}$$

The wetting efficiency of the trickle bed was correlated by Al-Dahhan et al.[38] as follows:

$$\varepsilon_W = 1.104\,\mathrm{Re}_L{}^{1/3}\left\{\frac{1+[(\Delta P/Z)/\rho_L g}{Ga_L}\right\}^{1/9} \tag{5-20}$$

where

$$\mathrm{Re}_L = \frac{U_L \rho_L d_p}{\mu_L} \tag{5-18}$$

and

$$Ga_L = \frac{{d_p}^3 {\rho_L}^2 g {\varepsilon_B}^3}{{\mu_L}^2 (1-\varepsilon_B)^3} \tag{5-21}$$

All the other physical properties were taken from the literature [43] or were estimated from existing correlations; values are given in Table 5-1.

Table 5-1. Physical properties used for trickle bed modeling

Description	Unit	Value
Particle size	m	0.0008
Particle porosity		0.6
Particle wet density	kg/m^3	1400
Catalyst Dry Bulk Density	kg/m^3	400
Bed depth	m	0.273
Bed porosity	-	0.5
Reactor radius	m	0.006
Liquid viscosity	kg/m/sec	0.00014
Liquid density	kg/m^3	1100
Gas viscosity	kg/m/sec	1.38E-05
Glycerol liquid diffusivity	m^2/sec	1.27E-08
Hydrogen liquid diffusivity	m^2/sec	5.5E-08
Liquid surface tension	kg/sec^2	0.0432

5.4. Solution Method and Kinetic Parameter Optimization

The mass and energy balance equations were numerically integrated over the reactor length using Euler's method in a program written in Microsoft Excel which is shown in Appendix B. At each point along the integration, the surface hydrogen concentration $C_{H2,S}$ was determined via the cubic equation shown in Eq. 5-15. All the concentrations and rates were then calculated at that point, and the step to the subsequent point was taken.

The reactor model was applied to several sets of steady state trickle bed reactor runs using different catalysts at widely varying conditions. For each set of data, the outlet glycerol conversion was predicted in each experiment from the model, and then the kinetic parameters in

the rate expression (Eq. 5-8), k_o, E_a, K_H, and the overall heat transfer coefficient U_o (Eq. 5-10), were varied for the entire set of data to minimize the sum of square differences between experimental and predicted glycerol concentrations.

$$obj.\,function = \sum_i (\sqrt{1 - X_{i,GO,\exp}} - \sqrt{1 - X_{i,GO,cal}})^2 \qquad (5\text{-}22)$$

An initial value of activation energy E_a was calculated based on the data from two experiments running at the different temperatures. Because the reaction is only partial order in glycerol, the objective function used in the regression was for a one-half order reaction. This gave a more even weighting of low and high conversion experiments than a simple linear model.

5.5. Results

5.5.1. Modeling of PNNL Trickle Bed Experiments

The trickle bed model was first applied to a large set of trickle bed reactor data collected at Pacific Northwest National Laboratory using one of their proprietary catalyst (PNNL 59260-51-65). The conditions are given in Table 5-2.

Table 5-2. Summary of PNNL Trickle Bed Run Conditions and Results

Exp. #	Feed Inlet Temp. (K)	Total Pressure (MPa)	Feed flow rate (ml/hr)	NaOH Conc. (M)	Experiment-al Glycerol Conversion	Predicted Glycerol Conversion
1	468	8.27	50	0.58	0.90	0.92
2	464	8.27	50	0.58	0.95	0.95
3	467	8.27	50	0.28	0.81	0.78
4	464	8.27	50	0.14	0.69	0.54
5	475	8.27	50	0.14	0.83	0.74
6	453	8.27	50	0.14	0.46	0.39
7	463	8.27	35	0.14	0.79	0.70
8	463	8.27	25	0.14	0.86	0.84
9	473	8.27	35	0.14	0.87	0.82
10	473	8.27	35	0.14	0.89	0.88
11	453	8.27	50	0.28	0.65	0.56
12	475	8.27	50	0.28	0.94	0.94
13	463	8.27	35	0.28	0.89	0.91
14	463	8.27	25	0.28	0.94	0.98
15	453	8.27	35	0.28	0.75	0.71
16	473	8.27	35	0.28	0.96	0.99
17	453	8.27	25	0.28	0.79	0.86
18	473	8.27	25	0.28	0.98	1.00
19	463	8.27	35	0.28	0.91	0.92
20	463	11.03	35	0.28	0.88	0.88
21	463	5.52	35	0.28	0.91	0.93
22	463	2.76	35	0.28	0.64	0.54
23	463	13.79	35	0.28	0.82	0.85
24	468	13.79	35	0.28	0.91	0.92
25	468	8.27	35	0.28	0.96	0.97

The optimized values of the kinetic constants for the glycerol hydrogenolysis rate expression (Eq. 5-8) are listed in Table 5-3. The predicted glycerol conversion was listed in the final column of Table 5-2 to be compared with experiment measurement.

Table 5-3. Optimal kinetic parameters for rate expression (PNNL data based)

Description	Unit	Value
Pre exponential factor k_o	m^3/kg catalyst /sec	8.99×10^8
Activation energy E_a	kJ/kmol	86,000
Hydrogen coeff. K_H	-	425
Heat transfer coeff. U_o	J/sec/m^2/K	100

A comparison of experimental and predicted outlet glycerol concentrations over a wide range of operating conditions is shown in Figures 5-2 and 5-3. It is seen that there is a good agreement between predicted and experimental values over all conditions - a remarkable outcome given that only the three kinetic constants (k_o, E_a, *and* K_H) are adjusted and all other constants and coefficients governing hydrodynamics and mass/heat transfer in the model are taken straight from literature or textbook correlations. For the optimized kinetic parameters, the value of the object function in Eq. 5-22 is 0.10; in simplified terms, the average value of the absolute difference between experimental and simulated outlet GO conversion is 0.042. Several temperature profiles along the bed are given in Figure 5-4; again, the model predicts with good accuracy the exotherm of about 10 K in the trickle bed reactor over the range of inlet temperatures examined.

The model can also illustrate species concentration profiles in the trickle bed; Figure 5-5 gives predicted GO concentration profiles as a function of a) inlet temperature, b) liquid feed flow rate, and c) feed base concentration at conditions that match those in the experiments identified. Figure 5-6 compares the experimental and predicted GO conversion on total reactor pressure; the sharp drop in conversion at the lowest pressure (2.76 MPa) is attributed to low

hydrogen partial pressure because water partial pressure at 463 K is 1.3 MPa, a significant fraction of the total. The observed drop in GO conversion as pressure increases above ~6 MPa is predicted by the mechanistically-based rate expression.

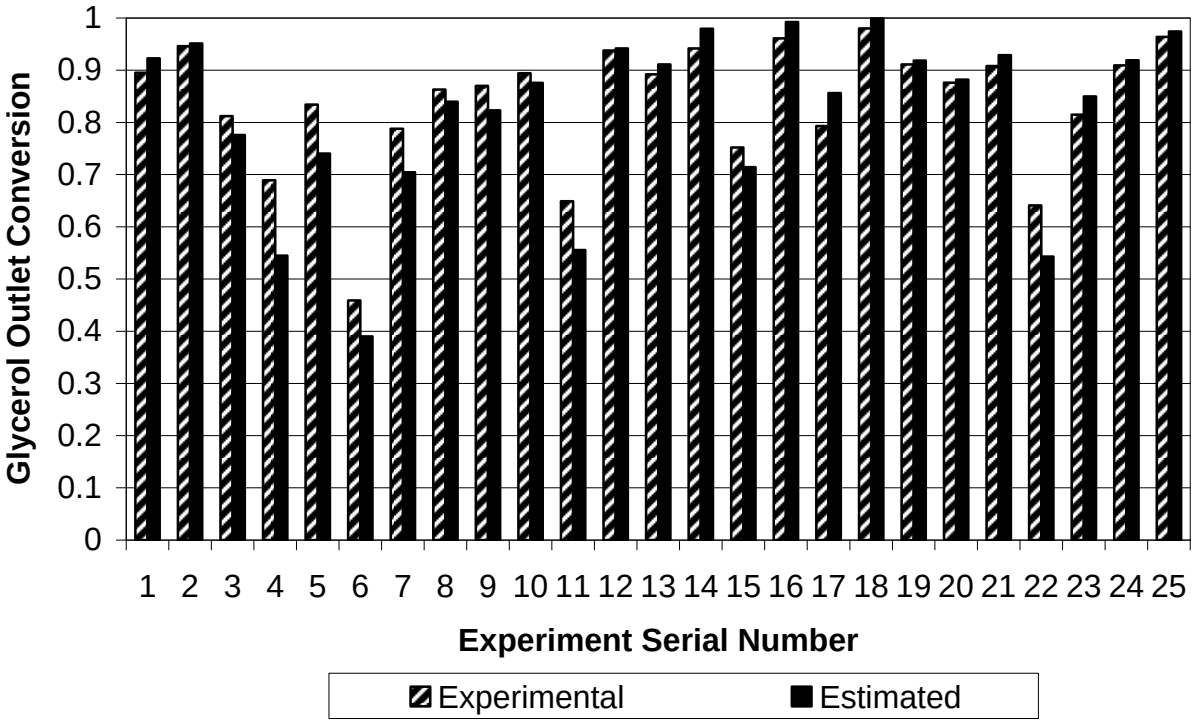

Figure 5-2. Outlet glycerol simulated and experimental conversions.

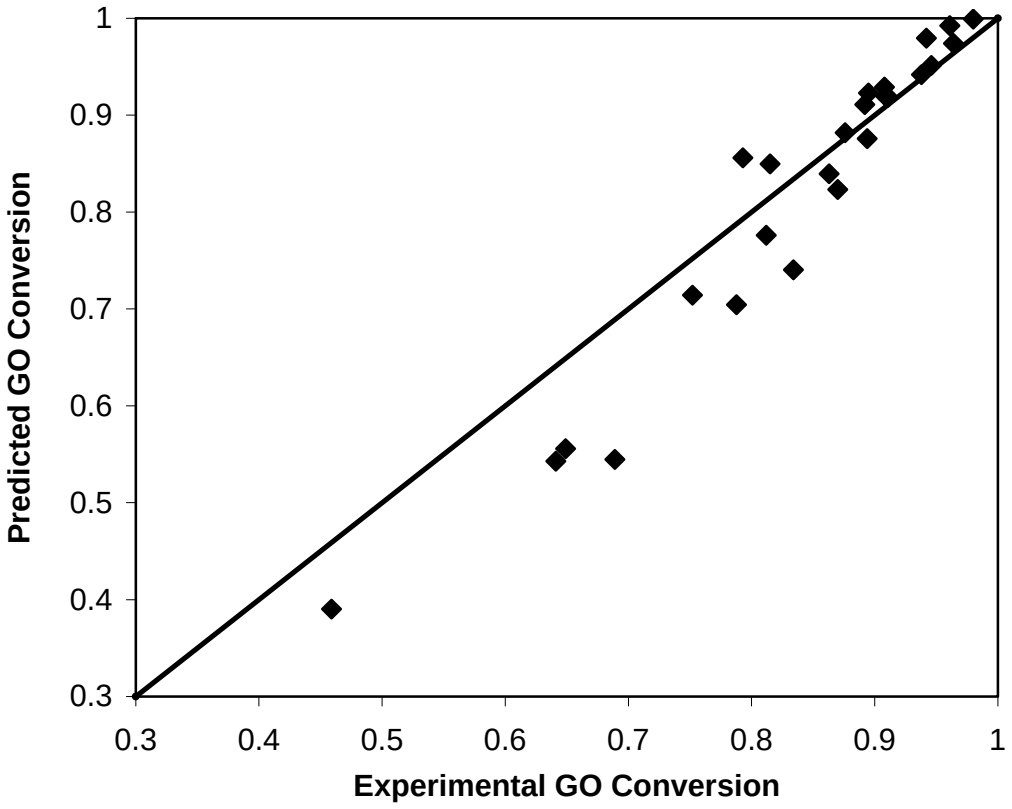

Figure 5-3. Parity plot of experimental versus predicted GO conversion.

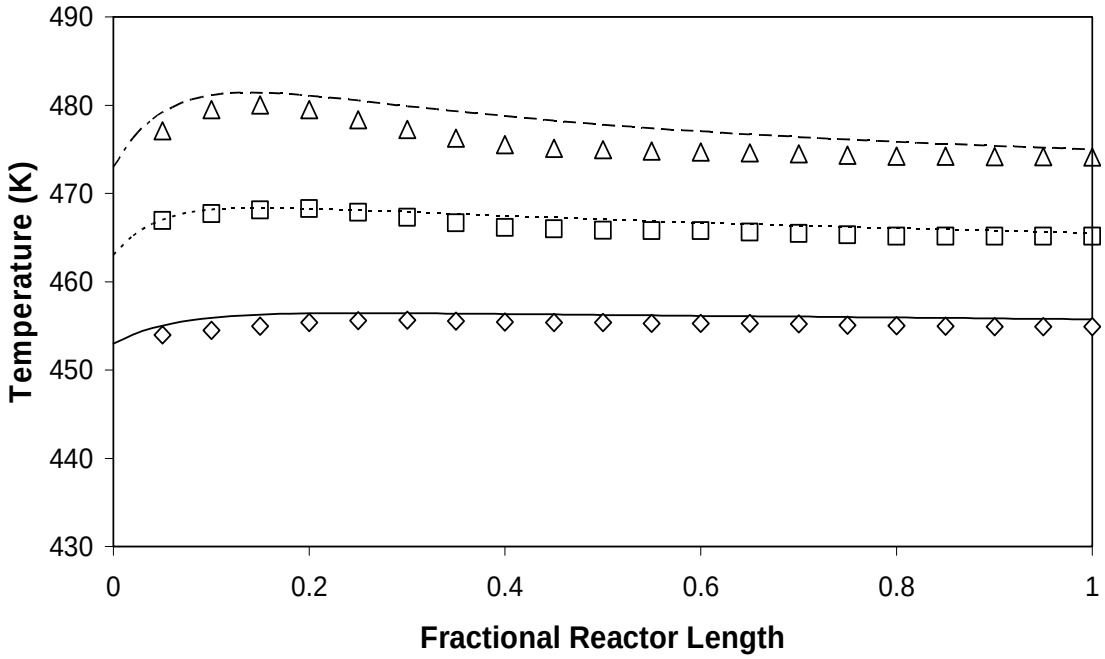

Figure 5-4. Predicted vs. experimental temperature profiles in trickle bed. Inlet temperature: 453 K : (——) – simulation, (◇) – experiment; 463 K: (- - -) – simulation, (□) – experiment; 473 K : (−·−·−) – simulation, (△) - experiment. Conditions: 8.27 MPa, liquid feed rate 35 ml/hr, 0.14 M NaOH.

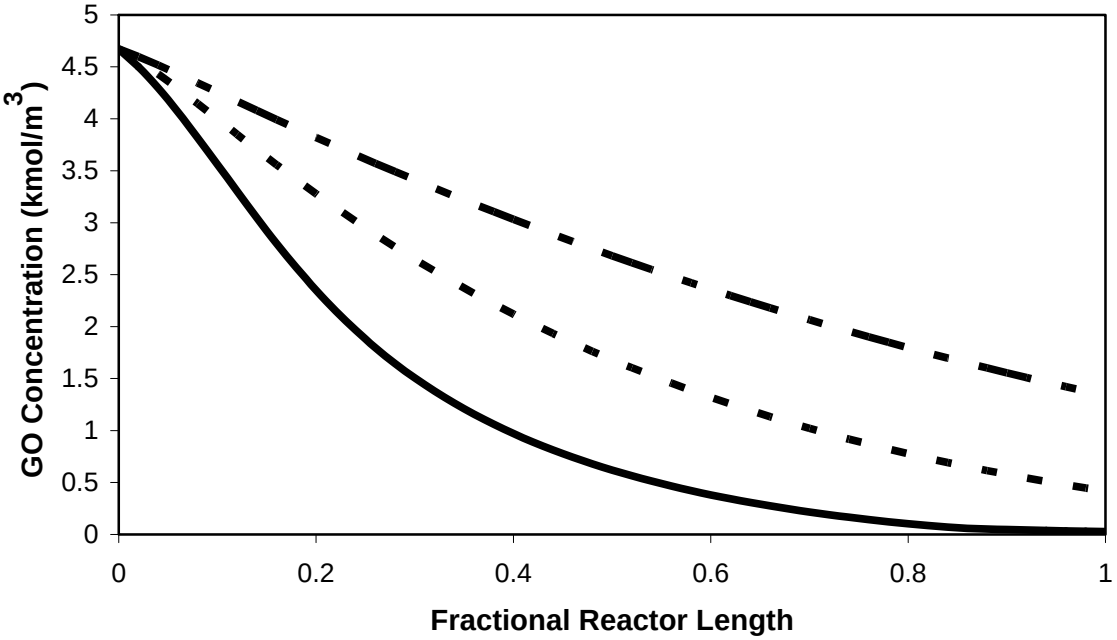

Figure 5-5a. Simulated GO concentration profiles in trickle bed for different inlet temperatures. (−−−) – 453 K ; (- - -) – 463 K; (——) – 473 K. Conditions: 8.27 MPa, liquid feed rate 35 ml/hr, 0.28 M NaOH.

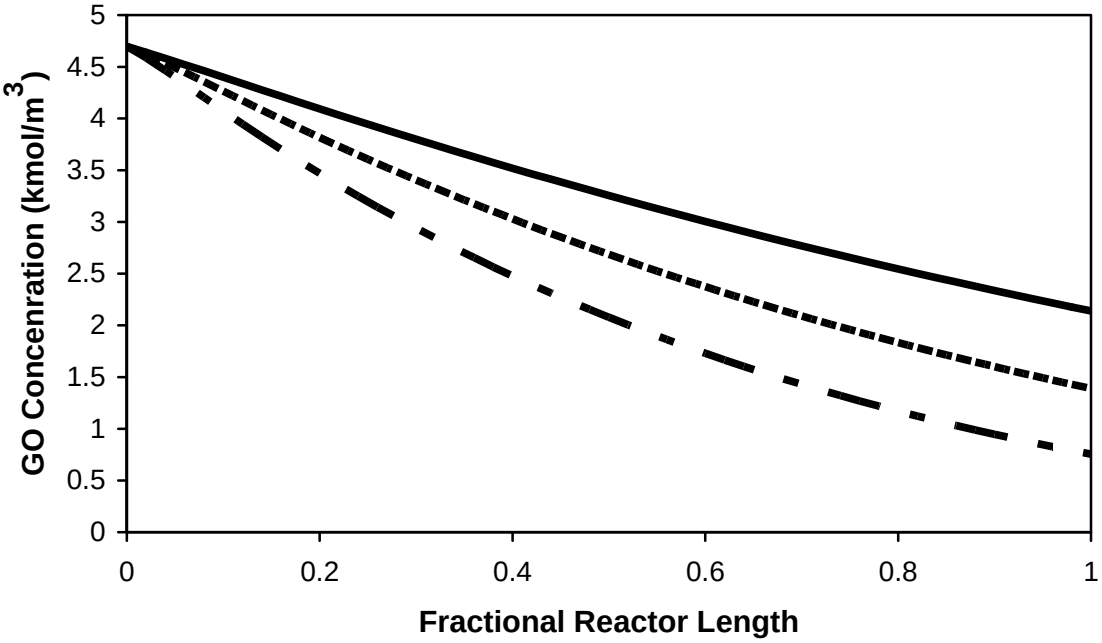

Figure 5-5b. Simulated GO concentration profiles in trickle bed for different liquid feed flow rates: (——) – 50 ml/hr ; (- - -) – 35 ml/hr; (−·−·−) – 25 ml/hr . Conditions: 8.27 MPa, 463 K, 0.14 M NaOH.

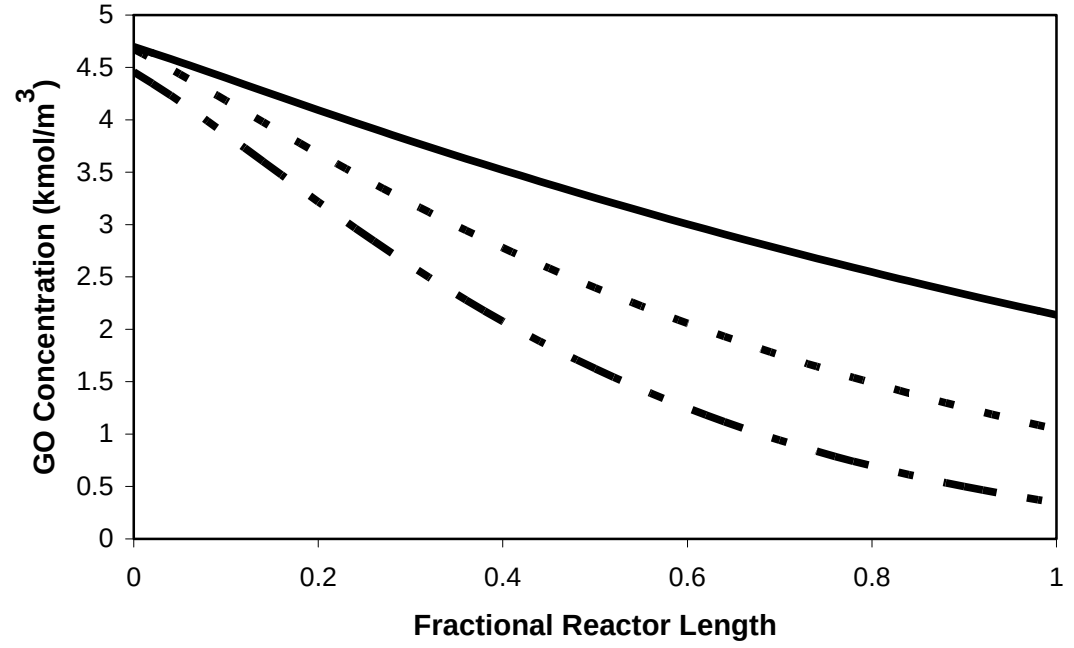

Figure 5-5c. Simulated GO concentration profiles in trickle bed at different NaOH concentrations: (−·−·−) - 0.58 M; (- - -) - 0.28 M ; (——) - 0.14 M . Conditions: 8.27 MPa, 464 K, liquid feed rate 50 ml/hr.

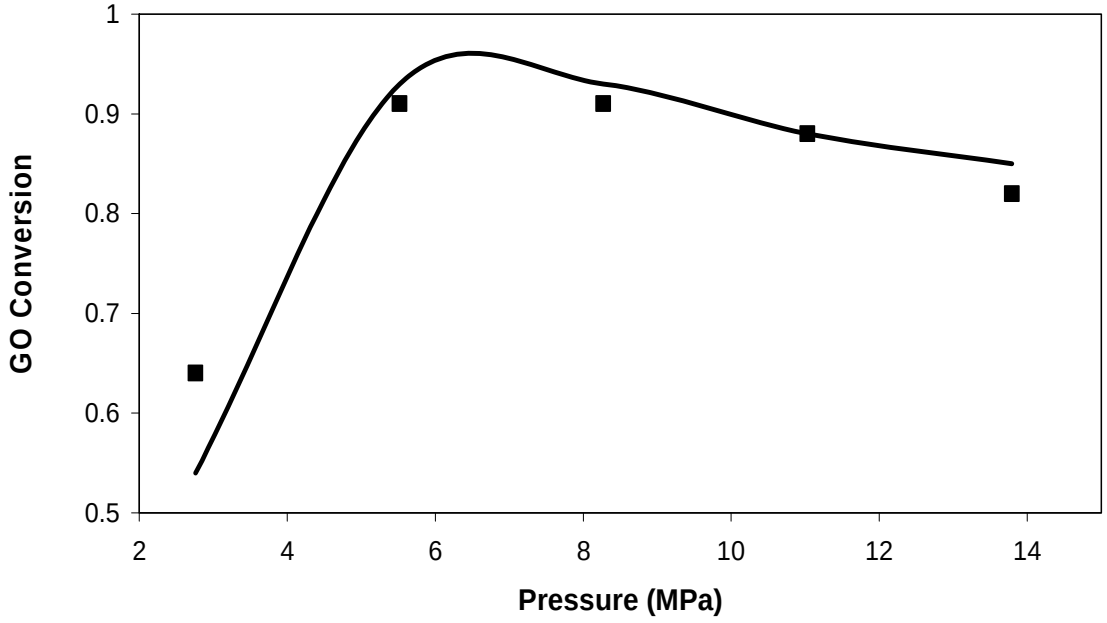

Figure 5-6. Effect of total pressure on outlet GO conversion from trickle bed reactor. (——) - simulation; (■) -experiment . Conditions: 463 K, liquid feed rate 35 ml/hr, 0.28 M NaOH.

5.5.2. Modeling of MSU Trickle Bed Experiments

Some data were also available from experiments run at MSU with low glycerol conversion. Modeling was done on these data, too. Kinetic parameters were optimized for glycerol conversion of TBR 15 through TBR 19 for catalyst PNNL-59260-33E, previously described in Chapter 4, and the agreement between experiments and simulations was good. These optimal kinetic parameters turned out different from those PNNL results due to different catalyst and trickle bed reactor dimension. Table 5-4 shows all the values.

Table 5-4. Optimal kinetic parameter summary (MSU TBR15~19 based)

Description	Unit	Value
Pre exponential factor k_o	m^3/kg catalyst /sec	8.99×10^8
Activation energy E_a	kJ/kmol	87,300
Hydrogen coeff K_H	-	3,160
Heat transfer coeff. U_o	J/sec/m^2/K	100

Further, our modeling study extended to fit glycerol conversion data of TBR 20 through TBR 30 where the same catalyst that was used in PNNL experiments (PNNL-59260-51-65) was used, and optimal kinetic parameters were fitted, and optimal values are listed in Table 5-5. Figure 5-7 shows the comparison between model simulation and experimental conversion. Our model gives a reasonably good simulation for glycerol conversion over various reaction conditions.

Table 5-5. Optimal kinetic parameter summary (MSU TBR 20~30 based)

Description	Unit	Value
Pre exponential factor k_o	m^3/kg catalyst /sec	8.99×10^8
Activation energy E_a	kJ/kmol	85,600
Hydrogen coeff K_H	-	1,110
Heat transfer coeff. U_o	J/sec/m^2/K	100

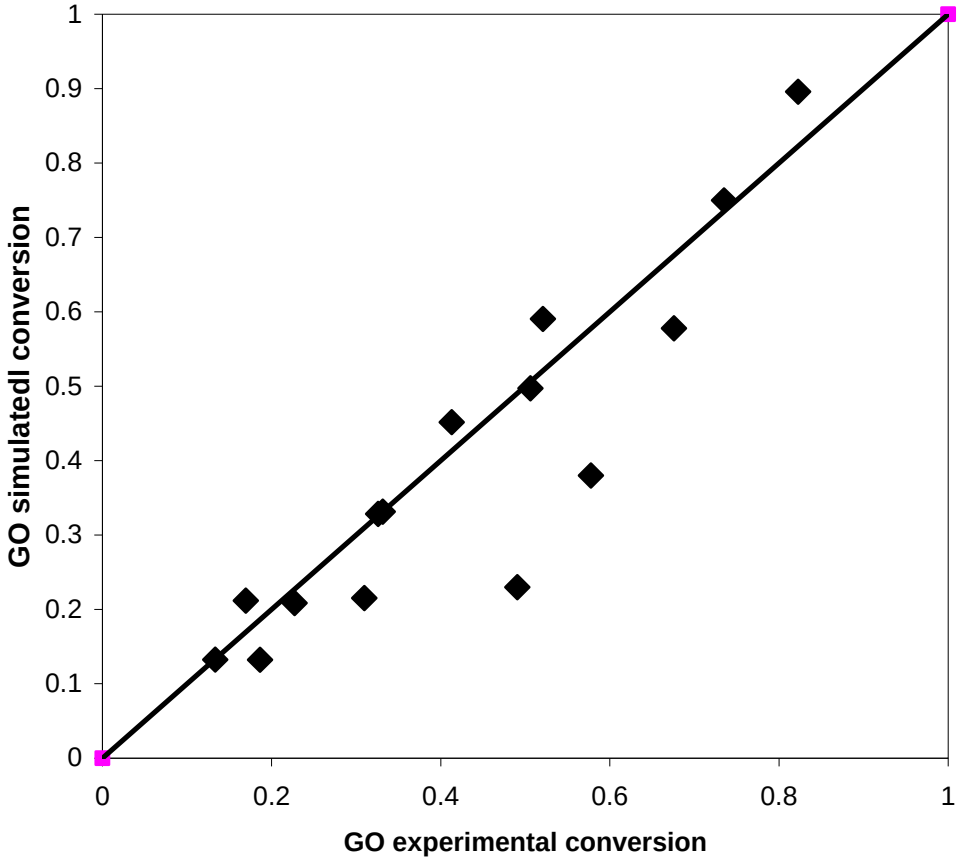

Figure 5-7. Parity plot for MSU experiments (TBR 15-30).

5.6. Extended Model with Partial Wetting Efficiency Correction Factor (ε)

5.6.1. Rationale and Methodology

The trickle bed model assumes reaction rate be the combination of fully wetted rate and unwetted rate, as shown in Eq. 5-11. In the unwetted rate term, catalyst is assumed to be completely accessible by hydrogen, and the model predicts the outlet glycerol concentration reasonably well. In order to better understand the effect of partial wetting, a partial wetting efficiency correction factor ω was introduced to the unwetted part of the rate expression as shown in Eq. 5-11-1 below. This factor allows us to better quantify the contribution of partial wetted catalyst to the overall reaction rate.

$$-R_G = \varepsilon_W(1-\varepsilon_B)\frac{\eta_{H_2} k_f C_{H_2,S} C_{GO} C_{OH^-}}{C_{GO}C_{OH^-} + K_H C_{H_2,S}^2} + \omega(1-\varepsilon_W)(1-\varepsilon_B)\frac{\eta_{H_2} k_f C_{H_2}^* C_{GO} C_{OH^-}}{C_{GO}C_{OH^-} + K_H C_{H_2}^{*2}} \quad (5\text{-}11\text{-}1)$$

Based on the optimal parameters (E_a , U_o , k_o , and K_H) from the previous simulation, the correction factor ω was fitted manually to bring the predicted conversion from the model to the value of the experimental conversion.

In some cases, the predicted conversion was lower than the actual glycerol outlet conversion even though the largest possible correction factor (1) was applied. Therefore, the preexponential factor k_o had to be increased to make it possible that predicted conversion equals the experimental conversion for correction factor values no greater than unity. Different values were tried for $k_{o,}$ and maximum value seems to be 2.1 times as large as original optimal k_o. Beyond 2.1 k_o, model crashes.

First, manual fitting of the correction factor was done for each experiment such that experimental and predicted outlet conversions agree. Based on these values, some efforts were made to correlate these values to operating conditions. This is a trial-and-error process, and tests

were done with different forms of equations (linear, logarithm, quadratic, etc.) and different operating parameters such as base concentration (C_{NaOH}) and liquid feed flow rate (m). With all the formulae fitted by computer, correction factors for each experiment could be calculated and put back in the model to get the prediction of glycerol outlet concentration. The best correlation is the one with minimum error summation from the same objective function used in the previous research.

5.6.2. Data Fitting Results

The values of the manually fitted correction factor ω are shown in the second sets of columns of Table 5-6. These values of partial wetting correction factor ω are best correlated to flow rate and base concentration:

$$\omega = 1000 m^{0.430} C_{NaOH}^{-0.235} \qquad (5\text{-}23)$$

where m is liquid feed flow rate (m^3/sec) and C_{NaOH} is inlet base concentration (kmol/m^3). The insertion of the correction factor ω into Eq. 5-11 and the subsequent prediction of outlet GO conversion from the model for the PNNL reactor data was done and is reported in the third set of columns in Table 5-6. With the correlation factor ω included, the overall objective function decreases from 0.100 to 0.052, and model's prediction is much more accurate. It is difficult to draw fundamental conclusions on partial wetting of the catalyst at this point; the partial wetting model of Al-Dahhan provides a reasonable estimate but it is clear that additional dependency on liquid flow rate comes into play in the current system.

Table 5-6. Partial wetting correction factor results

Run	Base model		Manually fitted		Best correlation		Correlation*	
	k_0 = 8.99E+8		k_0 = 1.89E+9		k_0 = 1.89E+9		k_0 = 1.89E+9	
	$X_{GO,exp}$	$X_{GO,cal}$	Partial wetting corr.	$X_{GO,cal}$	Partial wetting corr.	$X_{GO,cal}$	Partial wettin g corr.	$X_{GO,cal}$
1	0.895	0.923	0.473	0.895	0.473	0.895	0.565	0.958
2	0.946	0.951	0.494	0.9445	0.473	0.930	0.565	0.981
3	0.812	0.776	0.546	0.8115	0.563	0.825	0.565	0.827
4	0.689	0.545	0.713	0.6895	0.662	0.658	0.565	0.594
5	0.834	0.740	0.655	0.834	0.662	0.838	0.565	0.774
6	0.459	0.390	0.597	0.459	0.662	0.494	0.565	0.442
7	0.788	0.704	0.614	0.788	0.568	0.757	0.485	0.692
8	0.863	0.840	0.534	0.863	0.492	0.834	0.419	0.774
9	0.870	0.823	0.592	0.870	0.568	0.856	0.485	0.800
10	0.894	0.876	0.550	0.894	0.568	0.905	0.485	0.851
11	0.649	0.556	0.600	0.649	0.563	0.620	0.565	0.622
12	0.938	0.942	0.519	0.938	0.563	0.960	0.565	0.961
13	0.892	0.911	0.476	0.892	0.483	0.897	0.485	0.899
14	0.942	0.980	0.399	0.942	0.418	0.954	0.4195	0.955
15	0.752	0.714	0.529	0.752	0.483	0.712	0.485	0.714
16	0.961	0.992	0.396	0.961	0.483	0.996	0.485	0.996
17	0.793	0.856	0.414	0.793	0.418	0.797	0.4195	0.798
18	0.980	0.999	0.311	0.980	0.418	0.999	0.4195	0.999
19	0.911	0.919	0.492	0.911	0.477	0.900	0.485	0.906
20	0.876	0.882	0.491	0.876	0.479	0.867	0.485	0.871
21	0.908	0.929	0.480	0.908	0.479	0.907	0.485	0.912
22	0.641	0.543	0.590	0.641	0.479	0.514	0.485	0.521
23	0.815	0.850	0.448	0.815	0.479	0.839	0.485	0.843
24	0.909	0.919	0.478	0.909	0.479	0.909	0.485	0.913
25	0.964	0.974	0.485	0.964	0.479	0.961	0.485	0.964
	Error sum	0.1005		1.23E-5		0.052		0.112

* denotes that correction factor was calculated with Eq. 5-23-1.

Liquid feed flow rates play a more significant role in trickle bed wetting than any other parameter. Therefore, the correction factor ω was also numerically fitted only to flow rate, so Equation 5-23 can be rewritten as

$$\omega = 1359 m^{0.430} \qquad (5\text{-}23\text{-}1)$$

The last two columns of Table 5-6 list the corrector factor and corresponding outlet glycerol conversion. The value of the object function is 0.112, slightly worse than the original model and much worse than the correlation with Equation 5-21. This shows the base concentration plays a role in this correction factor, perhaps via changes in liquid viscosity or surface wetting that depend on base concentration.

5.7. Examination of Simplified Models for Trickle Bed Reactors

Previous discussion regarding the trickle bed model took mass and energy transport and reactor kinetics into account, and correction factor for partial wetting was introduced to better understand partial wetting, but how can we validate these considerations? In order to answer this question, examination of simplified models is necessary. The results from simplified models will be compared with those from the model discussed in Section 5.5 applied to the PNNL reactor data set in order to justify our work on modeling so far.

The trickle bed model incorporates several significant assumptions including a non-isothermal catalyst bed, mechanistically-based intrinsic rate expression, multiple mass transfer resistances, and partial wetting of the catalyst in the trickle bed. Here, we present simplifications of the original model that examine each of these assumptions to determine if their inclusion in the model is appropriate. The values of squared differences in outlet glycerol concentrations between experiment and model in the original and simplified models are used as criteria for the necessity of inclusion of each assumption in the model.

5.7.1. Isothermal Catalyst Bed

The reactor energy balance is eliminated for an isothermal catalyst bed, as temperature is constant at the specified value. The glycerol molar balance was integrated via Euler's method for all experiments, and new optimized values of the kinetic parameters k_o, K_H, and E_a were determined.

Table 5-7. Optimal parameters from isothermal catalyst bed assumption

Description	Unit	Value
Preexponential factor k_o	m^3/kg catalyst /sec	1.08E+9
Activation energy E_a	kJ/kmol	86,000
Hydrogen coeff. K_H	-	425
Heat transfer coeff. U_o	J/sec/m^2/K	100

With these optimal parameters, the value of the objective function (Eq. 5-22) for the isothermal trickle bed is 0.094, essentially equivalent to 0.100 from original comprehensive model. However, the observed temperature profile in the trickle bed cannot be represented by the isothermal model, so the inclusion of the energy balance in the trickle bed simulation is maintained.

It is entirely possible that the temperature gradient observed in reaction (Figure 5-4) arises because of radial heat transfer limitations, which are not accounted for in the current model. If this is true, then the isothermal model is a better representation of reality for GO hydrogenolysis because of water vaporization dampening gradients as described earlier. In either case, temperature effects do not play a large role in the trickle bed for GO hydrogenolysis.

5.7.2. Simplified Rate Expression

The mechanistically-based rate expression for GO hydrogenolysis (Eq. 5-8) includes two terms in the denominator. Under some experimental conditions, the C_{OH}-C_{GO} term is much larger than $K_H C_{H2}^{\ 2}$ at the reactor inlet, so the rate expression (Eq. 5-11) simplifies to the first order dependence on hydrogen only (Eq. 5-24).

$$-R_G = \varepsilon_W (1-\varepsilon_B)\eta_{H_2} k_f C_{H_2,S} + (1-\varepsilon_W)(1-\varepsilon_B)\eta_{H_2} k_f C^*_{H_2} \qquad (5\text{-}24)$$

With all the other assumptions the same, the simplified rate expression was implemented, and the trickle bed reactor balances were again integrated and kinetic parameters optimized. The resulting optimized kinetic parameters are listed in Table 5-8. With the simplified rate expression, the overall sum of squared differences (Eq. 5-22) is much larger (~3) than with the original model (0.100). Thus, the simplified rate expression assuming first order hydrogen dependence of rate does not predict trickle bed behavior as well as the rigorous rate expression (Eq. 5-11).

Table 5-8. Optimal parameters for model with simplified rate expression.

Description	Unit	Simplified rate expression	Analytical rate expression
Preexponential factor k_o	m^3/kg catalyst /sec	9.85E+7	1.15E+8
Activation energy E_a	kJ/kmol	86,000	86,000
Hydrogen coeff. k_H	-	-	425
Heat transfer coeff. U_o	J/sec/m^2/K	100	100

5.7.3. Fully Wetted Catalyst Bed

The low liquid velocities used in experiments necessitate application of the partial wetting correlation of Al-Dahhan.[38] Here we examine the effect of wetting on glycerol outlet conversion. First, the sensitivity of outlet GO conversion on fractional wetting was examined by varying ε_w from 50% to 200% of the value calculated by Al-Dahhan. For outlet GO conversions above 85%, varying the fraction wetted changed the outlet conversion by a maximum of 10% (e.g. at a conversion of 85%, down to 77% for ε_w twice its calculated value and up to 92% for ε_w half its calculated value). At lower conversion values, the fraction of the wetted bed had a greater effect on overall glycerol conversion in the trickle bed, illustrating the importance of partial wetting in the trickle bed process.

To examine the extreme condition of a fully wetted bed, the overall rate expression (Eq. 5-11) is simplified to contain only the term for the wetted catalyst as shown below (Eq. 5-25).

$$-R_G = (1-\varepsilon_B)\frac{\eta_{H_2} k_f C_{H_2,S} C_{GO} C_{OH^-}}{C_{GO} C_{OH^-} + K_H C_{H_2,S}^2} \qquad (5\text{-}25)$$

This fully-wetted bed rate expression was inserted into the reactor equations, and the integration/optimization process was performed for all the trickle bed experiments. In this form, the fully-wetted particle model significantly underpredicts outlet glycerol concentration from the trickle bed for all the experimental conditions. This is because the gas-liquid mass transfer resistance entirely limits the overall reaction rate in the fully-wetted bed, and the maximum possible reaction rate thus becomes the maximum gas-liquid mass transfer rate in the bed: $R_{G\text{-}L,\,max} = k_{GL,H2} a C^*_{H2}$ (Eq. 5-14). Assuming this value as constant throughout the trickle bed, the maximum possible glycerol conversion is about 55% at 8.5 MPa pressure, well below the values

obtained experimentally. Thus, either the value of the gas-liquid mass transfer coefficient is significantly higher than that predicted by the correlation of Goto and Smith,[42] or reaction rate is significantly enhanced by unwetted portions of the catalyst bed.

It is clear that partial wetting of the catalyst bed plays a significant role in determining trickle bed behavior at low flow conditions. The approach to model partial wetting for this reaction system leads to somewhat counterintuitive result that the unwetted portion of the bed must contribute significantly to overall reaction rate. Although others have looked in some detail at different ways to model partially wetted beds, the simplest approach, that of liquid replenishing of the unwetted region from bulk taken here, appears to be a reasonable means of characterizing wetting.

5.8. Gas-Liquid Mass Transfer Coefficient Sensitivity Analysis

The hydrogen gas-liquid mass transfer coefficient $k_{GL,H2}$ from the correlation of Goto and Smith[42] was varied from 50% to 200% of its calculated value and inserted into the partial-wetted trickle bed model for the PNNL reactor data set. For the full range of operating conditions, the outlet glycerol conversion varied by less than 5% over the range of $k_{GL,H2}$ investigated. This signifies that the unwetted portion of the bed is responsible for a significant portion of reaction, and that in the wetted portion gas-liquid mass transfer only moderately affects reaction rate.

5.9. Commercial Production Simulation

An initial commercial scale-up application of our model was done using the optimized kinetic constants from the PNNL reactor data set to simulate a trickle bed reactor with a yearly capacity of 100 million pounds of glycerol. Outlet glycerol conversion is over 90% with the right trickle bed configuration and operating conditions. Three scenarios were studied: one was done with the same WHSV as lab scale, the second with the same height/radius ratio as lab scale at given catalyst bed volume, and finally with different height/radius ratio.

With the same WHSV, the catalyst bed volume is proportional to incoming flow rate. In case of 100 MM lb/year glycerol capacity, the commercial bed volume is 9.8 m^3. Bed length was changed from 0.275 m (actual lab scale bed length) to 10 m. If the same diameter (0.0127 m) is used, the number of tubes can be calculated, and outlet glycerol concentration can be simulated by modifying our model accordingly.

For the other two cases, the same catalyst bed volume was used as case one, height and radius of catalyst bed was calculated and model was updated accordingly to get glycerol outlet concentrations. All the simulation glycerol conversion is listed in Table 5-9.

Table 5-9. Commercial process simulation summary

Scenario	Description	Glycerol Outlet Conversion (%)
Same WHSV	0.275 m	98%
	1.0 m	98%
	3.0 m	97%
	6.0 m	97%
	10.0 m	11%
Same H/radius ratio	H/radius=43.3	66%
Different H/radius ratio	H/radius=29	95%
	H/radius=30	90%
	H/radius=35	76%
	H/radius=40	69%

Chapter 6 Trickle Bed Model with Corrected Rate Expressions

During the derivation process in the previous chapter, stoichiometry in Eq. 5-3 was wrong. Two hydrogen molecules are needed in Eq. 5-3:

$$I \cdot S + 2H_2 \xrightarrow{k_3} PG + S \tag{6-1}.$$

Therefore, Eq. 5-6 becomes

$$r_3 = k_3 C_{I \cdot S} C_{H_2}^2 \tag{6-2}$$

and intrinsic rate expression changes to :

$$r_3 = \frac{k_f C_{GO} C_{OH^-} C_{H_2}^2}{C_{GO} C_{OH^-} + K_H C_{H_2}^3} \tag{6-3}.$$

The derivation process is discussed in the Appendix B.

With the updated rate expression, the overall rate expression has to change as well:

$$-R_G = \varepsilon_W (1-\varepsilon_B) \frac{k_f C_{GO} C_{OH^-} C_{H_2,S}^2}{C_{GO} C_{OH^-} + K_H C_{H_2,S}^3} + (1-\varepsilon_W)(1-\varepsilon_B) \frac{k_f C_{GO} C_{OH^-} C_{H_2}^{*2}}{C_{GO} C_{OH^-} + K_H C_{H_2}^{*3}} \tag{6-4}$$

The ensuing discussion is the correction made to reflect these changes with the rest the same.

6.1. Results

The corrected reactor model was applied to the same set of steady state trickle bed reactor experiments at a variety of operating conditions (Table 6-1) to predict outlet GO conversion in each experiment.

Table 6-1. Summary of Trickle Bed Run Conditions and Results

Exp. Number	Feed Inlet Temp (K)	Total Pressure (MPa)	Feed flow rate (ml/hr)	NaOH Conc. (M)	Experimental Glycerol Conversion	Predicted Glycerol Conversion
1	468	8.27	50	0.58	0.90	0.97
2	464	8.27	50	0.58	0.95	0.98
3	467	8.27	50	0.28	0.81	0.84
4	464	8.27	50	0.14	0.69	0.55
5	475	8.27	50	0.14	0.83	0.75
6	453	8.27	50	0.14	0.46	0.38
7	463	8.27	35	0.14	0.79	0.67
8	463	8.27	25	0.14	0.86	0.81
9	473	8.27	35	0.14	0.87	0.85
10	473	8.27	35	0.14	0.89	0.85
11	453	8.27	50	0.28	0.65	0.58
12	475	8.27	50	0.28	0.94	0.95
13	463	8.27	35	0.28	0.89	0.90
14	463	8.27	25	0.28	0.94	0.97
15	453	8.27	35	0.28	0.75	0.72
16	473	8.27	35	0.28	0.96	0.99
17	453	8.27	25	0.28	0.79	0.85
18	473	8.27	25	0.28	0.98	1.00
19	463	8.27	35	0.28	0.91	0.90
20	463	11.03	35	0.28	0.88	0.83
21	463	5.52	35	0.28	0.91	0.96
22	463	2.76	35	0.28	0.64	0.60
23	463	13.79	35	0.28	0.82	0.79
24	468	13.79	35	0.28	0.91	0.87
25	468	8.27	35	0.28	0.96	0.96

The strategy of the modeling exercise was to identify the set of kinetic parameters k_o, E_a (used for calculation of k_f which is assumed to follow Arrhenius equation), and K_H in the rate expression (Eq. 6-3) that minimizes the objective function defined in Eq. 5-22 (essentially the sum over all 25 experiments of the square of the differences in square roots of the experimental and predicted GO outlet concentrations from the trickle bed reactor). Because the reaction is only partial order in GO, this objective function, defined for a one-half order reaction, was found to

lead to the best overall fit of the data at both low and high GO conversions. To help in the optimization, an initial value of activation energy E_a, calculated from batch reactor initial rate data, was used in order to facilitate more rapid error minimization.

$$obj.function = \sum_i (\sqrt{1 - X_{i,GO,\exp}} - \sqrt{1 - X_{i,GO,cal}})^2 \qquad (5\text{-}22)$$

Optimized values of the kinetic parameters are listed in Table 6-2. A comparison of experimental and predicted outlet GO conversions for all experiments is given in Table 6-2 and as a parity plot in Figure 6-1.

Table 6-2. Optimized kinetics parameters for rate expression (Eq. 6-3).

Description	Unit	Value
k_o	m^6 fluid/kmol/m^3 catalyst/sec	8.26×10^{10}
E_a	kJ/kmol	86,000
K_H	m^3/kmol	4.86×10^4

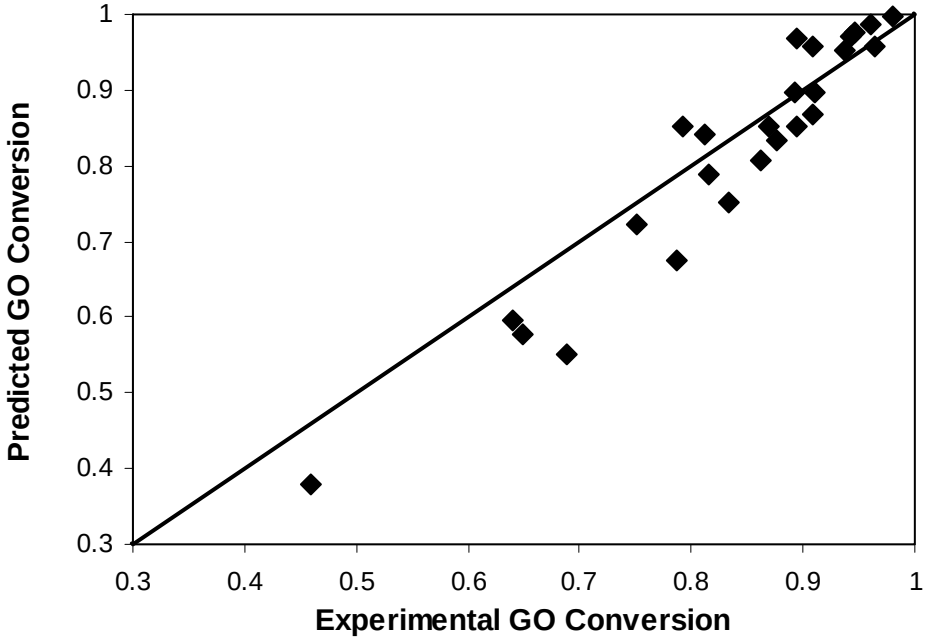

Figure 6-1. Trickle bed simulation parity plot with corrected rate expression.

In general, there is good agreement between predicted and experimental reactor performance – a remarkable outcome given that only the three kinetic constants are adjusted and all other constants and coefficients governing hydrodynamics and mass/heat transfer in the model are taken straight from literature or textbook correlations. For the optimized kinetic parameters, the value of the objective function in Eq. 5-22 is 0.123; in simplified terms, the average value of the absolute difference between experimental and simulated outlet GO conversion is 0.0455. An example of the experimental and predicted temperature profiles along the trickle bed at three different inlet temperatures is given in Figure 6-2; the model reasonably predicts the mild exotherms in the trickle bed reactor over the temperature range examined.

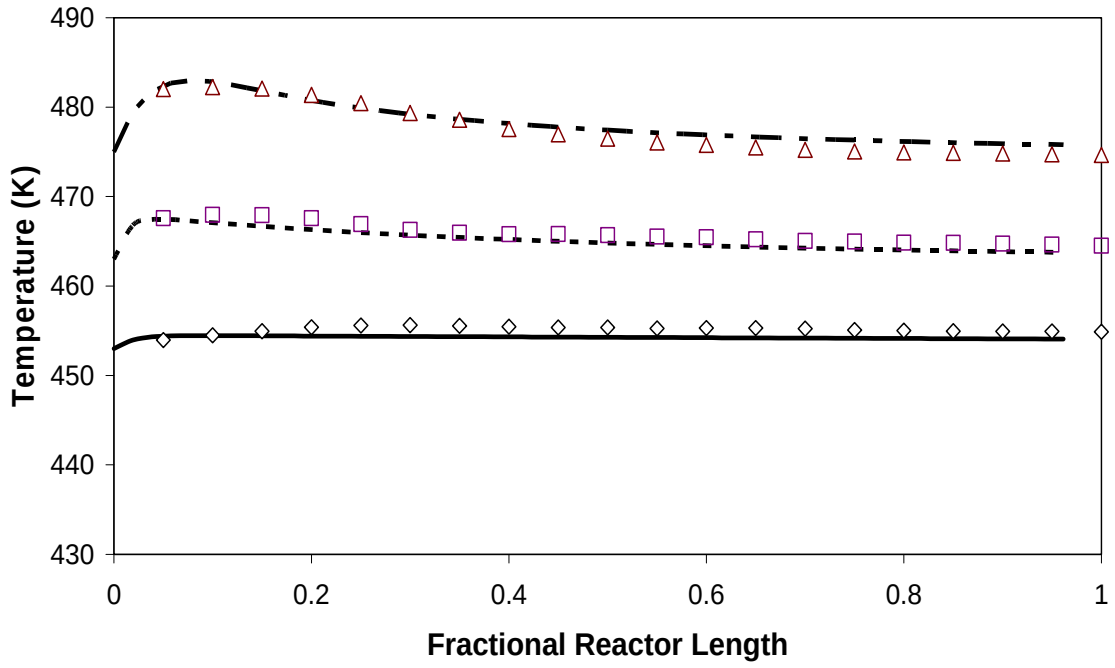

Figure 6-2. Predicted vs. experimental temperature profile in trickle bed. Inlet temperature: 453 K (Exp. 6): (—) – simulation, (◇) – experiment; 463 K (Exp. 7): (- - -) – simulation, (□) – experiment; 473 K (Exp. 9): (−·−·−) – simulation, (△) - experiment. Conditions: 8.27 MPa, liquid feed rate 35 ml/hr, 0.14 M NaOH.

The model can also illustrate species concentration profiles in the trickle bed; Figure 6-3 gives predicted GO concentration profiles as a function of a) inlet temperature, b) liquid feed flow rate, and c) feed base concentration at conditions that match those in the experiments identified. Figure 6-4 compares the experimental and predicted GO conversion on total reactor pressure; the sharp drop in conversion at the lowest pressure (2.76 MPa, Exp. 22) is attributed to low hydrogen partial pressure because water partial pressure at 463 K is 1.3 MPa, a significant fraction of the total. The observed drop in GO conversion as pressure increases above ~6 MPa is predicted by the mechanistically-based rate expression.

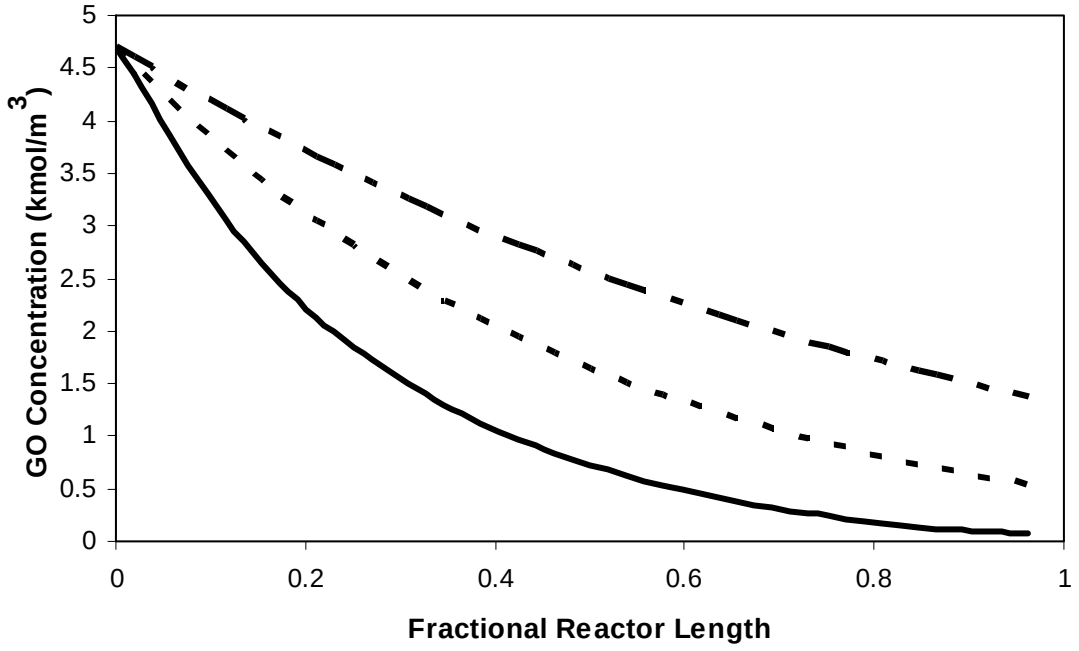

Figure 6-3a. Simulated GO concentration profiles in trickle bed for different inlet temperatures. (−·−·−) – 453 K (Exp. 15); (- - -) – 463 K (Exp. 13); (——) – 473 K (Exp. 16). Conditions: 8.27 MPa, liquid feed rate 35 ml/hr, 0.28 M NaOH.

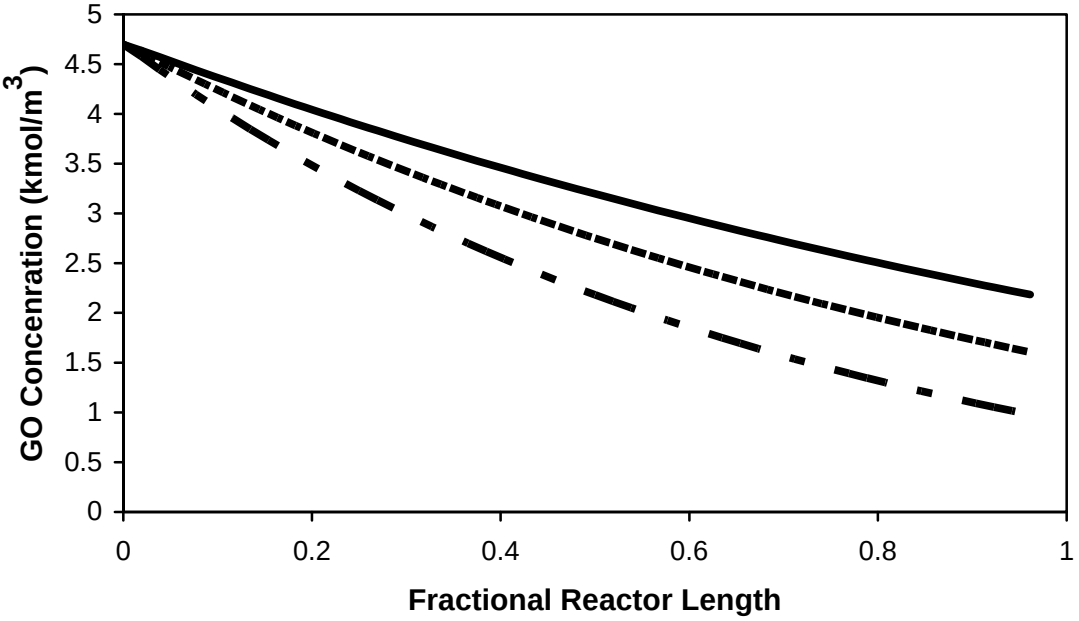

Figure 6-3b. Simulated GO concentration profiles in trickle bed for different liquid feed flow rates: (——) – 50 ml/hr (Exp. 4); (- - -) – 35 ml/hr (Exp. 7); (−·−·−) – 25 ml/hr (Exp. 8). Conditions: 8.27 Mpa, 463 K, 0.14 M NaOH.

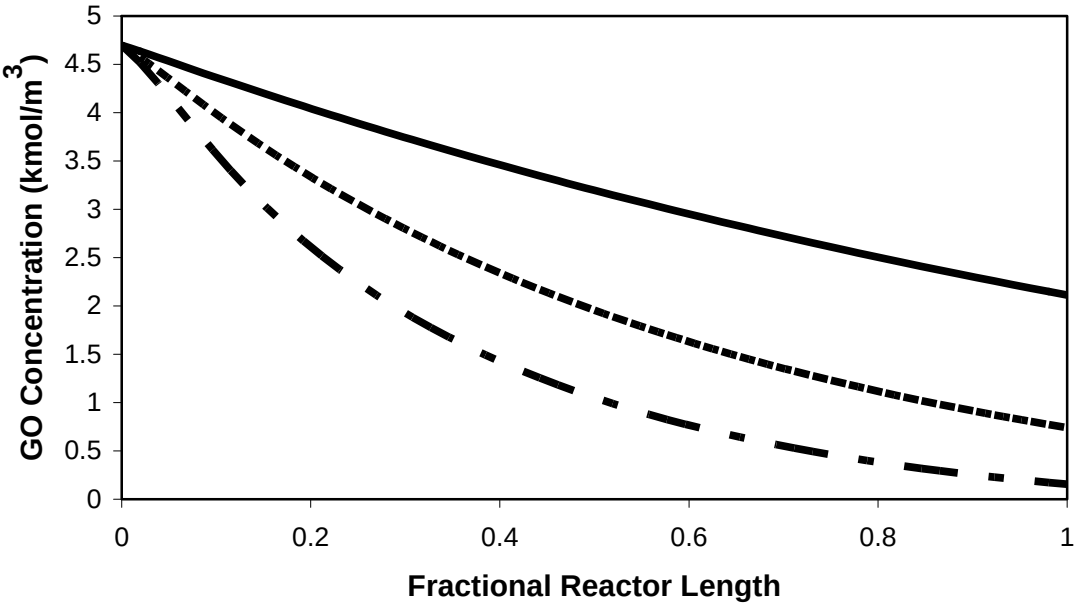

Figure 6-3c. Simulated GO concentration profiles in trickle bed at different NaOH concentrations: (−·−·−) - 0.58 M (Exp. 2); (- - -) - 0.28 M (Exp. 3); (——) - 0.14 M (Exp. 4). Conditions: 8.27 MPa, 464 K, liquid feed rate 50 ml/hr.

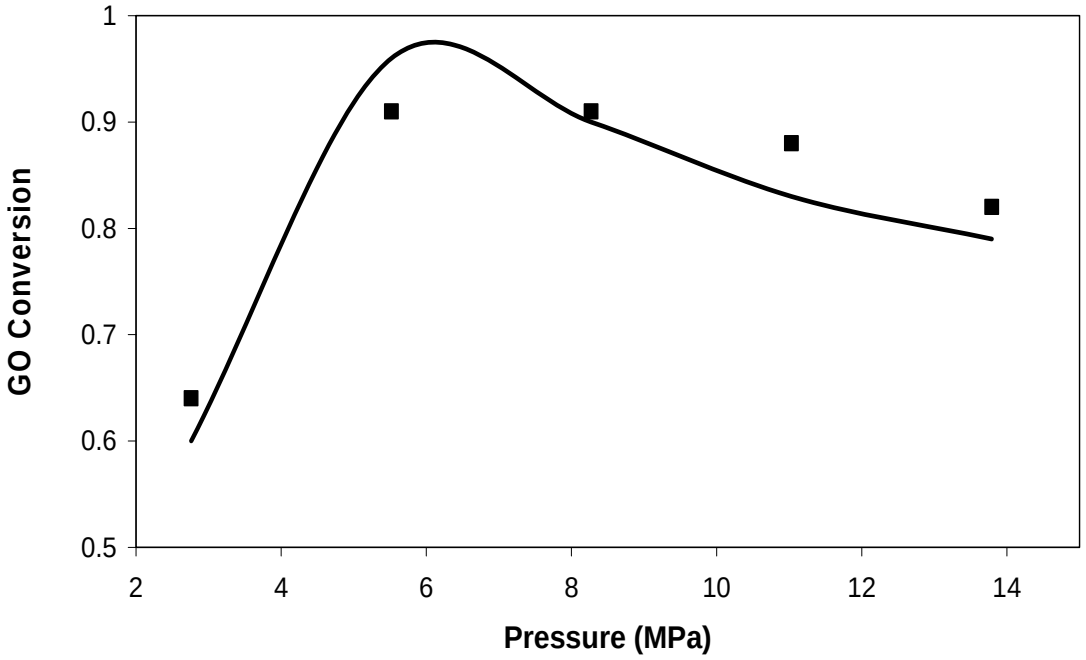

Figure 6-4. Effect of pressure on outlet GO conversion from trickle bed reactor. (—) - simulation; (■) -experiment . Conditions: 463 K, liquid feed rate 35 ml/hr, 0.28 M NaOH.

If the rate expression (Eq. 6-3) with coefficients from Table 6-2 is evaluated at 463 K at the reactor inlet (C_{GO} = 4.6 M; C_{OH^-} = 0.28 M; P_{H2} = 8.3 MPa) and normalized to the catalyst site density of 1.3×10^{-5} kmol/kg, the resulting turnover frequency (TOF) is approximately 0.31 kmol H_2/kmol metal site/sec. This is a reasonable value for GO hydrogenolysis at these conditions.

6.2. Evaluation of Model Assumptions

The trickle bed model incorporates several significant features including a non-isothermal catalyst bed, mechanistically-based intrinsic rate expression, multiple mass transfer resistances, and partial wetting of the catalyst in the trickle bed. Here we present simplifications of the

original model that examine each of these assumptions to determine if their inclusion in the model is appropriate. The difference in value of the objective function given in Eq. 5-22 in the original and simplified models is used as a criterion for the validity of inclusion of each assumption in the model.

It is noted here that attempts were made to model glycerol hydrogenolysis with simple n^{th}-order reaction kinetics in glycerol and hydrogen along with the mass transfer effects. None of these kinetic models gave a reasonably approximation of the experimental trickle bed data. Thus, inclusion of the mechanistically based rate expression with the observed dependence on glycerol and hydrogen is an integral part of the modeling process.

6.2.1. Isothermal Catalyst Bed

The reactor energy balance Eq. 5-10 is eliminated for an isothermal catalyst bed, as temperature is constant at the specified inlet value. The GO molar balance was integrated via Euler's method for all experiments, and the kinetic parameters k_O and K_H were re-optimized to minimize the objective function. The new optimized values are $K_H = 4.6 \times 10^4$ m^3/kmol and $k_O = 8.83 \times 10^{10}$ m^6 fluid/kmol/m^3 catalyst/sec. With these optimal isothermal bed parameters, the value of the objective function Eq. 5-22 for the isothermal trickle bed is 0.106, a value slightly smaller than the value of 0.123 obtained for the complete model. The average difference between predicted and experimental GO conversions for the isothermal model is 0.040 vs. 0.045 for the complete model.

Although the isothermal model thus appears to fit the GO conversion data slightly better than the complete model, the fact that it cannot predict temperature gradients in the trickle bed,

which may be important in an expanded range of operation, makes it less attractive than the complete model.

It is possible that reactor temperature gradients measured experimentally (Figure 6-3a) arise in part because of radial heat transfer resistances, which are not accounted for in the model. At this point, it is not possible to distinguish the effects of radial from axial temperature gradients because of limited measurement capabilities.

6.2.2. Fully Wetted Catalyst Bed

The low liquid velocities used in experiments necessitate application of the partial wetting correlation of Al-Dahhan. Here, we examine the effect of fractional wetting (ε_w) of the catalyst bed on outlet conversion. First, the sensitivity of outlet GO conversion on fractional wetting was examined by varying ε_w from 50% to 200% of the value calculated by Al-Dahhan. For outlet GO conversions above 85%, varying the fraction wetted changed the outlet conversion by a maximum of 10% (e.g. at a conversion of 85%, down to 77% for ε_w of twice its calculated value and up to 92% for ε_w of half its calculated value). At lower conversion values, the fraction wetted had a greater effect on overall GO conversion in the trickle bed, illustrating the importance of partial wetting in the trickle bed process.

To examine the extreme condition of a fully wetted bed, the overall rate expression (Eq. 6-4) is simplified to contain only the term for the wetted catalyst as shown below (Eq. 6-5).

$$-R_G = (1-\varepsilon_B)\frac{k_f C_{GO} C_{OH^-} C_{H_2,S}^2}{C_{GO} C_{OH^-} + K_H C_{H_2,S}^3} \qquad (6\text{-}5)$$

This fully-wetted bed rate expression was inserted into the reactor equations and the integration/optimization process was performed over all trickle bed data. In this form, the fully-wetted particle model significantly underpredicts outlet GO concentration from the trickle bed at all but the highest pressure (13.8 MPa) investigated. At the lower pressures, gas-liquid mass transfer resistance limits the overall reaction rate in the fully-wetted bed, and the maximum possible reaction rate thus becomes the maximum gas-liquid mass transfer rate in the bed: $R_{G\text{-}L,\ max} = k_{GL,H2} a C^{*}_{H2}$. Assuming this value as constant throughout the trickle bed, the maximum possible GO conversion is about 57% at 8.3 MPa pressure (7.5 MPa H_2 pressure), well below the values obtained experimentally. At the highest pressure (13.8 MPa, Runs 23 and 24), the predicted conversions are close to the experimental values, suggesting that the reaction is moving away from being hydrogen mass transfer limited in the wetted fraction at high pressures. Overall, however, the conclusion must be drawn that the unwetted portion of the catalyst bed contributes significantly to reaction rate. It is possible that the actual value of the gas-liquid mass transfer coefficient is significantly larger than that predicted by the correlation of Goto and Smith[42] and thus the bed could be nearly fully wetted and giving the observed conversions, but that notion is inconsistent with the literature and the correlations used for both wetting and mass transfer.

Further, the substantial body of literature on trickle bed reactors clearly indicates that partial wetting of the catalyst bed plays a significant role in determining trickle bed behavior at low flow conditions. The question of how the unwetted portion of a trickle bed reactor contributes to reaction, as assumed here, seems difficult at first to reconcile. We make the assumption that the pore volume of all catalyst particles in the bed are filled with liquid, and that

the bulk liquid flowing over part of the catalyst is continuously changing its path along the trickle bed. Thus, while only a portion of the catalyst is wetted at any instant, the particular portion wetted changes continuously. When catalyst particles are wetted, the liquid inside them exchanges reactants and products with the bulk liquid, hence facilitating reaction when again unwetted. This continuous liquid replenishing of the unwetted region from bulk liquid appears a reasonable first approximation of characterizing partial wetted trickle beds, and avoids the major challenges associated with attempting to model bed hydrodynamics.

6.2.3. Gas-Liquid Mass Transfer Coefficient Sensitivity Analysis

The hydrogen gas-liquid mass transfer coefficient $k_{GL,H2}$ from the correlation of Goto and Smith was varied from 50% to 200% of its calculated value and inserted into the partial-wetted trickle bed model. Over the full range of experimental conditions, the outlet GO conversion varied by less than five percentage points over the range of $k_{GL,H2}$ investigated. This outcome is partially explained by the fact that the reaction rate (Eq. 6-3) is weakly or even negatively dependent on hydrogen concentration ($C_{H2,\,S}$) at the catalyst particle, and also by the fact that the unwetted portion of the trickle bed makes a substantial contribution to overall reaction rate.

6.3. Conclusions

Experimental data of GO hydrogenolysis in a laboratory-scale trickle bed reactor have been described with a one-dimensional, nonisothermal trickle bed reactor model involving a mechanistically-based kinetic rate expression, intraparticle mass transport, interphase mass

transport, and partial wetting of the catalyst bed. The model is fit to the experimental data by optimizing values of the kinetic constants in the rate expression. The rate expression predicts rate dependencies on GO and H_2 that vary significantly in order depending on particular experimental conditions, indicating that the interplay between mass transport resistances, fractional wetting of catalyst, and observed reaction rate is complex. Axial temperature gradients are small ($<10^oC$) yet play a role in the trickle bed, and the unwetted portion of the bed contributes significantly to overall reaction rate. Accounting for all complexities and assumptions, the model reasonably predicts the outlet conversion of GO from the trickle bed.

Chapter 7 Intrinsic Reaction Rate Correlation for Batch and Trickle Bed Reactors

Trickle bed reactors are commonly used on a commercial scale for hydrogenolysis of liquid-phase reactants.[44-46] Much work has been done to study mass transfer, energy transfer, reaction kinetics, and partial wetting [47-50] of trickle bed reactors for the purpose of better predicting and characterizing their operation. Even so, trickle bed reactors remain complex unit operations that are often subject to mass transport and hydrodynamic limitations at practical operating conditions. Because of these complications, laboratory and pilot-scale trickle bed reaction studies often give results that are difficult to interpret from a fundamental viewpoint, and scale-up of trickle beds is subject to uncertainty and risk.

In contrast to trickle beds, bench-scale batch reactors are easy to operate in an intrinsic kinetic reaction mode and are thus effective tools for evaluating catalysts and conditions for three-phase reactions. With greater control of mass transfer by vigorous agitation of fully-wetted catalyst and temperature to control rate, batch reactors are efficient and reliable tools.

Despite the utility of batch reactors for fundamental reaction characterization, little work has been done[51-55] so far to relate batch reactor results to actual or potential trickle bed operation for three phase reaction systems, particularly hydrogenolysis of aqueous-phase reactants derived from biomass sources. This chapter will take such a step by examining the hydrogenolysis of aqueous solutions of lactic acid to propylene glycol, a reaction system with high selectivity to PG and few byproducts,[56-58] over a carbon supported ruthenium catalyst in both trickle-bed and batch reaction systems. The goal of this work is to gain the ability to predict trickle-bed performance based on batch reaction studies to facilitate more efficient scale-up and design. We

do this by comparing reaction rates at different conditions and then analyzing to gain a better understanding of the roles that mass transfer, heat transfer, and wetting play in the hydrogenolysis.

7.1. Kinetic Model for Lactic Acid Conversion

Lactic acid hydrogenolysis kinetics in a stirred batch reactor with a catalyst similar to that used in this work have been reported previously by Zhang et al.[59] Experimental data were fit to a mechanistically based Langmuir-Hinshelwood rate expression as is shown in Eq. 7-1. Reaction rate coefficients, k, K_{H2}, and K_{LA}, were fit with MathCad to data at 403 K and 423K with different catalyst loadings (0.5g, 1.0g, and 1.5g) in 100 g 1.15 M lactic acid solution at different pressures (6.8 MPa, 10.2 MPa, and 13.6 MPa).

$$-r_{LA} = \frac{kC_{LA}P_{H_2}}{(1 + K_{H_2}P_{H_2} + K_{LA}C_{LA})^2} \qquad (7\text{-}1)$$

To apply Eq. 7-1 to this study, rate constants determined at 403 and 423 K were extrapolated using an Arrhenius expression to the temperatures (353 K and 363 K) at which reactions were carried out. Table 7-1 lists the values of the constants in the rate expression at all five temperatures, with rate written on a unit catalyst volume basis.

Table 7-1. Constants in Kinetic Model for Lactic Acid Hydrogenation

Constant*	Preexponential factor (k_o or A_o)	Activation energy (E_a) or heat of adsorption (ΔH_i) (kJ/kmol)
k (m^3/m^3 catalyst/MPa/s)	2.4 E-2	12,400
K_{H2} (MPa^{-1})	1.6 E-13	-79,800
K_{LA} (m^3/kmol)	8.0 E-8	-47,800

*$k = k_o \exp(-E_a/RT)$; $K_i = A_o \exp(-\Delta H_i/RT)$

7.2. Parallel Experiment Runs

In order to compare reaction rates in batch and trickle bed systems, identical conditions were applied to catalyst reduction, hydrogenolysis reactions, and sampling methods in each reactor. A temperature of 363 K was found to give high enough reaction rates to be easily measured yet not so high as to become mass transport limited, as the Weisz-Prater observable modulus for hydrogen was less than 0.05 for all experiments. Experiments in both reactors showed excellent mass conservation and carbon balances. Mass loss was less than 5% in both reactors, and carbon balances were 100% ± 5% in batch runs and 96% ± 5% in trickle bed runs. The experiments at these low temperatures showed no gas product formation; hence all yield calculations were based only on HPLC analyses of aqueous phase products.

7.2.1. Batch Reactor Experiments

Experiments were carried out at 363 K, 8.3 MPa hydrogen pressure, an initial lactic acid solution concentration in water of 1.0 kmol/m^3, and a total liquid volume of 5.0×10^{-5} m^3. Three different catalyst loadings (0.125g, 0.25g, and 0.5g) were examined to validate that reactions take place in the intrinsic kinetic regime. Figure 7-1 shows propylene glycol yield with respect to time for the different catalyst loadings.

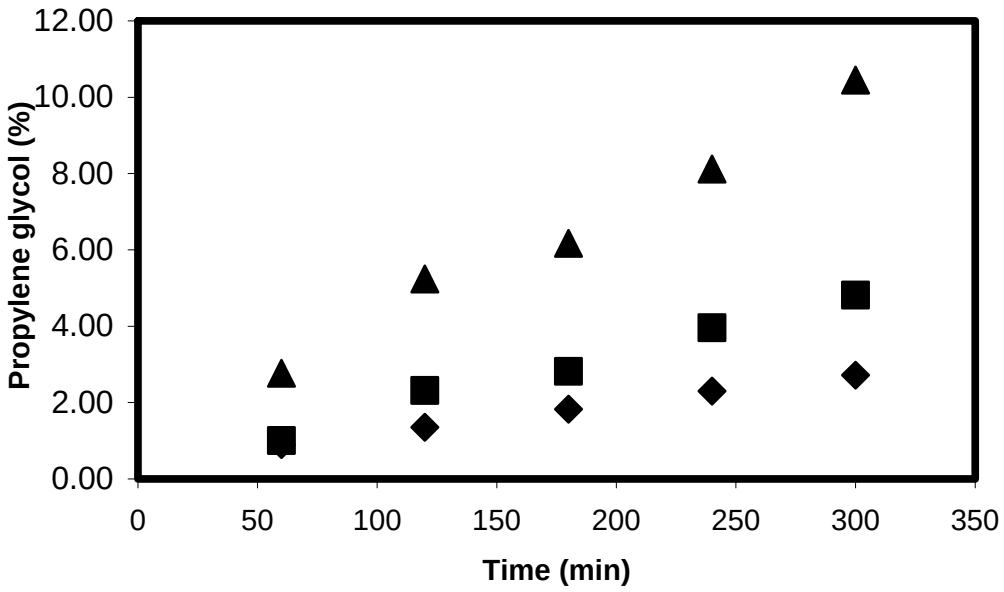

Figure 7-1. Propylene glycol yield versus time in a batch reactor at 363 K and 8.3 MPa H_2 (▲- 0.5 g catalyst; ■ - 0.25 g catalyst; ♦ - 0.125 g catalyst).

Figure 7-1 shows that propylene glycol yield is linear at low conversion, so lactic acid hydrogenolysis rate is constant over the course of reaction. The value of the rate on a per unit catalyst mass basis, determined from the slopes of the curves in Figure 7-1, is $5.8 \times 10^{-7} \pm 3 \times 10^{-8}$ kmol/kg catalyst/sec. The value predicted by Eq. 7-1 is 5.3×10^{-7} kmol/kg catalyst/sec at

the same conditions, somewhat low but in reasonable agreement considering that the kinetic constants were determined at significantly higher temperatures and extrapolated to 363 K.

7.2.2. Trickle Bed Reactor Experiments

For the trickle bed runs, three catalyst beds were constructed: one containing 19.0 g (45 cm^3) catalyst, another 9.1 g (22.5 cm^3) catalyst, and a third containing 9.0 g (22.5 cm^3) catalyst diluted with 22.5 cm^3 inert glass beads as fines. The beds are noted according to volume in Tables 7.2; the bed with glass bead fines is denoted with a star. The inert glass bead diameter for the diluted bed (d_{fines} ~ 0.02 cm) was chosen to be approximately one-tenth of the catalyst particle's diameter, as suggested by Tsamatsoulis et al.[60] to enhance wetting of the catalyst.

The feed rate of lactic acid solution (1.0 M) was varied to investigate the effect of catalyst particle wetting on lactic acid conversion and reaction rate. In order to achieve experimental conditions consistent with those in the batch reactor, relatively high liquid feed flow rates (up to 200 ml/hr) were applied. Several temperatures from 353 K to 373 K were examined in trickle bed runs, and hydrogen flow rate was adjusted to maintain excess hydrogen (a 2.5:1 molar ratio of hydrogen: lactic acid). It generally took 2-3 hours to reach steady state in the trickle bed reactor. Reaction conditions are listed in Table 7-2 for all the trickle bed runs.

Table 7-2. Lactic Acid Hydrogenolysis Trickle Bed Experiments (at 1200 psi, 1.0 M initial lactic acid solution, and catalyst 3224-25-1)

Experiment Serial No.	Temperature (℃)	Feedstock flow rate (ml/hr)	Catalyst volume (cm^3)	LA Conversion	PG Selectivity	Carbon Balance
TBR 34	140	25	45	0.999	0.464	0.466
TBR 35	140	50	45	1	0.684	0.684
TBR 36	140	75	45	0.995	0.676	0.683
TBR 37	140	100	45	1	0.584	0.584
TBR 38	140	200	45	0.994	0.508	0.511
TBR 39	120	200	45	0.886	0.726	0.758
TBR 40	120	100	45	0.921	0.699	0.723
TBR 41	120	75	45	0.9	0.73	0.757
TBR 42	120	50	45	0.952	0.668	0.683
TBR 43	120	25	45	0.86	0.636	0.687
TBR 44	100	50	45	0.991	0.784	0.786
TBR 45	100	50	45	0.98	0.827	0.83
TBR 46	100	100	45	0.841	0.824	0.852
TBR 47	80	50	45	0.649	0.564	0.915
TBR 48	60	50	45	0.243	0.222	0.979
TBR 49	80	200	45	0.205	0.9	0.98
TBR 50	90	200	45	0.356	0.851	0.947
TBR 51	90	100	45	0.617	0.856	0.911
TBR 53	80	100	45	0.389	0.812	0.927
TBR 54	90	200	22.5	0.127	0.898	0.987
TBR 55	90	100	22.5	0.217	0.953	0.99
TBR 56	80	100	22.5	0.147	0.924	0.988
TBR 57	80	200	22.5	0.052	1	1.013
TBR 58	90	100	22.5*	0.232	0.851	0.965
TBR 59	90	200	22.5*	0.108	0.979	0.998
TBR 60	90	1.0	22.5*	0.416	0.76	0.9
TBR 61	90	1.0	22.5*	0.551	0.867	0.927
TBR 62	80	25	22.5*	0.395	0.899	0.96
TBR 63	80	50	22.5*	0.245	0.917	0.98
TBR 64	80	100	22.5*	0.162	0.762	0.962
TBR 65	80	200	22.5*	0.081	0.756	0.98

The approach to steady state operation for each of the three different trickle bed reactors at 363 K, 8.3 MPa H_2, and flow rates of 100~200 ml/hr aqueous solution of lactic acid is shown

in Figure 7-2. Given that overall conversion is relatively low for the two smaller catalyst beds (<20%), we make the assumption, in accordance with rate behavior in the batch reactor, that lactic acid reaction rate is essentially constant in the trickle bed. The average reaction rate was thus readily calculated as $-R_{LA,G} = C_{LAo}X_{LA}/(1-\varepsilon_B)/\tau$ from inlet flow rate, lactic acid conversion, and catalyst mass. Values of these average rates determined from the trickle bed reactor operating in a "differential" mode are given in Table 7-3.

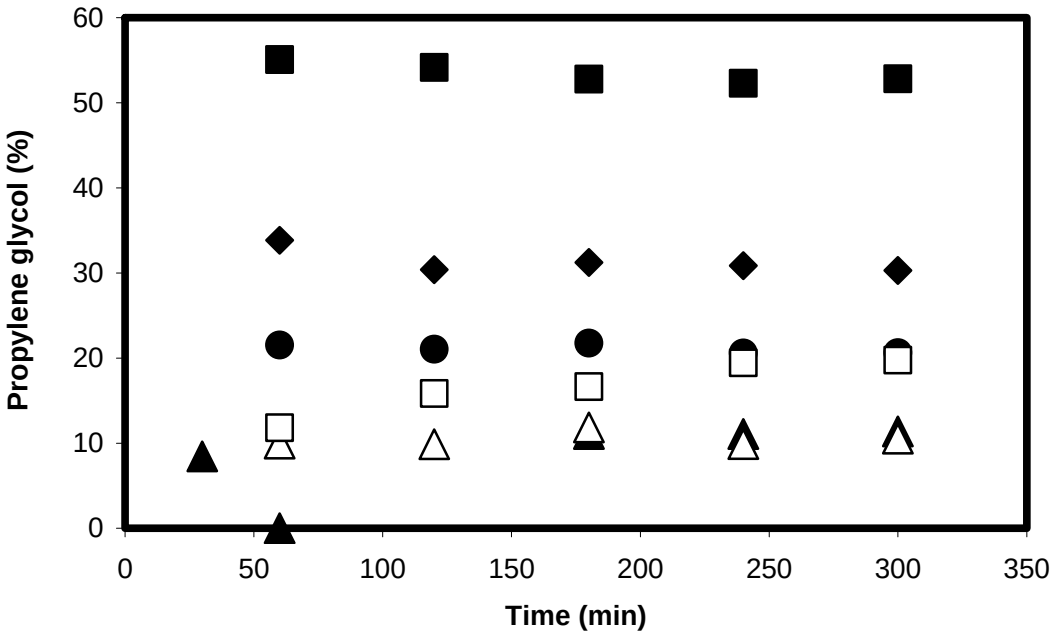

Figure 7-2. Propylene glycol yield (363 K; 8.3 MPa H_2) versus time with different flow rates. ♦ - 45 ml catalyst at 200 ml/hr; ■ - 45 ml catalyst at 100 ml/hr; ▲ - 22.5 ml catalyst at 200 ml/hr; ● - 22.5 ml catalyst bed at 100 ml/hr; □ - 22.5 ml catalyst and 22.5 ml inert glass beads at 100 ml/hr; Δ - 22.5 ml catalyst and 22.5 ml inert glass beads at 200 ml/hr.

Under these reaction conditions, the literature wetting efficiency correlation of Al-Dahhan[38] indicates that the trickle beds are only partially wetted (ε_W = 0.35 at 100 ml/hr and ε_W = 0.44 at 200 ml/hr). Interestingly, the conversion in the 22.5 cm^3 Ru/C catalyst bed with and

without fines is essentially the same – this suggests that either the addition of fines has relatively little effect on the fraction of catalyst wetted, or that both beds are fully wetted and thus the

Table 7-3. Propylene glycol formation rates in trickle bed and batch reactors (T = 363 K; 8.3 MPa H_2; 1.0 M solution lactic acid feed)

Flow rate (ml/hr)	200	100
Catalyst bed mass (g)	$R_{PG,G}$ (kmol/m^3cat/sec)	
9.1	$5.5\pm0.4 \times 10^{-4}$	$5.1\pm0.4 \times 10^{-4}$
9.1 + fines	$5.1\pm0.4 \times 10^{-4}$	$4.9\pm0.4 \times 10^{-4}$
Batch	$4.6\pm0.3 \times 10^{-4}$	

correlation of Al-Dahhan is not applicable to this aqueous phase system. The close agreement of trickle bed and batch reaction rate, especially in the shorter bed and with fines present, is further evidence that the trickle bed under these high liquid flow rates is essentially operating under intrinsic kinetic conditions, and is thus fully wetted.

The higher average rate in the larger (45 cm^3) trickle bed is not readily explained. The conversion (30% and 55%) at these conditions is clearly higher than what could be considered the differential mode of operation, but that would lead to a lower, not a higher, overall rate in the bed because rate increases with lactic acid concentration in the range used. Wetting efficiency should be the same in shorter and longer beds at the same flow rate, because the liquid velocity ($kg/m^2/sec$) is unchanged. Other possibilities, including liquid channeling, could lead to higher conversions if the catalyst becomes only partially wetted in the lower regions of the larger beds.

At this point, we attribute the higher rate either to channeling which results in partial wetting or to a greater exotherm in the bed because of the higher conversions, and thus a slight increase in overall bed temperature results.

The results represent, to our knowledge, the first case of direct comparison of reaction rates under identical conditions in aqueous batch and trickle bed reactions, and indicate that it is possible to achieve intrinsic kinetics in a trickle bed reactor, albeit at conditions (e.g. high flow rates and low conversions) that are far from those that would be chosen to optimize product yields.

7.3. Trickle Bed Reactor Modeling

To further explore the relationship between trickle bed performance and intrinsic reaction kinetics, experiments were completed in the trickle bed reactor at 353 K and 363 K at four different flow rates (25 ml/hr, 50 ml/hr, 100ml/hr, and 200 ml/hr) with the 22.5 ml Ru/C catalyst bed diluted with 22.5 ml inert glass beads as fines. Initial lactic acid concentration for all experiments was 1.0 M, and hydrogen pressure was maintained constant at 8.3 MPa.

We have previously developed a detailed trickle bed reactor model for glycerol hydrogenolysis that accounts for interphase mass transfer, temperature gradients, and catalyst particle partial wetting. We apply that model here, in several simplified forms, to hydrogenolysis of lactic acid, including the intrinsic kinetic expression shown in Eq. 7-1 to describe reaction rate. The goal of this modeling is to identify those aspects and assumptions of the trickle bed model that are important in predicting trickle bed reactor behavior.

The trickle bed reactor is modeled as a one-dimensional system with liquid in plug flow, such that the molar balance for lactic acid can be written as

$$-\frac{dC_{LA}}{d\tau} = (1-\varepsilon_B)R_{LA,G} \qquad (7\text{-}2)$$

No balance for the gas phase is required – the gas phase is composed solely of water at its vapor pressure and hydrogen, since there are no gas-phase products formed in LA hydrogenolysis as is proved by the gas sample analysis. The reactor is assumed to be isothermal for two reasons – first, its temperature is controlled by silicon oil that circulating at a high rate through the jacket surrounding the reactor; and second, changes in reactor temperature are dampened by water vaporization as temperature is increased to maintain saturation of the vapor phase.

For the trickle bed, the rate expression (Eq. 7-1) can be written in terms of hydrogen concentration instead of partial pressure using Henry's law

$$P_{H_2} = H_A \cdot C_{H_2} \qquad (7\text{-}3)$$

with the Henry's law constant for hydrogen in water is equal to 120 MPa/M. [43]

In the wetted fraction of the trickle bed reactor, the diffusion of hydrogen limits reaction to a greater degree than lactic acid because it must diffuse across the gas-liquid interface and because of its low concentration (solubility) in water (C_{H2}^{*} = 0.068 M at 8.3 MPa pressure) relative to lactic acid (~1.0 M). The trickle bed model must therefore account for mass transport resistances of hydrogen across the gas-liquid and liquid-solid interfaces in the wetted fraction of the trickle bed. At steady state, the hydrogen mass transfer rates must equal the hydrogen consumption rate in the catalyst ($-r_{H2} = 2(-r_{LA})$):

$$k_{GL}a(C_{H_2}^{*} - C_{H_2,L}) = k_{LS}a(C_{H_2,L} - C_{H_2,S}) = 2\eta_{H_2}(1-\varepsilon_B)(-r_{LA}) \qquad (7\text{-}4)$$

Inserting the rate expression (Equation 7-1) into Equation 7-4, the actual hydrogen concentration in the liquid phase ($C_{H2,\,L}$) and at the catalyst surface ($C_{H2,\,S}$) can be found from the resulting equations:

$$C_{H_2,L} = \frac{k_{GL}a \cdot C^*_{H_2} + k_{LS}a \cdot C_{H_2,S}}{k_{GL}a + k_{LS}a} \tag{7-5}$$

and

$$\begin{aligned} &k_{GL}a \cdot k_{LS}a \cdot K^2_{H_2} H^2_A C^3_{H_2,S} + k_{GL}a \cdot k_{LS}a \cdot K_{H_2} H_A (2 + 2K_{LA}C_{LA} - K_{H_2} C^*_{H_2} H_A) C^2_{H_2,S} \\ &+ (k_{GL}a \cdot k_{LS}a \cdot \left(1 + 2K_{LA}C_{LA} + K^2_{LA}C^2_{LA} - 2K_{H_2}H_A C^*_{H_2} - 2K_{H_2}H_A C^*_{H_2} K_{LA}C_{LA}\right) \\ &+ 2\eta_{H_2}(1-\varepsilon_B) k H_A C_{LA} (k_{GL}a + k_{LS}a)) C_{H_2,S} \\ &- K^2_{LA}C^2_{LA} k_{GL}a \cdot k_{LS}a \cdot C^*_{H_2} - 2k_{LS}a \cdot k_{GL}a \cdot C^*_{H_2} K_{LA}C_{LA} - k_{GL}a \cdot k_{LS}a \cdot C^*_{H_2} = 0 \end{aligned} \tag{7-6}$$

Mass transfer coefficients ($k_{GL}a$, $k_{LS}a$) are calculated using the correlations of Goto and Smith; [42] wetting efficiency (ε_W) is based on Al-Dahhan's correlation; [38] both are given in Chapter 5.

The observed reaction rate in the trickle bed reactor can be written most generally as the sum of rates in a wetted fraction and in an unwetted fraction that is periodically replenished with liquid and is thus reactive. [38] In this unwetted fraction, the liquid phase hydrogen concentration is equal to its solubility from Henry's law, as there is no liquid layer surrounding the catalyst for hydrogen to diffuse through.

$$-R_{LA,G} = \varepsilon_W \frac{\eta_{H_2} k C_{LA} H_A C_{H_2,S}}{(1 + K_{LA}C_{LA} + K_{H_2}H_A C_{H_2,S})^2} + (1-\varepsilon_W) \frac{\eta_{H_2} k C_{LA} H_A C^*_{H_2}}{(1 + K_{LA}C_{LA} + K_{H_2}H_A C^*_{H_2})^2} \tag{7-7}$$

The intraparticle hydrogen mass transfer limitations are characterized by the generalized Thiele modulus for hydrogen in the catalyst particles [61]

$$\phi = 2L(-r_{LA})\left[4\int_0^{C_{H_2,S}} D_e(-r_{LA})dC_{H_2}\right]^{-0.5} \tag{7-8}$$

which takes the following form when $-r_{LA}$ (Equation 7-1) is inserted:

$$\phi = \frac{d_p}{6}\cdot\frac{2kC_{LA}H_AC_{H_2}}{(1+K_{LA}C_{LA}+K_{H_2}H_AC_{H_2})^2}\left(4D_{H_2}\varepsilon_p^2kC_{LA}H_A\int_0^{C_{H_2,S}}\frac{C_{H_2}dC_{H_2}}{(1+K_{LA}C_{LA}+K_{H_2}H_AC_{H_2})^2}\right)^{-0.5} \tag{7-9}$$

The value of the generalized modulus is less than 0.2 for all reaction conditions, so we assume that the effectiveness factor is essentially unity in the model.

The molar balance (Eq. 7-2) is integrated numerically across the trickle bed volume using Euler's method in Microsoft Excel. At any position in the trickle bed reactor, where H_2 pressure and LA concentration are known, the value of $C_{H2,S}$ can be determined by solving Equation 7-6, a cubic equation, with the Solver function in Microsoft Excel 7.0. With $C_{H2,S}$, $C_{H2,L}$, and η_{H2} known, the reaction rate (Eq. 7-1) can be calculated and then lactic acid concentration determined at the next increment along the reactor. In this way, the concentration profiles and outlet conversion can be determined at each set of experimental conditions.

7.4. Results and Discussion

The trickle bed model described in Equation 7-2 to Equation 7-9 is referred to herein as Case 1, or the complete model for the trickle bed. We have also examined several variations of the model in order to better understand which model assumptions are important. These are given

below, and their results along with those of Case 1 are presented in Table 7-4. The catalyst beds in Table 7-4 correspond to those described in Section 7.2.2 examined in this study.

Case 2 is the same as Case 1 except that the trickle bed is assumed to be fully wetted (ε_W=1). Therefore, Equation 7-7 simplifies to

$$-R_{LA,G} = \frac{\eta_{H_2} k C_{LA} H_A C_{H_2,S}}{(1 + K_{LA} C_{LA} + K_{H_2} H_A C_{H_2,S})^2} \tag{7-10}$$

Case 3 is similar to Case 2, but reaction is assumed to take place only in the wetted fraction of the catalyst in the trickle bed, with the wetted fraction (ε_W) given by the correlation of Al-Dahhan. [38] In this case, Equation 7-7 is given as

$$-R_{LA,G} = \varepsilon_W \frac{\eta_{H_2} k C_{LA} H_A C_{H_2,S}}{(1 + K_{LA} C_{LA} + K_{H_2} H_A C_{H_2,S})^2} \tag{7-11}$$

In Case 4, it is assumed that the trickle bed is fully wetted (ε_W=1), that there are no gas-liquid or liquid-solid mass transfer resistances in the trickle bed (C^*_{H2}= $C_{H2,\,S}$), and that there are no intraparticle resistances (η_{H2}=1). The reactor is thus considered as a plug flow reactor with intrinsic reaction kinetics. The observed reaction rate is thus given by Eq. 7-1, and Equations 7-4 to 7-9 do not apply.

Table 7-4. Results of Trickle Bed Modeling (Cases 1-4) of Lactic Acid Hydrogenolysis

#	TBR S/N	Temperature (K)	Flow Rate (ml/hr)	Exp. Conversion	Catalyst mass (g)	Case 1	Case 2	Case 3	Case 4	ε_W [1]	ε_W [2]	$C_{H2,S}$ inlet (mol/l) Case 1
1	59	363	200	0.108	9.1*	0.136	0.113	0.050	0.153	0.436	0.706	0.042
2	58	363	100	0.232	9.1*	0.264	0.203	0.071	0.294	0.346	0.638	0.037
3	60	363	50	0.416	9.1*	0.491	0.352	0.100	0.535	0.274	0.576	0.031
4	61	363	25	0.551	9.1*	0.802	0.584	0.136	0.836	0.218	0.521	0.026
5	65	353	200	0.081	9.1*	0.068	0.064	0.028	0.071	0.436	0.706	0.053
6	64	353	100	0.162	9.1*	0.134	0.123	0.043	0.140	0.346	0.638	0.049
7	63	353	50	0.245	9.1*	0.260	0.229	0.064	0.272	0.274	0.576	0.045
8	62	353	25	0.395	9.1*	0.486	0.414	0.094	0.504	0.218	0.521	0.039
9	54	363	200	0.127	9.1	0.136	0.113	0.05	0.153	0.436	0.706	0.042
10	55	363	100	0.217	9.1	0.264	0.203	0.071	0.294	0.346	0.638	0.037
11	57	353	200	0.052	9.1	0.068	0.064	0.028	0.071	0.436	0.706	0.053
12	56	353	100	0.147	9.1	0.134	0.122	0.043	0.140	0.346	0.638	0.049

* denotes the diluted trickle bed

Table 7.4. (Cont'd)

#	TBR S/N	Temperature (K)	Flow Rate (ml/hr)	Exp. Conversion	Catalyst mass (g)	Case 1	Case 2	Case 3	Case 4	ε_W [1]	ε_W [2]	$C_{H2,S}$ inlet (mol/l) Case 1
13	50	363	200	0.356	19.0	0.264	0.222	0.099	0.294	0.436	0.706	0.042
14	51	363	100	0.617	19.0	0.490	0.392	0.141	0.535	0.346	0.638	0.037
15	49	353	200	0.205	19.0	0.134	0.127	0.056	0.140	0.436	0.706	0.053
16	53	353	100	0.389	19.0	0.261	0.240	0.085	0.272	0.346	0.638	0.049
17	47	353	50	0.649	19.0	0.487	0.439	0.127	0.504	0.274	0.576	0.045
18	46	373	100	0.840	19.0	0.700	0.496	0.181	0.768	0.346	0.638	0.028
19	45	373	50	0.980	19.0	0.951	0.773	0.242	0.967	0.274	0.576	0.023

1 Wetting efficiency was calculated as per Al-Dahhan's correlation:

$$\varepsilon_W = 1.104\,\mathrm{Re}_L^{1/3}\left[\frac{1+\left[(\Delta P/Z)/\rho_L g\right]}{Ga_L}\right]^{1/9}$$

2 Wetting efficiency was calculated as per Al-Dahhan's correlation at low pressure:

$$\varepsilon_W = 1.617\,\mathrm{Re}_L^{0.1461}\,Ga_L^{-0.0711}$$

where

$$\mathrm{Re}_L = \frac{Ld_P}{\mu_L}, Ga_L = \frac{d_P^3 g \rho_L^2}{\mu_L^2}$$

In analyzing the results given by the four cases, it is important to note that under all conditions that reaction rate increases with lactic acid concentration and with hydrogen concentration. Thus, the presence of mass transport resistances always decreases overall rate; thus Case 4 represents the maximum possible conversion rate in the trickle bed, and Case 3 the minimum possible conversion. It should also be noted that no parameters were adjusted to fit the model results to experimental data; extrapolated kinetic constants were used from Table 7-1 and mass transfer coefficients were calculated directly from literature correlations.[42] The following parity plot shows the comparison between model simulation and experiment results.

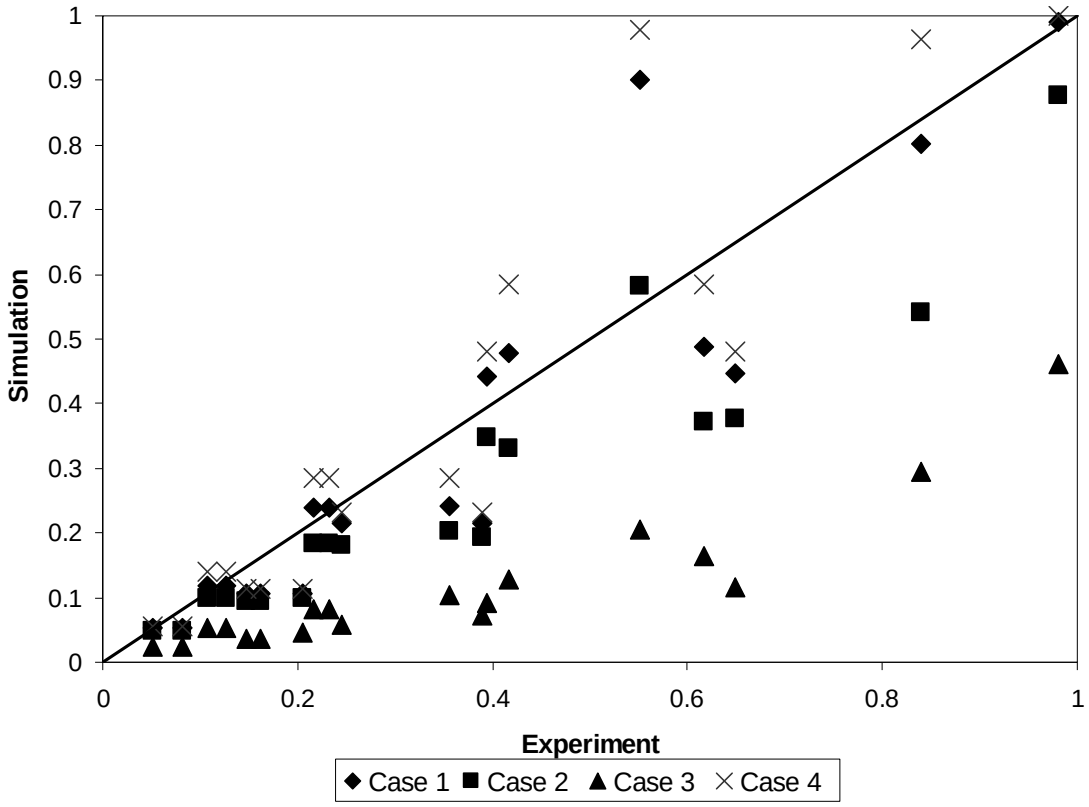

Figure 7-3. Parity plot of model simulation versus experiment results.

7.4.1. Comparison of Trickle Bed Models (Cases 1-4) with Experiments

Table 7-4 gives predicted outlet LA conversion for each of the four models (Cases 1-4) developed for LA hydrogenolysis in the trickle bed. In analyzing the results for the four cases, it is important to note that under all conditions the reaction rate increases with LA concentration and with hydrogen concentration. Thus, the presence of mass transport resistances always decreases overall rate. Case 4 therefore represents the maximum possible conversion in the trickle bed, and Case 3 the minimum possible conversion. It should also be noted that the same kinetic parameters, determined by fitting the data to the partially-wetted model (Case 1), were used in all four models. All physical properties, wetted fractions, and mass transfer coefficients were calculated directly from literature correlations as stated above.

The partially-wetted model (Case 1) presented in Eq. 7-2 – 7-9 predicts the outlet conversions for all trickle bed runs reasonably well, except at low flow rates in the reactor bed with fines (Runs 4 and 8), where it overpredicts conversion, and in the large reactor bed (Runs 15-19) where it underpredicts conversion. For the reactor bed with fines (Runs 1-8), the fully-wetted model predicts the low flow rate conversion somewhat better – this makes sense in terms of fines enhancing the fraction of catalyst wetted and hence matching the fully wetted model more closely. We note that rate constants fitted to Runs 1-8 with the fully-wetted model (Case 2) are essentially identical to those reported in Table 7-2, so the fully-wetted model is clearly preferred for reactions in trickle beds with fines. The results for Case 3, with only the wetted fraction reactive, clearly underpredict the experimental conversions for nearly all reactions; results for Case 4, with no mass transfer resistances, clearly overpredict conversion, especially at lower flow rates.

The value of the surface concentration ($C_{H2,S}$) at the reactor inlet, given in the rightmost column of Table 7-4, is a measure of the extent of mass transport resistances across the gas-liquid and liquid-solid interfaces. At 353 K, where reaction is relatively slow, the value of $C_{H2,S}$ is fairly close to that of the bulk liquid hydrogen concentration (0.068 M), indicating that gas-liquid and liquid-solid mass transport cannot influence rate. As such, Cases 1, 2, and 4 give nearly the same conversion at 353 K, because wetted and unwetted fractions give the same rate when mass transfer resistances are minimal. At 363 K, and especially at 373 K (Runs 18-19), the value of $C_{H2,S}$ in the wetted portion of the reaction is much less than the bulk liquid hydrogen concentration, and each model predict a significantly different outlet conversion. Here the partially wetted model gives a clearly superior fit of experimental results relative to the other models (Cases 2-4).

In the partially-wetted model (Case 1), the reaction rate in the unwetted fraction is higher than that in the wetted fraction, because the resistance to hydrogen transport across the liquid film reduces the hydrogen concentration at the catalyst surface ($C_{H2,S}$) in the wetted fraction of the bed. Thus, Case 2, where the reactor is assumed fully wetted, always gives a lower conversion than the partially-wetted model. For the partially-wetted model to be valid from a physical standpoint, it is necessary to imagine that the wetting of the trickle bed is a dynamic phenomenon such that the unwetted fraction is continuously replenished with the liquid phase. This postulate appears to hold in LA hydrogenolysis, in part because the carbon support is readily wetted by water and thus, although the liquid flows only over a portion of the catalyst particles in the bed, the entire catalyst is internally wetted and therefore reactive.

Experimentally, there is little effect of fines on LA conversion in the trickle bed reactor at high liquid flow rates (100 and 200 ml/hr), as evidenced by comparison of Runs 1, 2, 5, and 6 with Runs 9-12 in Table 7-1. This lack of influence of fines in the catalyst bed suggests that either 1) the catalyst is partially wetted and the fines do not increase the fraction wetted, or 2) at these flow rates the catalyst bed is nearly fully wetted with and without fines. Since the bed was carefully packed and since the fully wetted model (Case 2) fits the experimental behavior in the bed with fines well at low flow rates, we conclude that it is most likely that the bed is fully wetted under the operating conditions used. Thus the correlations of Al-Dahhan et al.[38] and El-Hiswani et al.[62] that were developed for hydrocarbons on metal oxides do not apparently predict wetted fractions accurately for this aqueous phase system in which, as stated before, the carbon support is hydrophilic. Yet despite the likelihood that these correlations underpredict fraction wetted in this system, the reactor model accounting for partial wetting (Case 1), with the wetted fraction predicted by the correlation of Al-Dahhan et al.[38] does give the best fit of any model to the collective experimental data and thus remains the preferred means of approaching trickle bed modeling, especially at low liquid mass velocities. This suggests that the approach to modeling is correct, even if the values of the wetted fractions are not.

Finally, the experimental conversions in the larger trickle bed reactor (Runs 13-18) are greater than those predicted by the models in every experiment. The models consistently predict the same conversion at similar residence times (catalyst mass/liquid flow rate) in small and large beds, (Runs 10 and 13, Runs 12 and 15, Runs 3 and 14, Runs 7 and 16), but the experimentally observed conversion in the larger reactor bed is consistently greater than that at the same residence time in the smaller bed. The reason for this behavior is not known, but the results

suggest that laboratory trickle reactors should be preferably shorter rather than longer in order to be best modeled and controlled.

7.4.2. Comparison of Batch and Trickle Bed Reaction Rates

Given that overall conversion is relatively low for the two smaller trickle catalyst beds (<25%), we make the assumption, in accordance with the zero-order rate behavior in the batch reactor, that hydrogenolysis rate is essentially constant in the trickle bed at these conditions. The average reaction rate in the trickle bed is thus readily calculated via Eq. 7-12 as

$$R_{PG,G} = C_{PG}/(1-\varepsilon_B)/\tau \qquad (7\text{-}12)$$

from the inlet flow rate, propylene glycol outlet concentration, and bed volume. Values of the average rates determined from the trickle bed experiments at high flow rates in the two smaller trickle beds are given in Table 7-3.

The average reaction rates in the trickle bed reactor (Table 7-3) approach those measured in the batch reactor, especially in the shorter beds and with fines present. This result indicates that the trickle bed reactors operating under these high liquid flow rates approach the intrinsic kinetic regime of operation.

The similarity between batch and trickle bed rates is further evidence that the catalyst in the trickle bed reactor is fully wetted, or nearly so, at these reaction conditions. As discussed above, the fraction wetted predicted by Al-Dahhan et al.[38] ($\varepsilon_W = 0.35$ at 100 ml/hr and $\varepsilon_W = 0.44$ at 200 ml/hr at these conditions) is apparently less than that actually wetted in the water/activated carbon system present for LA hydrogenolysis. It is clear that predicting the effects of partial wetting remains a challenging aspect of trickle bed reactor analysis.

The results in Table 7-3 represent, to our knowledge, one of few cases where trickle bed reactors are purposefully operated in a "differential" model to achieve rates similar to those obtained in a batch reactor. It is also noteworthy that product selectivity, which is a second major issue in relating batch and trickle bed reactors, especially with biorenewable substrates, is similar in both reactors under these conditions. It is therefore possible to approach intrinsic kinetic rates and selectivity in a trickle bed reactor, albeit at conditions (e.g. high flow rates and low conversions) that are far from those that would be chosen to optimize product yields in feasibility or screening studies.

7.5. **Conclusions**

Laboratory-scale trickle bed reactors must be used carefully in order to characterize heterogeneous reaction systems such as lactic acid hydrogenolysis that are gaseous reactant limited. Under conditions of high flow rate and low temperature, and thus low reactant conversion, it is possible to approach intrinsic kinetic reaction rates that are similar to those found in conventional stirred batch systems. Under such conditions, the trickle bed approaches fully-wetted behavior and essentially acts as a differential reactor. These conditions are thus preferable for fundamental characterization of reaction kinetics and pathways.

Applying results of laboratory trickle bed reactor experiments at conditions aimed at maximizing conversion and product yields must be done with caution, as the effects of partial wetting and mass transport disguise reaction kinetics and product selectivities. It is possible to model reactor behavior under these conditions by including wetting and mass transport, but results must be viewed carefully in light of the challenges of predicting fractional wetting and mass transport coefficients for different physical systems. Nevertheless, the use of such models,

based on intrinsic kinetics developed in batch reactors, appears to be a step forward in understanding trickle bed behavior and in facilitating reasonable scale-up of trickle reactor systems.

Chapter 8 Conclusion and Recommendations for Future Work

During the course of my thesis projects discussed in the prior chapters, systematic investigation was carried out to screen multiple proprietary catalysts in terms of glycerol conversion and selectivity toward propylene glycol in the batch reactors. Process optimization was done with attention paid to catalyst loadings, temperature, reaction pressure, various organic solvents other than water, and impurities present in the commercial manufacturing. This investigation in the batch reactors provided important information and feedback to our project collaborator and helped guide through catalyst synthesis and preparation.

Based on the study in the batch reactors, some candidates were selected for catalyst scale-up in a pilot scale trickle bed reactor to investigate how flow dynamics influence the catalysis and kinetics of glycerol hydrogenolysis system. Partial wetting of catalyst particle has a pronounced effect on glycerol conversion and reaction rates, and a 5 to 10 K temperature profile was observed along the catalyst bed central axis. All the assumptions adopted during the model establishment were thoroughly examined by simplifying the original comprehensive model. Predictions from such simplified models were compared with the experimental results and the simulation from original comprehensive model, which proves and justifies the usage of assumptions.

With all the experimental data available from vigorous runs from both MSU and PNNL trickle beds, mechanistically based model was established to integrate mass and energy transfer and partial wetting phenomenon for the data collected in PNNL. This comprehensive model gives a reasonable simulation of the catalyst bed and a prediction of glycerol conversion over a

wide range of conditions. Moreover, temperature gradient observed inside the trickle bed was simulated, too. Model gives a realistic depiction for isothermal bed.

Since experiments were run in both batch and trickle bed reactors, intrinsic rate correlation was considered for the next stage of this research for a better understanding of reaction kinetics and a possibly faster screening process. Given few side products and high selectivity, lactic acid hydrogenolysis was chosen for this part of research. Our study shows that intrinsic reaction rate stays the same regardless the reactors as long as the reaction lies in the intrinsic reaction regime. Mechanistically based model for lactic acid hydrogenolysis predicts outlet conversion in the trickle bed well.

As for the future work, I will recommend three points for the consideration:

1. Other active metals or oxides should be tested for the possible constituents.

   There are a great number of literatures that investigated other active metals for glycerol hydrogenolysis. Ruthenium and platinum were studied by Maris et al.[15] with carbon as support. Wang et al.[16] studied Cu-ZnO catalyst for glycerol hydrogenolysis. Mane et al.[17] tried copper and aluminum for this process. Other candidates include iron, chromium, magnesium oxide, and palladium.[63-66]

2. Surface structure and treatment is correlated to catalyst performance and explore alternative reaction pathway and catalysis mechanism.

   A great deal of efforts in this research was made to understand mass transport limit and interaction between catalyst particle surface and reactants by calculating Weisz-Prater numbers, for instance. On the other hand, catalyst surface structure and how to treat the surface and modify the structure often has a significant impact on the catalyst activity and

potentially change reaction mechanism and route. This structure-performance correlation has been a popular topic for catalysis research in recent years with advanced characterization instruments widely available.[67-69] It gives the direct information about the interaction between catalyst active size, reactants, and intermediates, and therefore makes it possible or easier to elucidate the catalysis mechanism and pathway. It also helps evaluate a specific support material.

3. Better understanding partial wetting and its effect on the reaction by conducting reactions in a trickle bed reactor with reactants recycled. At present, the trickle bed used in our research facility does not recycle the reactants. In order to improve system efficiency, exiting liquid phase should be redirected to the top of trickle bed for a better conversion. Given the phenomenon we have observed thus far that unwetted fraction of catalyst surface contributes more to the overall reaction rate, feed flow rate or feed pumping speed needs to be thoroughly investigated along with bed holdup and resident time.

APPENDICES

Appendix A. Detailed Derivation of Kinetic Model

Our model of glycerol hydrogenolysis investigated steady state scenario when all data were collected and where catalyst was partially wetted. The establishment of this model started with reaction mechanism proposal. Based on the available literature regarding typical hydrogenolysis process, the mechanism proposal here works as follows:

$$GO + S \underset{k_{-1}}{\overset{k_1}{\rightleftarrows}} GA \cdot S + H_2$$

$$GA \cdot S + OH^- \underset{k_{-2}}{\overset{k_2}{\rightleftarrows}} I \cdot S + OH^-$$

$$I \cdot S + H_2 \xrightarrow{k_3} PG + S$$

The reaction starts with glycerol dehydrogenolysis on catalyst surface. Intermediate GA·S will then turn into intermediate I·S under basic environment, which is followed by hydrogenolysis to product propylene glycol.

The rate expression for each step shown above can be written as following when reaction system reaches equilibrium:

$$r_1 = k_1 C_{GO} \cdot C_S - k_{-1} C_{GA \cdot S} C_{H_2}$$
$$r_2 = k_2 C_{GA \cdot S} C_{OH^-} - k_{-2} C_{I \cdot S} C_{OH^-}$$
$$r_3 = k_3 C_{I \cdot S} C_{H_2}$$

At steady state all three reaction rates equal and therefore

$$r_1 = r_2 = r_3$$

In order to development model in terms of glycerol, base, and hydrogen, terms involving intermediates such as GA·S, I·S, and free catalyst surface S should be eliminated. To solve

equation group with three unknown variables, three independent equations are needed. Steady state provides two, and one boundary condition is required.

$$C_{total} = C_S + C_{GA\cdot S} + C_{I\cdot S}$$

This boundary condition depicts free catalyst surface and surface occupied by intermediates such as GA·S and I·S add up to the total catalyst surface.

With all three equations available, the relationship between variables can be determined:

$$C_{I\cdot S} = \frac{k_1 C_{GO} C_S}{k_3 C_{H_2} + \frac{k_{-1} k_3 C_{H_2}{}^2}{k_2 C_{OH^-}} + \frac{k_{-2} k_{-1} C_{H_2}}{k_2}}$$

$$C_{GA\cdot S} = \frac{k_3 C_{H_2} + k_{-2} C_{OH^-}}{k_2 C_{OH^-}} \cdot \frac{k_1 C_{GO}}{k_3 C_{H_2} + \frac{k_{-1} k_3 C_{H_2}{}^2}{k_2 C_{OH^-}} + \frac{k_{-2} k_{-1} C_{H_2}}{k_2}} \cdot C_S$$

Since GA·S and I·S concentration has been denoted in terms of Cs, Cs can be determined as follows:

$$CTotal = CS + CGA\cdot S + CI\cdot S$$

$$= \left[1 + \frac{k_1 C_{GO}}{k_3 C_{H_2} + \frac{k_{-1} k_3 C_{H_2}{}^2}{k_2 C_{OH^-}} + \frac{k_{-2} k_{-1} C_{H_2}}{k_2}} \left(1 + \frac{k_3 C_{H_2} + k_{-2} C_{OH^-}}{k_2 C_{OH^-}} \right) \right] \cdot C_S$$

where C_{total} is known through chemisorption performed on Micromeritics ASAP 2010.

Therefore, reaction rate expression can be further written as:

$$r = r_3 = k_3 C_{I\cdot S} C_{H_2}$$

$$= \frac{k_3 C_{H_2} k_1 C_{GO}}{k_3 C_{H_2} + \frac{k_{-1} k_3 C_{H_2}{}^2}{k_2 C_{OH^-}} + \frac{k_{-2} k_{-1} C_{H_2}}{k_2}} \cdot \frac{C_{Total}}{1 + \frac{k_1 C_{GO}}{k_3 C_{H_2} + \frac{k_{-1} k_3 C_{H_2}{}^2}{k_2 C_{OH^-}} + \frac{k_{-2} k_{-1} C_{H_2}}{k_2}} \left(1 + \frac{k_3 C_{H_2} + k_{-2} C_{OH^-}}{k_2 C_{OH^-}}\right)}$$

After rearrangement, reaction rate expression becomes

$$r_1 = \frac{k_1 k_2 k_3 C_{total} C_{H_2} C_{GO} C_{OH^-}}{(k_3 k_2 + k_{-2} k_{-1}) C_{H_2} C_{OH^-} + (k_1 k_2 + k_{-2} k_1) C_{GO} C_{OH^-} + k_{-1} k_3 C^2{}_{H_2} + k_1 k_3 C_{H_2} C_{GO}}$$

Simplify this reaction rate expression by dismissing two cross terms in denominator while retaining dependencies on hydrogen and base:

$$(k_3 k_2 + k_{-2} k_{-1}) C_{H_2} C_{OH^-}$$

$$k_1 k_3 C_{H_2} C_{GO}$$

Therefore, simplified reaction rate expression is

$$r = r_1 = \frac{k_f C_{H_2} C_{GO} C_{OH^-}}{C_{GO} C_{OH^-} + K_H C^2{}_{H_2}}$$

where

$$k_f = k_1 k_2 k_3 C_{total} \Big/ k_1 k_2 + k_{-2} k_1 = k_0 e^{(-E_a / RT)}$$

and

$$K_H = k_{-1} k_3 \Big/ k_1 k_2 + k_{-2} k_1$$

Appendix B. Corrected Derivation of Kinetic Model

Our model of glycerol hydrogenolysis investigated steady state scenario when all data were collected and where catalyst was partially wetted. The establishment of this model started with reaction mechanism proposal. Based on the available literature regarding typical hydrogenolysis process, the mechanism proposal here works as follows:

$$GO + S \underset{k_{-1}}{\overset{k_1}{\rightleftharpoons}} GA \cdot S + H_2$$

$$GA \cdot S + OH^- \underset{k_{-2}}{\overset{k_2}{\rightleftharpoons}} I \cdot S + OH^-$$

$$I \cdot S + 2H_2 \xrightarrow{k_3} PG + S$$

The reaction starts with glycerol dehydrogenolysis on catalyst surface. Intermediate GA·S will then turn into intermediate I·S under basic environment, which is followed by hydrogenolysis to product propylene glycol.

The rate expression for each step shown above can be written as following when reaction system reaches equilibrium:

$$r_1 = k_1 C_{GO} \cdot C_S - k_{-1} C_{GA \cdot S} C_{H_2}$$
$$r_2 = k_2 C_{GA \cdot S} C_{OH^-} - k_{-2} C_{I \cdot S} C_{OH^-}$$
$$r_3 = k_3 C_{I \cdot S} C^2_{H_2}$$

At steady state, all three reaction rates equal and therefore

$$r_1 = r_2 = r_3$$

In order to development model in terms of glycerol, base, and hydrogen, terms involving intermediates such as GA·S, I·S, and free catalyst surface S should be eliminated. To solve

equation group with three unknown variables, three independent equations are needed. Steady state provides two, and one boundary condition is required.

$$C_{total} = C_S + C_{GA\cdot S} + C_{I\cdot S}$$

This boundary condition depicts free catalyst surface and surface occupied by intermediates such as *GA·S* and *I·S* add up to the total catalyst surface. With all three equations available, the relationship between variables can be determined:

$$C_{I\cdot S} = \frac{k_1 k_2 C_{GO} C_S C_{OH^-}}{k_{-1}k_{-2}C_{OH^-}C_{H_2} + k_{-1}k_3 C_{H_2}^3 + k_2 k_{-2} C_{OH^-}^2 + k_2 k_3 C_{OH^-} C_{H_2}^2 - k_2 k_{-2} C_{OH^-}^2}$$

$$C_{G\cdot S} = \frac{k_1 C_{GO} C_S (k_{-2} C_{OH^-} + k_3 C_{H_2}^2)}{k_{-1}k_{-2}C_{OH^-}C_{H_2} + k_{-1}k_3 C_{H_2}^3 + k_2 k_{-2} C_{OH^-}^2 + k_2 k_3 C_{OH^-} C_{H_2}^2}$$

Given the boundary condition listed above, CS can be solved with $C_{I\cdot S}$ and $C_{G\cdot S}$ available

$$C_S = \frac{C_{total}(k_{-1}C_{H_2} + k_2 C_{OH^-})(k_{-2}C_{OH^-} + k_3 C_{H_2}^2) - k_2 k_{-2} C_{OH^-}^2}{(k_{-1}C_{H_2} + k_2 C_{OH^-} + k_1 C_{GO})(k_{-2}C_{OH^-} + k_3 C_{H_2}^2) - k_2 k_{-2} C_{OH^-}^2 + k_1 k_2 C_{GO} C_{OH^-}}$$

and r_3.

$$r_3 = \frac{k_1 k_2 k_3 C_{total} C_{OH^-} C_{GO} C_{H_2}^2}{k_{-1}k_{-2}C_{H_2}C_{OH^-} + k_2 k_3 C_{OH^-} C_{H_2}^2 + k_1 k_3 C_{GO} C_{H_2}^2 + k_{-1}k_3 C_{H_2}^3 + k_1(k_2 + k_{-2}) C_{GO} C_{OH^-}}$$

Simplify this reaction rate expression by dismissing three cross terms in denominator while retaining dependencies on hydrogen and base:

$$k_{-1}k_{-2}C_{H_2}C_{OH^-},$$

$$k_2k_3C_{OH^-}C_{H_2}^2,$$

and $k_1k_3C_{GO}C_{H_2}^2$.

Final simplified intrinsic rate expression is

$$r_3 = \frac{k_f C_{GO} C_{OH^-} C_{H_2}^2}{C_{GO}C_{OH^-} + K_H C_{H_2}^3}$$

where $k_f = {k_2k_3C_{total}}\big/{(k_2 + k_{-2})}$

and $K_H = {k_{-1}k_3}\big/{k_1(k_2 + k_{-2})}$

Appendix C. Microsoft Excel Macro Program

Solutions to the cubic equation are found with macro program which was written to perform solver functionality at each incremental distance throughout the trickle bed reactor.

In order to run this macro, you need to open the spreadsheet of interest and click TOOLS>MACRO>MACROS. When a window pops up, copy and paste the following program into the window:

```
**********************************************************************
Sub Macro1()
'
' Macro1 Macro
' Macro recorded 2/14/2007 by Stazy
'
    currentrow = U
    Do Until currentrow > V
    SolverOk SetCell:="$X" & currentrow, MaxMinVal:=3, ValueOf:="0",
ByChange:="$Y" & currentrow
    SolverSolve userFinish:=True
    SolverFinish keepFinal:=1
    currentrow = currentrow + 1
    Loop
End Sub
**********************************************************************
```

X and Y in the macro program stand for two columns in the spreadsheet. X is cubic equation expression, and Y is the solution to it. U indicates the starting point for the iteration and V for the end.

Despite of macro's versatility, some adjustments to the solver in the individual spreadsheet are needed given the fact that cubic equation has three solutions in theory. However, not all the mathematical solutions make sense from chemical kinetic perspectives. Some conditions are needed in order for solver to produce sensible solution which makes mass fluxes across interfaces equal each other.

REFERENCES

REFERENCES

[1] Gunkel, D. (2006). Alternative energy sources. Detroit: Greenhaven Press.

[2] Sheahan, R. (1981). Alternative energy sources: a strategy planning guide. Rockville, Md: Aspen Systems Corp.

[3] Berinstein, P. (2001). Alternative energy: facts, statistics, and issues. Westport, CT: Oryx Press.

[4] Baumgartner, T. and Burns, T. (1984). Transitions to alternative energy systems: entrepreneurs, new technologies, and social change. Boulder: Westview Press.

[5] Maclean, H. (2004). Alternative transport fuels for the future. *Int. J. Vehicle Des*. **35** (1-2), 27-49.

[6] Scott, Elinor , Peter, F, et al. (2007). Biomass in the manufacture of industrial products - the use of proteins and amino acids. *Appl. Microbiol. Biot*. **75** (4), 751-762.

[7] Huber, George W, Corma, Avelino. (2007). Synergies between bio- and oil refineries for the production of fuels from biomass. *Angew. Chem. Int. Edit.* **46** (38), 7184-7201.

[8] Wise, D. (1981). Fuel gas production from biomass. Boca Raton, Fla: CRC Press.

[9] Passero, B. (2006). Energy alternatives. Detroit: Greenhaven Press/Thomson Gale.

[10] Hall, C. (1981). Biomass as an alternative fuel. Rockville, Md: Government Institutes.

[11] Montharu, J., Le Guellec, S. and Kittel, B. et al. (2010). Evaluation of lung tolerance of ethanol, propylene glycol, and sorbitan monooleate as solvents in medical aerosols. *J. Aerosol. Med. Pulm. D.* **23** (1), 41-46.

[12] Herkenne, C., Naik, A., and Kalia, Y. et al. (2008). Effect of propylene glycol on ibuprofen absorption into human skin in vivo. *J. Pharm. Sci*. **97** (1), 185-197.

[13] Yang, K. et al. (2006). Dendrimers for pharmaceutical and biomedical applications. *J. Biomat. Sci-Polym. E*. **17** (1-2), 3-19.

[14] Alli, A, Hazer, B, Menceloglu, Y, et al. (2006). Synthesis, characterization and surface properties of amphiphilic polystyrene-b-polypropylene glycol block copolymers. *Eur. Polym. J*. **42** (4), 740-750.

[15] Maris, E., Davis R. (2007). Hydrogenolysis of glycerol over carbon-supported Ru and Pt catalysts. *J. Catal*. **249** (2), 328-337.

[16] Wang S., Liu, H. (2007). Selective hydrogenolysis of glycerol to propylene glycol on Cu-ZnO catalyst. *Catal. Lett*. **117** (1-2), 62-67.

[17] Mane, R., Hengne, A., Ghalwadkar, A. et al. (2010). Cu : Al nano catalyst for selective hydrogenolysis of glycerol to 1, 2-propanediol. *Catal. Lett*. **135** (1-2), 141-147.

[18] Casale, B. and Gomez, A. (1994). Catalytic method of hydrogenating glycerol. US Patent 5,276,181.

[19] Schuster, L. and Eggersdorfer, M. (1997). Preparation of 1,2-propanediol. US Patent 5,616,817.

[20] Werpy, T., Fyre, J. and Zacher, A. et al. (2005). Hydrogenolysis of 6-Carbon Sugars and Other Organic Compounds. US Patent 6,841,085 B2.

[21] Hass, T., Neher, A., Arntz, D. et al. (1995). Process for the Simultaneous Production of 1,2- and 1,3- propanediol. US Patent 5,426,249.

[22] Miyazawa, T., Koso, S. et al. Glycerol hydrogenolysis to 1,2-propanediol catalyzed by a heat-resistant ion-exchange resin combined with Ru/C. *Appl. Catal. A-Gen.* **329**, 30-35.

[23] Suppes, G., Dasari, M., and Kiatsimkul, Pim-Pahn et al. (2005). Low-Pressure Hydrogenolysis of Glycerol to Propylene Glycol. *App.Catal. A: Gen.* **281**, 225-231.

[24] Shanks, B., and Lahr, D. (2003). Kinetic Analysis of the Hydrogenolysis of Lower Polyhydric Alcohols: Glycerol to Glycols. *Ind. Eng. Chem. Res*. **42**, 5467-5472.

[25] Dudukovic, M., and Larachi, F. et al. (1999). Multiphase reactors-revisited. *Chem. Eng. Sci.* **54** (13-14), 1975-1995.

[26] Dudukovic, M. (1999). Trends in catalytic reaction engineering. *Catal. Today*. **48** (1-4), 5-15.

[27] Biardi, G., Baldi, C. (1999). Three-phase catalytic reactors. *Catal. today*. **52**, 223-234.

[28] Wang, T., Wang, J., Jin, Y. (2007) Slurry Reactors for Gas-to-Liquid Processes: A Review. *Ind. Eng. Chem. Res.* **46** (18), 5824-5847.

[29] Chaudhari, R., Mills, P. Multiphase catalysis and reaction engineering for emerging pharmaceutical processes. *Chem. Eng. Sci*. **59** (22-23), 5337- 5344

[30] Dudukovic, M., Larachi, F., Mills, P. (2002). Multiphase catalytic reactors: a perspective on current knowledge and future trends. *Catal. Rev.* **44** (1), 123-246.

[31] Al-Dahhan, M. and Dudukovic, M. et al. (1996). Catalyst bed dilution for improving catalyst wetting in laboratory trickle-bed reactors. *AICHE J*. **42** (9), 2594-2606.

[32] Dianetto, A., Specchia, V. (1992). Trickle-bed reactors: state of art and prospectives. *Chem. Eng. Sci*. **47** , 3197-3213.

[33] Schubert, M., Bauer, T., and Lange, R. (2006). Unsteady-state operation for

enhancement of the performance of technical trickle-bed reactors. *Chemie. Ingenieu. Technik*. **78** (8),1023-1032.

[34] Larachi, F., Cassanello, M. et al. (1998). Gas-liquid interfacial mass transfer in trickle-bed reactors at Elevated Pressures. *Ind. Eng. Chem. Res*. **37**, 718-733.

[35] Iliuta, I., Ortiz-Arroyo and Arturo et al. (1999). Hydrodynamics and mass transfer in trickle bed reactor: an overview. *Chem. Eng. Scien.* **54**, 5329-5337.

[36] Al-Dahhan, M., Larachi, F., Dudukovic, M., Laurent, A. (1997). High-pressure trickle-bed reactors : a review. *Ind. Eng. Chem. Res.* **36** (8), 3292-3314.

[37] Huang, X. and Varma, A. et al. (2004). Heat transfer characterization of gas-liquid flows in a trickle bed. *Chem. Eng. Sci.* **59** (15), 3767-3776.

[38] Al-Dahhan M. and Dudukovic, M. (1995). Catalyst Wetting Efficiency in trickle bed reactors at high pressure. *Chem. Eng. Sci.* **50**, 2377-2389.

[39] Tronconi, E., Ferlazzo, N. et al. (1992). A mathematical model for the catalytic hydrogenolysis of carbohydrates. *Chem. Eng. Sci.,* **47**, 2451-2456.

[40] Linke, W. F. and Seidell, A. (1958). Solubilities, inorganic and metal organic compounds; a compilation of solubility data from the periodical literature. Vol. I. 4th Ed., Van Nostrand : Princeton, New Jersey.

[41] Smith, J.M. (1981). Chemical Engineering Kinetics, 3rd Ed., McGraw-Hill: New York.

[42] Goto, S. and Smith. J. (1975). Trickle-bed reactor performance. Part I. holdup and mass transfer effects. *AICHE J*. **21** (4), 706-713.

[43] Perry, R., Green, D., and Maloney, J. (1997). Perry's Chemical Engineering

Handbooks. McGraw-Hill: New York.

[44] Mederos, F., Ancheyta, J., and Chen, J. (2009). Review on criteria to ensure ideal behaviors in trickle-bed reactors. *Appl. Catal. A: Gen*. **355**, 1-19.

[45] Maiti, R. and Nigam, K. (2007). Gas-liquid distributors for trickle-bed reactors: a review. *Ind. Eng. Chem. Res*. **46**, 6164-6182.

[46] Bhaskar, M., Valavarasu, G., Sairam, B. and Balaraman, K. (2006). Performance evaluation of certain commercial hydrotreating catalysts in a pilot plant reactor. **24** (2), 217-234.

[47] Chen, J., Wang, N., Mederos, F. and Ancheyta, J. (2009). Vapor-liquid equilibrium study in trickle-bed reactor. *Ind. Eng. Chem. Res*. **48**, 1096-1106.

[48] Mogalicherla, A., Sharma, G., and Kunzru, D. (2009). Estimation of wetting efficiency in trickle-bed reactors for nonlinear kinetics. **48**, 1443-1450.

[49] Metaxas, K. and Papayannakos, N. (2006). Kinetics and mass transfer of benzene hydrogenolysis in a trickle-bed reactor. *Ind. Eng. Chem. Res.* **45**, 7110-7119.

[50] Eftaxias, A., Font, J., Fortuny, A., Fabregat, A., and Stuber, F. (2005). Kinetics of phenol oxidation in a trickle bed reactor over active carbon catalyst. *J. Chem. Technol. Biot.* **80**, 677-687.

[51] Popken, T., Geisler, R. and Gotze, L. et al. (1999). Reaction kinetics and reactive distillation – on the transfer of kinetic data from a batch reactor to a trickle-bed reactor. *Chem. Eng. Technol.* **21**(5), 401-404.

[52] Hickman, D., Weidenbach, M. and Friedhoff D. (2004). A comparison of a batch recycle reactor and an integral reactor with fines for scale-up of an industrial trickle bed reactor from laboratory data. *Chem. Eng. Sci.* **59**, 5425-5430.

[53] Kulkarni, R., Natividad, R., Wood, J., Stitt, E., and Winterbottom, J. (2005). A comparative study of residence time distribution and selectivity in a monolith CDC reactor and a trickle bed reactor", *Catal. Today*, **105**, 455-463.

[54] Manole, C., Julcour-Lebigue, C., Wilhelm, A., and Delmas, H. (2007). Catalytic oxidation of 4-hydroxybenzoic acid on activated carbon in batch autoclave and fixed-bed reactors. *Ind. Eng. Chem. Res*. **46**, 8388-8396.

[55] Guettel, R. and Turek, T. (2009). Comparison of different reactor types for low temperature Fischer-Tropsch systhesis: a simulation study. *Chem. Eng. Sci*. **64**, 955-964.

[56] Zhang, Z., Jackson, J., and Miller, D. (2008). Effect of biogenic fermentation impurities on lactic acid hydrogenolysis to propylene glycol. *Bioresource Technol*. **99**, 5873-5880.

[57] Chen, Y., Miller, D., and Jackson, J. (2007). Kinetics of aqueous-phase hydrogenolysis of organic acids and their mixtures over carbon supported ruthenium catalyst. *Ind. Eng. Chem. Res*. **46**, 3334-3340.

[58] Cortright, R., Sanchez-Castillo, M. and Dumesic J. (2002). Conversion of biomass to 1,2- propanediol by selective catalytic hydrogenolysis of lactic acid over silica-supported copper. *Appl. Catal. B: Environ.* **39**, 353-359.

[59] Zhang, Z., Jackson, J. and Miller, D. (2002). Kinetics of aqueous-phase hydrogenation of lactic acid to propylene glycol. *Ind. Eng. Chem. Res*. **41**(4), 691-696.

[60] Tsamatsoulis, D., Al-Dahhan, M., Larachi, F. and Papayannakos, N. (2001). The effect of particle dilution on wetting efficiency and liquid film thickness in small trickle beds. *Chem. Eng. Commu*. **185**, 67-77.

[61] Lee, H. (1985). Heterogeneous reactor design. Boston: Butterworth Publishers.

[62] El-Hisnawi, A.A.; Dudukovic, M.P.; Miller, P.L. (1982). Trickle bed reactors: dynamic tracer test, reaction studies, and modeling of reactor performance. ACS Symposium Series, *196*, 431.

[63] Anand, K.A., Anisia, K.S., Agarwal, A.K., et al.(2010). Hydrogenolysis of glycerol

with FeCo macrocyclic complex bonded to Raney Nickel support under mild reaction conditions. *Can. J. Chem. Eng.* **88** (2), 208-216.

[64] Kim, N.D., Oh, S., Joo, J.B., et al. (2010). Effect of preparation method on structure and catalytic activity of Cr-promoted Cu catalyst in glycerol hydrogenolysis. *Korean J. Chem. Eng.* **27** (2), 431-434.

[65] Guo, X.H., Li, Y., Shi, R. J., et al. (2009). Co/MgO catalysts for hydrogenolysis of glycerol to 1, 2-propanediol. *Appl. Catal. A-Gen.* **371** (1-2), 108-113.

[66] Musolino, M.G., Scarpino, L.A., Mauriello, F., et al. (2009). Selective transfer hydrogenolysis of glycerol promoted by palladium catalysts in absence of hydrogen. *Green Chem*. **11**(10), 1511-1513.

[67] Huang, Z.W., Cui, F., Kang, H.X., et al. (2008). Highly dispersed silica-supported copper nanoparticles prepared by precipitation-gel method: A simple but efficient and stable catalyst for glycerol hydrogenolysis. *Chem. Mater.* **20**(15), 5090-5099.

[68] Shinmi, Y., Koso, S., Kubota, T., et al. (2010). Modification of Rh/SiO2 catalyst for the hydrogenolysis of glycerol in water. *Appl. Catal. B-Environ.* **94**(3-4), 318-326.

[69] Tanksale A, Beltramini JN, Dumesic JA, et al.(2008). Effect of Pt and Pd promoter on Ni supported catalysts - A TPR/TPO/TPD and microcalorimetry study. *J. Catal.* **258**(2), 366-377.